Wave slamming forces on truss structures for wind turbines

Christy Ushanth Navaratnam

ERASMUS MUNDUS MSc PROGRAMME

COASTAL AND MARINE ENGINEERING AND MANAGEMENT
CoMEM

WAVE SLAMMING FORCES ON TRUSS STRUCTURES FOR WIND TURBINES

Norwegian University of Science and Technology, Trondheim, Norway
1st July, 2013

Navaratnam Christy Ushanth
4192338

The Erasmus Mundus MSc Coastal and Marine Engineering and Management
is an integrated programme organized by five European partner institutions,
coordinated by Delft University of Technology (TU Delft).
The joint study programme of 120 ECTS credits (two years full-time) has been
obtained at three of the five CoMEM partner institutions:

- Norges Teknisk- Naturvitenskapelige Universitet (NTNU) Trondheim, Norway
- Technische Universiteit (TU) Delft, The Netherlands
- City University London, Great Britain
- Universitat Politècnica de Catalunya (UPC), Barcelona, Spain
- University of Southampton, Southampton, Great Britain

The first year consists of the first and second semesters of 30 ECTS each, spent at
NTNU, Trondheim and Delft University of Technology respectively.
The second year allows for specialization in three subjects and during the third semester
courses are taken with a focus on advanced topics in the selected area of specialization:
- Engineering
- Management
- Environment
In the fourth and final semester an MSc project and thesis have to be completed.
The two year CoMEM programme leads to three officially recognized MSc diploma
certificates. These will be issued by the three universities which have been attended by
the student. The transcripts issued with the MSc Diploma Certificate of each university
include grades/marks for each subject. A complete overview of subjects and ECTS
credits is included in the Diploma Supplement, as received from the CoMEM coordinating
university, Delft University of Technology (TU Delft).

Information regarding the CoMEM programme can be obtained from the programme
coordinator and director

Prof. Dr. Ir. Marcel J.F. Stive
Delft University of Technology
Faculty of Civil Engineering and geosciences
P.O. Box 5048
2600 GA Delft
The Netherlands

NORWEGIAN UNIVERSITY OF SCIENCE AND TECHNOLOGY
DEPARTMENT OF CIVIL AND TRANSPORT ENGINEERING

Report Title:	Date: 1st July, 2013
Wave slamming forces on truss structures for wind turbines	Number of pages (incl. appendices): 128
	Master Thesis X Project Work

Name: Navaratnam Christy Ushanth

Professor in charge/supervisor: Øivind Asgeir Arntsen

Alf Tørum

Other external professional contacts/supervisors:

Abstract:

Generally the foundations of offshore wind turbines are steel truss structures which are exposed to wave slamming forces due to breaking waves, typically plunging breaking waves in shallow water. Calculations show that the forces from the plunging breaking waves are governing the design responses of the structure and the foundations. However, there are considerable uncertainties on the calculated plunging breaking wave forces. This research study is to investigate the wave slamming forces acting on different sections of the truss structure for wind turbines.

A physical model of 1:50 scale was built at the hydrodynamic laboratory, NTNU. A large number of experiments were carried out on various sections of the truss structure such as front section and side section. Besides, two different size individual piles places at the position of the vertical legs of the truss structure were tested in order to check the size effects. All the tests carried out for regular waves with different wave height and wave periods.The recorded total responses have been decomposed into quasi static and dynamic components. Then dynamic component of the total response is analysed using frequency response function (FRF) method or the transfer function method. The transfer function relates the impact force and the responses and an impulse hammer was used to obtain the transfer function. Duhamel integral method was used only for two individual cylinders in addition to the frequency response function method.

The analysed results show that the measured slamming forces are much lesser than the calculated slamming forces in all the cases. This discrepancies could be due to the size effects, scale effects and unfavourable wave form when it hits the structure. The entrained air during breaking process also influences in the results as it is different in the small scale test and in reality. It is recommended to perform the large scale tests to overcome such discrepancies.

Keywords:

1. Breaking waves
2. Slamming forces
3. Response
4. Frequency Response Function

MASTER DEGREE THESIS

Spring 2013

for

CoMEM student

Navaratnam Christy Ushanth

Thesis Title

Wave slamming forces on truss structures for wind turbines
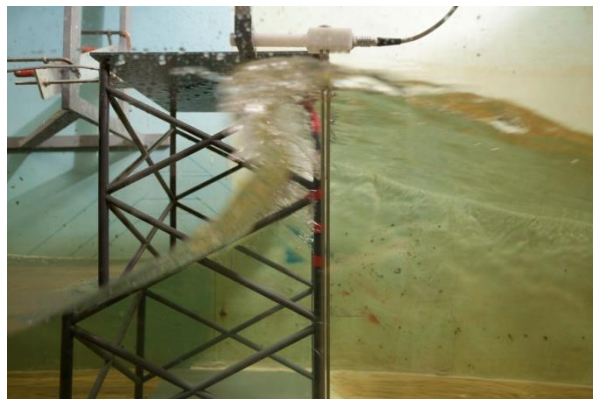
BACKGROUND

Figure 1. NTNU 1:50 scale model

Wind turbine foundation structures in shallow water may be prone to slamming forces from breaking waves in shallow water, typically plunging breaking waves. The Norwegian company Reinertsen A/S has been involved in the design of a truss support structure for wind turbines on the Thornton Bank, Belgian Coast. Plunging breaking waves has been specified for this area. Calculations show that the forces from the plunging breaking waves are governing the design responses of the structure and the foundations. However, there are considerable uncertainties on the calculated plunging breaking wave forces.

Miriam Aashamar (2012) conducting tests on a 1:50 scale model of a truss structure, Figure 1, to obtain wave slamming forces. The test set-up for the model used is shown in Figure 2.

NTNU

Faculty of Engineering Science and Technology
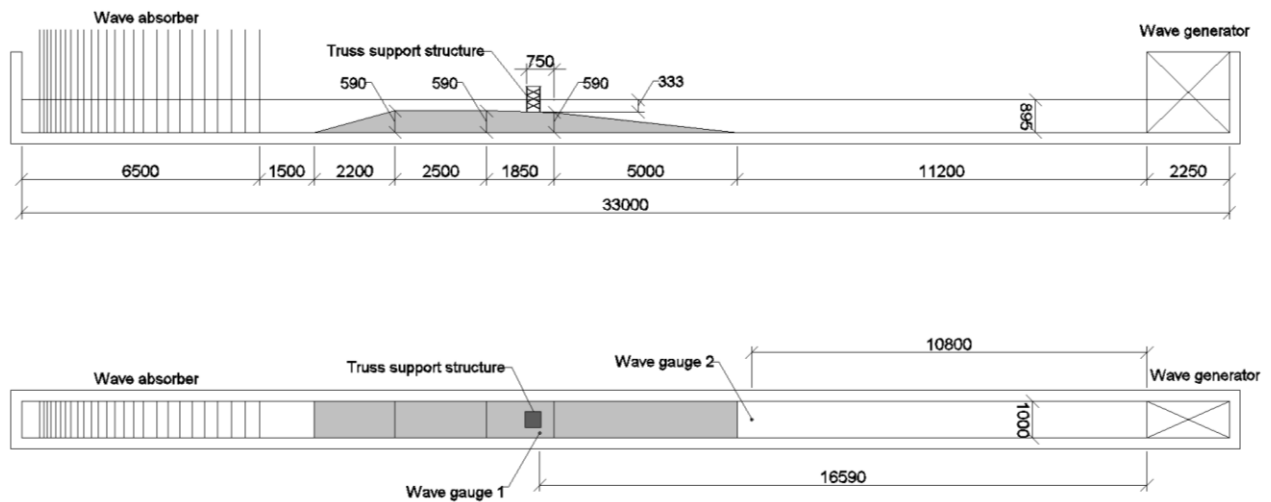Institute of Civil and Transport Engineering

Figure 2. Wave flume with model truss structure. Aashamar (2012).

Slamming forces is supposed to occur on the vertical legs as well as on the bracings of a truss structure. It is thus a challenging task to resolve the slamming forces on the individual members of the truss structure. Large scale tests have been planned in late spring of 2013 in the Hydralab facility The Large Wave Channel (GWK) in Hannover, Germany, (scale 1:8) of the same structure as we have tested in scale 1:50. During these tests it is planned to measure wave slamming forces locally on vertical leg and on some bracings in the expected breaking wave hit area, in addition to the total wave forces on the structure.

TASK DESCRIPTION

For the Master's thesis during the spring semester 2013, the plan is that the student shall carry out some laboratory tests to explore the simultaneous action on different parts of the truss structure:

1. Measuring simultaneously the forces on two different size vertical cylinders placed parallel to the wave crest with spacing between them corresponding to the distance between the two front vertical legs.

2. Measuring the forces on a section corresponding to the front section and side section of the truss structure.

The type of breaking (surging, plunging etc) is depending on the wave steepness and the bottom slope. The bottom slope in front of the model structure has been approximately 1:10 in the tests run by Ros (2011), Aune (2011) and Aashamar (2012). Plunging waves have been obtained in this case. If time permit during the tests of a Master student in the spring semester 2013, the bottom slope will be 1:20 or 1:50 For these slopes it may be that mainly surging waves will occur.

The tests will be run with regular waves.

The Master thesis work implies also some contact and co-operation with Reinertsen AS.

The attached preliminary note "Analysis of force response data from tests on a model of a truss structure subjected to plunging breaking waves" of 24 May 2012 gives an overview of wave slamming forces on piles and of different analysis methods applied for analyzing test results of wave slamming force experiments. In addition some comparison of forces obtained by Aashamar (2012) and calculated forces by existing calculation methods.

BIBLIOGRAPHY

Appelt, C.J. and Piorewicz, J. (1987): Laboratory studies of breaking wave forces acting on vertical cylinders in shallow water. Coastal Engineering, Vol. 11, 1987, pp 263 – 282.

Arntsen, Ø., Ros, X. and Tørum, A. (2011): Impact forces on a vertical pile from plunging breaking waves. Proceedings of the international conference "Coastal Structures 2011".

Aashamar, M. (2012): Wave slamming forces on truss support structures for wind turbines. Master thesis, submitted June 12, 2012, Norwegian University of Science and Technology, Department of Civil and Transport Engineering, Trondheim, Norway.

Aune, L. (2011): Forces from plunging breaking waves on a truss structure. Master thesis submitted June 2011, Norwegian University of Science and Technology, Department of Civil and Transport Engineering, Trondheim, Norway.

Chaplin, J.R., Flintham, T.P., Greated, C.A. and Skyner, D.J.(1992): Breaking wave forces on a vertical cylinder. Health and Safety Executive – Offshore Technology Report OTH 90 324, UK.

Cuomo, G., Trinidelli, M . and Allsop, W. (2007): Wave-in-deck loads on exposed jetties. Coastal Engineering, 54, pp 657 – 679, Elsvier,

Gjøsund, S. H., Moe, G., Arntsen, Ø. A., "Kinematics in broad-banded irregular ocean waves by a Lagrangian formulation", 20th Offshore Mechanics and Arctic Engineering Conference, 3rd-8th June, 2001, Rio de Janeiro, Brazil

Goda, Y., Haranaka, S., and Kitahata, M. (1966): Study of impulsive breaking wave forces on piles. Report of Port and Harbor Research Institute, Japan, Vol. 5. No. 6, pp. 1 – 30 (in Japanese).. Concept also in English language in Watanabe, A. and Horikawa, K. (1974): Breaking wave forces on lkarge diameter cell. Proc. Of 14th International Conference on Coastal Engineering, Chapter 102, pp 1741 – 1760.

Goda (2010): Reanalysis of regular and random breaking wave statistics. Coastal Engineering Journal, Vol. 52, No. 1 (2010) 71 – 106.

Goda, Y. (2010a): Random seas and design of maritime structures. 3rd Edition. World Scientific.

Grønsund Hanssen, A. and Tørum, A. (1999): Breaking wave forces on tripod concrete structure on shoal. Journal of Waterway, Port, Coastal, and Ocean Engineering, Vol. 125, No. 6, November 1999. ASCE.

Gudmestad, O.T. (1993): Measured and predicted deep water wave kinematics in regular and irregular seas. Marine Structures, vol.6, pp 1 – 73.

Kyte, A. and Tørum, A. (1996): Wave forces on a vertical cylinders upon shoals. Coastal Engineering, Vol. 27, 1996, pp 263 – 286.

Moe G, Verley R: Hydrodynamic Damping of Offshore Structures in Waves and Current, OTC Paper No 3798, Houston, Texas, May 1980

Moe G: Morison type wave loading, In: Tørum A, Gudmestad OT (Ed): Water Wave Kinematics, NATO ASI Series, Seies E: Applied Sciences, Vol 178, 1990, Kluwer Akademic Publishers, Dordrecht

Moe G and Gudmestad O T: "Predictions of Morison Type Forces in Irregular High Reynolds Number Waves", Int J of Offshore and Polar Engineering, Vol 8, No. 4, Dec 1998

Ros, X. (2011): Impact forces on a vertical pile from plunging breaking waves. Master thesis, Norwegian University of Science and Technology, Department of Civil and Transport Engineering, Trondheim, Norway.

Sawaragi, T. and Nochino, M. (1984): Impact forces of nearly breaking waves on a vertical circular cylinder. Coastal Engineering in Japan, Vol. 27, 1984.

Tanimoto, K., Takahashi, S., Kaneko, T. and Shiota, K. (1986): Impulsive breaking wave forces on an inclined pile exerted by random waves. Proceedings International Conference on Coastal Engineering, 1986.

Timoshenko, S. and Young, D.H. (1951): Engineering mechanics. McGraw-Hill Book Company.

Tørum, A. (1989): Wave forces on pile in surface zone. Journal of Waterway, Port, Coastal, and Ocean Engineering, Vol. 115, No. 4, July 1989. ASCE.

Wienke, J. and Oumeraci, H. (2005): Breaking wave impact forces on vertical and inclined slender pile – theoretical and large scale model investigations. Coastal Engineering, Elsevier, 52 (2005), pp 435 – 462.

General about content, work and presentation

The text for the master thesis is meant as a framework for the work of the candidate. Adjustments might be done as the work progresses. Tentative changes must be done in cooperation and agreement with the professor in charge at the Department.

In the evaluation thoroughness in the work will be emphasized, as will be documentation of independence in assessments and conclusions. Furthermore the presentation (report) should be well organized and edited; providing clear, precise and orderly descriptions without being unnecessary voluminous.

The report shall include:

- Standard report front page (from DAIM, http://daim.idi.ntnu.no/)
- Title page with abstract and keywords.(template on: http://www.ntnu.no/bat/skjemabank)
- Preface
- Summary and acknowledgement. The summary shall include the objectives of the work, explain how the work has been conducted, present the main results achieved and give the main conclusions of the work.
- Table of content including list of figures, tables, enclosures and appendices.
- If useful and applicable a list explaining important terms and abbreviations should be included.
- The main text.
- Clear and complete references to material used, both in text and figures/tables. This also applies for personal and/or oral communication and information.
- The Thesis Task Description (these pages) signed by professor in charge as Attachment 1.
- The report musts have a complete page numbering.

Advice and guidelines for writing of the report is given in: "Writing Reports" by Øivind Arntsen. Additional information on report writing is found in "Råd og retningslinjer for rapportskriving ved prosjekt og masteroppgave ved Institutt for bygg, anlegg og transport" (In Norwegian). Both are posted on http://www.ntnu.no/bat/skjemabank

Submission procedure

Procedures relating to the submission of the thesis are described in DAIM (http://daim.idi.ntnu.no/). Printing of the thesis is ordered through DAIM directly to Skipnes Printing delivering the printed paper to the department office 2-4 days later. The department will pay for 3 copies, of which the institute retains two copies. Additional copies must be paid for by the candidate / external partner.

On submission of the thesis the candidate shall submit a CD with the paper in digital form in pdf and Word version, the underlying material (such as data collection) in digital form (eg. Excel). Students

NTNU
Faculty of Engineering Science and Technology
Institute of Civil and Transport Engineering

Page 5 of 5 pages

must submit the submission form (from DAIM) where both the Ark-Bibl in SBI and Public Services (Building Safety) of SB II has signed the form. The submission form including the appropriate signatures must be signed by the department office before the form is delivered Faculty Office.

Documentation collected during the work, with support from the Department, shall be handed in to the Department together with the report.

According to the current laws and regulations at NTNU, the report is the property of NTNU. The report and associated results can only be used following approval from NTNU (and external cooperation partner if applicable). The Department has the right to make use of the results from the work as if conducted by a Department employee, as long as other arrangements are not agreed upon beforehand.

Tentative agreement on external supervision, work outside NTNU, economic support etc.
Separate description to be developed, if and when applicable. See
http://www.ntnu.no/bat/skjemabank for agreement forms.

Health, environment and safety (HSE) http://www.ntnu.edu/hse
NTNU emphasizes the safety for the individual employee and student. The individual safety shall be in the forefront and no one shall take unnecessary chances in carrying out the work. In particular, if the student is to participate in field work, visits, field courses, excursions etc. during the Master Thesis work, he/she shall make himself/herself familiar with " Fieldwork HSE Guidelines". The document is found on the NTNU HMS-pages at
http://www.ntnu.no/hms/retningslinjer/HMSR07E.pdf

The students do not have a full insurance coverage as a student at NTNU. If you as a student want the same insurance coverage as the employees at the university, you must take out individual travel and personal injury insurance.

Start and submission deadlines
The work on the Master Thesis starts on 4th February 2013

The thesis report as described above shall be submitted digitally in DAIM at the latest
1st July, 2013 at 3pm

Professor in charge: Øivind A. Arntsen

Other supervisors: Alf Tørum

Trondheim, June 28, 2013. (revised: dd.mm.yyyy)

Professor in charge (sign)

I lovingly dedicate this thesis to my mother who has been supporting me in each step of my life

1ˢᵗ July 2013, Trondheim, Norway

ACKNOWLEDGEMENT

I would like to express my sincere gratitude to a number of people who supported and helped me in several ways throughout my master's thesis. First of all, I would like to thank my supervisors Prof. Øivind Asgeir Arntsen and Prof. Alf Tørum for the guidance, useful comments, remarks and engagement through the learning process of this master thesis. My special thanks to Prof. Alf Tørum for helping me by organizing regular meetings even during his illness. I would also like to express my gratitude to Torgeir Jensen and Gustav Jakobsen for assisting me in experimental set-up and instrumentation; it would not have been possible to do the experiments without your frequent support. I am most grateful to Mayilvahanan Alagan Chella for assisting me whenever I come up with problems.

I would like to thank to my mother and my brother for being with me in all successes and motivating me in many ways. Finally, I would like thank to all of my friends, especially CoMEM friends for your support and love. I will be grateful to you all forever.

TABLE OF CONTENTS

LIST OF FIGURES

LIST OF TABLES

1.0   INTRODUCTION

Although hydropower is the major energy production in Norway, wind energy is becoming more popular these days. Norway has excellent wind power potential as it has typical sites along the long coastline with promising annual mean wind speed which is better than that in Denmark or northern Germany (Wind Energy-IFE, 2013). Wind energy is being produced from onshore and offshore wind farms. Approximately 10% of the total wind power is produced from offshore wind turbines.

1.1   Background

The foundations of offshore wind turbines could be a truss structure and might be placed in shallow waters, which is exposed to high amount of wave impacts. This wave impact will also be called as 'wave slamming forces'. Reinertsen A/S, a Norwegian company had been involved in the design of truss structure for wind turbines on the Thornton Bank, Belgian Coast (Figure 1.1) where plunging braking waves were specified.

Figure 1.1: Thornton Bank wind farm (Innogy, 2013)

A lot of researches have been carried out by several researchers to investigate the wave slamming forces on structures, most of them were vertical slender piles. There were not many researches done on the truss structures of wind turbines. Aashamar (2012), investigated the

wave slamming forces on truss support structure as part of her master's thesis. It was found that the slamming forces were very small compared to the calculated forces. Generally, unlike oil and gas platforms, hundreds or thousands of offshore wind turbines are installed at a site. Overdesigning them would result in high amount of costs. So, it is always better to investigate very deeply and validate the previous results.

1.2 Scopes and Objectives

The main objective of this research project is to carry out the laboratory tests to explore the simultaneous actions on different part of the truss structure in the following ways,

- Measuring the forces simultaneously on two vertical cylinders (different in sizes) placed parallel to the wave crest with spacing between them corresponding to the distance between the two front vertical legs
- Measuring the forces on a front section of the truss structure
- Measuring the forces on a side section of the truss structure

2.0   LITERATURE REVIEW

Many researches about wave slamming forces or breaking wave forces have been carried out and still being carried out all over the world. In this chapter, findings from previous researches have been described.

2.1   Morison's Equation

The non-breaking wave forces acting on a vertical pile can be calculated using Morison's equation (Morison, et al., 1950) which is the summation of the quasi static inertia and drag forces.

$$dF = dF_D + dF_M = \frac{1}{2} \rho_w C_D D |u| u \, dz + \rho_w \frac{\pi D^2}{4} C_M \frac{du}{dt} \, dz \qquad (2.1)$$

Where ρ_w is the water density, C_D is the drag coefficient, C_M is the inertia coefficient, D is the diameter of the pile, u is the water particle velocity, z is the water depth and t is the time. The values of the drag and coefficients are depending on the Reynolds number, Keulagen Carpenter number, roughness parameters and interaction parameters (Morison, et al., 1950). The total force can be obtained by integrating the equation (2.1) along the height of the pile.

$$F = F_D + F_M = \int_{-d}^{\eta} \frac{1}{2} \rho_w C_D D |u| u \, dz + \int_{-d}^{\eta} \rho_w \frac{\pi D^2}{4} C_M \frac{du}{dt} \, dz \qquad (2.2)$$

Where, η is the water surface elevation and the d is the total water depth.

The force coefficients C_D and C_M have been obtained with laboratory experiments. Different range of values were found for a non-breaking wave for various flow conditions. Generally the Morison equation is valid for small diameter members that don't significantly modify the incident waves, and it depends on the ratio of the wavelength to the member diameter. If this ratio is more than 5, the Morison equation is applicable (Chella, et. al., 2012).

When it comes to breaking wave attack, an additional force of short duration because of the impact of the vertical breaker front and the breaker tongue has to be considered (Irschik, et. al., 2002). So, an additional force term which is called 'slamming force' (F_S) has to be added to the Morison equation as given in the equation (2.3).

$$F = F_D + F_M + F_S \qquad (2.3)$$

2.2   Wave Slamming Force

The first wave impact model and theoretical formulation of water impact force on rigid body was derived by von Karman (von Karman, 1929). In his research, he considered a horizontal cylindrical body with a wedged-shaped under surface as it strikes the horizontal surface of water and calculated the force acting between the cylindrical body and the water. As it's shown in the Figure 2.1, a cylinder is approximated by a flat plate of width *c(t)* which is equal to the

immersed portion of the cylinder at each instant of the impact. The force on this plate could be calculated by considering the potential flow under the plate and integrating the pressures which can be found by the Bernoulli's equation and for this, the time history of the width of the plate should be known as well.
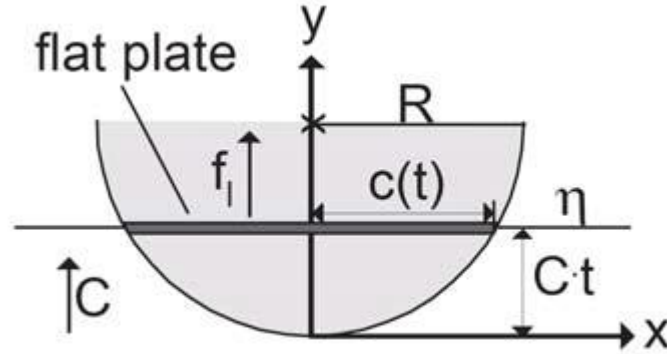
Figure 2.1: Definition sketch of von Karman's model (Ros Collados, 2011)

According to von Karman theory, the line force *f(t)* is given by the following equation,

$$f(t) = 0.5\, C_s\, \rho_w D\, C_b^2 \qquad (2.4)$$

$$C_s = \pi \left(1 - \frac{C_b}{R} t\right) \qquad (2.5)$$

Where, C_s is the slamming factor, C_b is the wave celerity and D is the diameter of the cylinder and R is the radius of the cylinder. The maximum line force occurs when the time t is zero ($t=0$, i.e. beginning of the impact), and the slamming factor becomes π.

As this line force is two dimensional and was derived for an infinite length of cylinder based on von Karman's model, it should be integrated over the length of the impact area (Figure 2.2) of cylinder assuming the same line force acting everywhere in the cylinder.
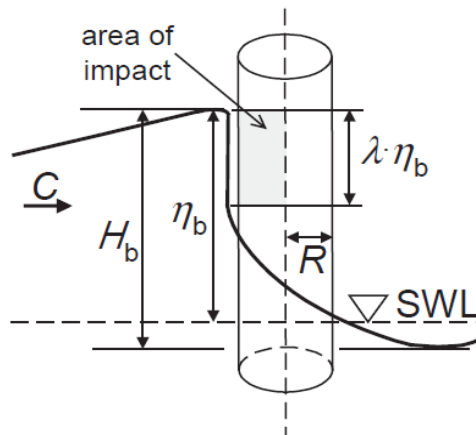
Figure 2.2: Definition sketch of impact force on vertical cylinder (Wienke & Oumeraci, 2005)

As Figure 2.2 shows, the height of the impact area was found to be the multiplication of the curling factor λ and the maximum breaking wave crest height η_b (Goda, et. al.,1966). So, the slamming force F_s on the cylinder,

$$F_s(t) = 0.5 \, \rho_w D \, C_b^2 \, \pi \left(1 - \frac{C_b}{R} t\right) \lambda \, \eta_b \tag{2.6}$$

$$F_s(t) = \pi \, \rho_w R \, C_b^2 \left(1 - \frac{C_b}{R} t\right) \lambda \, \eta_b \tag{2.7}$$

At the beginning of the impact with $t=0$ the equation (2.7) follows,

$$F_s = \pi \, \rho_w R \, \lambda \, \eta_b C_b^2 \tag{2.8}$$

From equation (2.4), the line force based on von Karman (1929),

$$f(t) = \pi \, \rho_w R \, C_b^2 \tag{2.9}$$
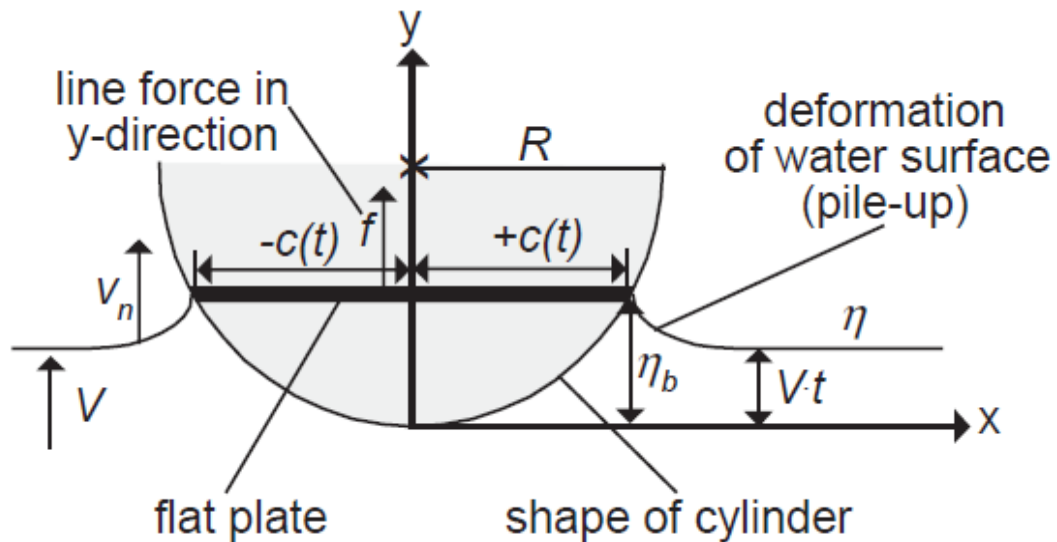
Figure 2.3: Definition sketch of 2D impact distribution (Wienke & Oumeraci, 2005)

The line force given in equation (2.9) was obtained by considering the momentum conservation during the impact. By taking into consideration not only the momentum conservation, but also the flow beside the flat plate would result in the so-called 'pile-up effect', that is the deformation of the water free surface (Figure 2.3). Because of this pile-up effect, the 'immersion' of the cylinder occurs earlier. As a result, the duration of impact decreases and the maximum line force increases (Wienke & Oumeraci, 2005).

According to Wagner (1932), the maximum line force is given as follows,

$$f(t) = 2\pi \, \rho_w R \, C_b^2 \tag{2.10}$$

The maximum line force calculated by Wagner's theory is twice the maximum line force calculated by von Karman's theory. Generally this maximum line force is described as a function 'Slamming Coefficient' C_s.

$$f(t) = C_S\, \rho_w R\, C_b^2 \tag{2.11}$$

2.3 Slamming Coefficients

So, the general form of wave slamming force is given in the following equation.

$$F_s = C_S \rho_w R\, \lambda\, \eta_b C_b^2 \tag{2.12}$$

According to von Karman (1929) and Goda et. al. (1966), Cs is π and Wagner's theory suggests a C_s value of 2π. Wienke & Oumeraci (2005) suggest a C_s value of 2π as they show that the formulation of Wagner's theory is more accurate even though Goda et. al (1966)'s description of the impact is based on von Karman (1929). Ros Collados (2011) investigated the slamming coefficient on a vertical cylinder in his master's thesis and estimated a C_s value of 4.3 for a triangular load case, and this value is between π and 2π. This experiment was done with a vertical cylinder with a series of force transducers placed on it in different elevations as shown in Figure 2.4.
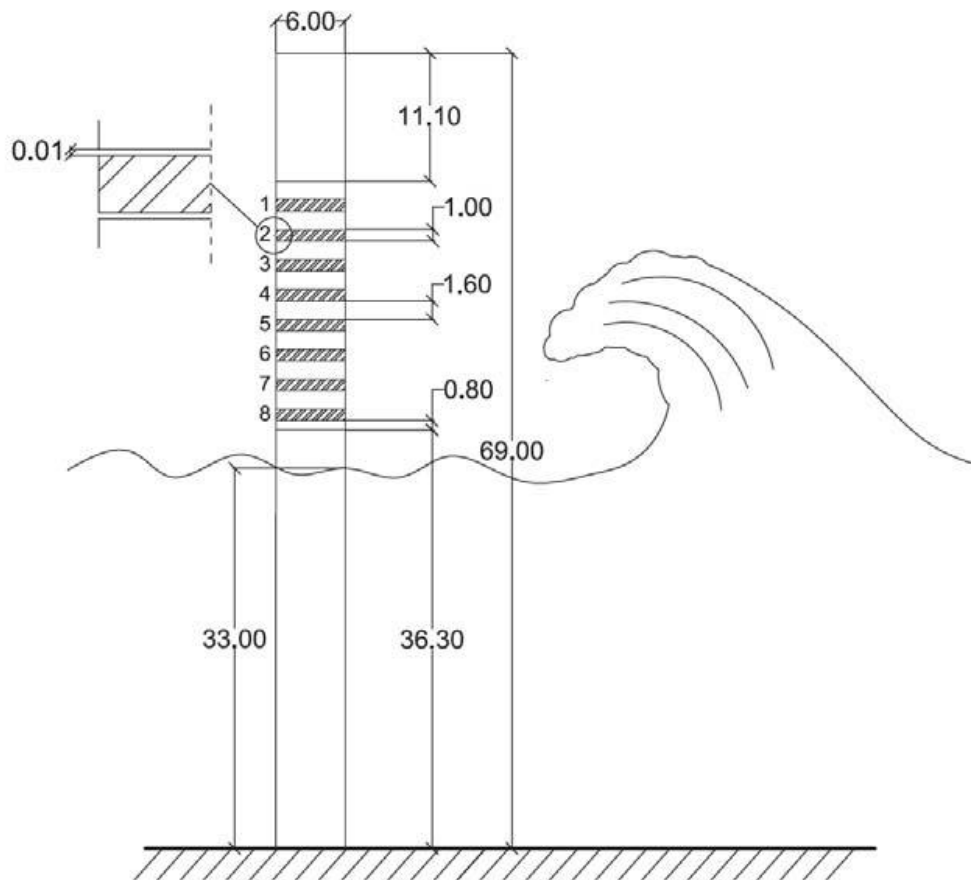
Figure 2.4: Instrumented cylinder [cm]. (Tørum, 2013)

The C_s values were found by considering the maximum impact force at the third transducer. It should be noted that the impact duration time was set as 0.008s for all the cases, which was defined at the same time as the triangular load.

Another experiment was carried out by Aune (2011) as part of his master's thesis and he calculated a C_s value of 4.77. But, in this experiment was performed on a truss structure.

Wienke and Oumeraci (2005) obtained a time history of the impact line force. This is shown in Figure 2.5. This shows that the value of the line force at the beginning of the impact (t=0), i.e. the maximum line force that is calculated by their proposed model is equal to the value obtained from the Wagner's model.
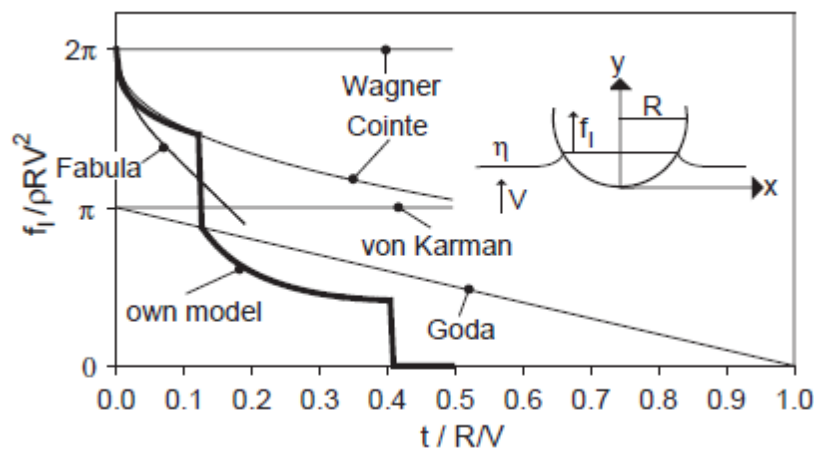
Figure 2.5: Time histories of line forces according to different theories (Wienke & Oumeraci, 2005)

2.4　Curling Factor

Wienke and Oumeraci (2005) investigated about the curling factor for the vertical and inclined cylinders. The ratio of the impact force F_s to the line force $f(t)$ provides the height area of the impact η_b, where η_b is the maximum surface elevation of the breaking wave and the λ is the curling factor. Figure 2.6 shows the variation of the cylinder factor with the different inclination of the cylinder, i.e. yaw angle α.

For a vertical cylinder, the maximum curling factor is $\lambda=0.46$ and this is in agreement with the values of curling factors cited in literature, for example, Goda, et. al. (1966) proposed a range of curling factors $\lambda=0.4$-0.5 for plunging wave breakers.
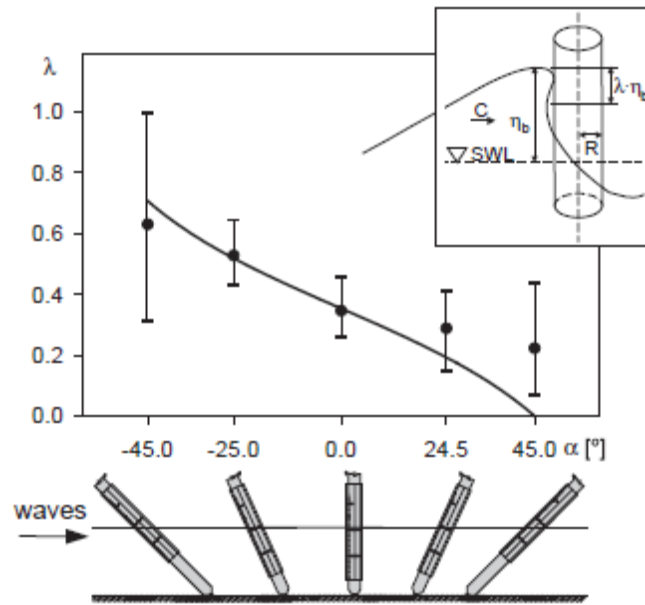
Figure 2.6: Curling factor for different inclination of the pile (Wienke & Oumeraci, 2005)

2.5 Breaking Waves

Waves breaking process is taken place in various different ways depending on the wave properties and angle of bed slope (Judith & Marcel, 2012). Battjes (1974) showed that the Iribarren parameter influences in the wave breaking process. The Iribarren parameter is difined as follows,

$$\xi_0 = \frac{\tan \alpha}{\sqrt{H_0/L_0}}$$

(2.13)

where, $\tan \alpha$ is the steepness of the bed, H_0 is the deep water wave height and L_0 is the wave length in deep water.

The Iribarren number ξ_0 represents the ratio of the slope of the bed and the deep water wave steepness. A distinction is made between spilling, plunging, collapsing and surging breakers based on the value of ξ_0 (Figure 2.7). The values of Iribarren number are indicative and the transition between the various breaker types is gradual. Spilling breakers are generally found along the flat bed. Plunging breaking occurs on a mild slope bed and the curling top is characteristic of such a wave. When the curling top breaks over the lower part of the wave, a lot of energy is dissipated into turbulence.
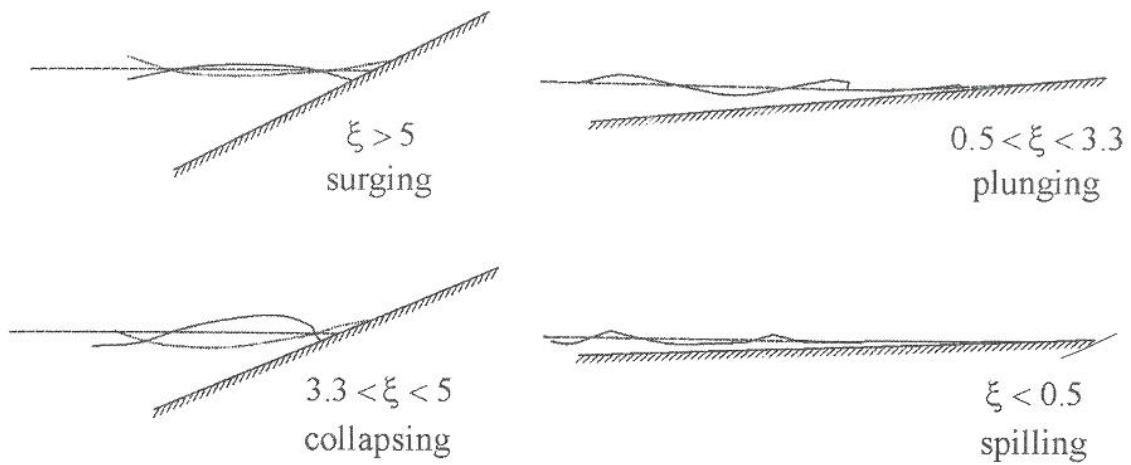
Figure 2.7: Breaker types based on Iribarren parameter (Judith & Marcel, 2012)

3.0 MATERIALS AND METHODOLOGY

Since this research project is a laboratory experimental study, there were several laboratory instruments used to perform the experiments. This chapter is starting with describing all the laboratory devices and materials used for the experiments and later sections describe how the test were carried out, how the data were recorded and finally the detailed description of the data analysing methods with their theoretical background.

3.1 Wave Flume

The wave flume in which all the experiments were carried out was so-called, 'Sjøfrid' at the hydrodynamic laboratory, NTNU, Trondheim. This flume is 33m long, 1m wide and 1.8m deep. There is a hydraulically driven (piston-type wave maker) wave generator with paddles which move back and forth. Normally the input parameters of the wave generators are the wave period (or frequency) and the eccentricity. The eccentricity is related with the displacement of the flap. Wave heights are dependent on this eccentricity and the frequency of the waves and the variation of the wave height with the eccentricity for different wave period is discussed in the section 5.1. The detail cross section and the plan view of this wave flume is given in the Figure 3.2. There are wave absorbers placed at the rear end of the flume and they are made out of perforated steel plates. These wave absorbers are used to prevent the disturbance of the reflecting waves.

The deep water part of the flume is about 11.2m and shallow water was achieved by constructing of a 1:10 slope wooden ramp as shown in Figure 3.2. This 1:10 slope was later modified to 1:20 to get the spilling breaker and this will be discussed in section 4.2.4. The water depth at the structure is about 33.3cm. All the experiments carried out in this flume were regular waves.

Figure 3.1: Wave flume at hydrodynamics laboratory, NTNU
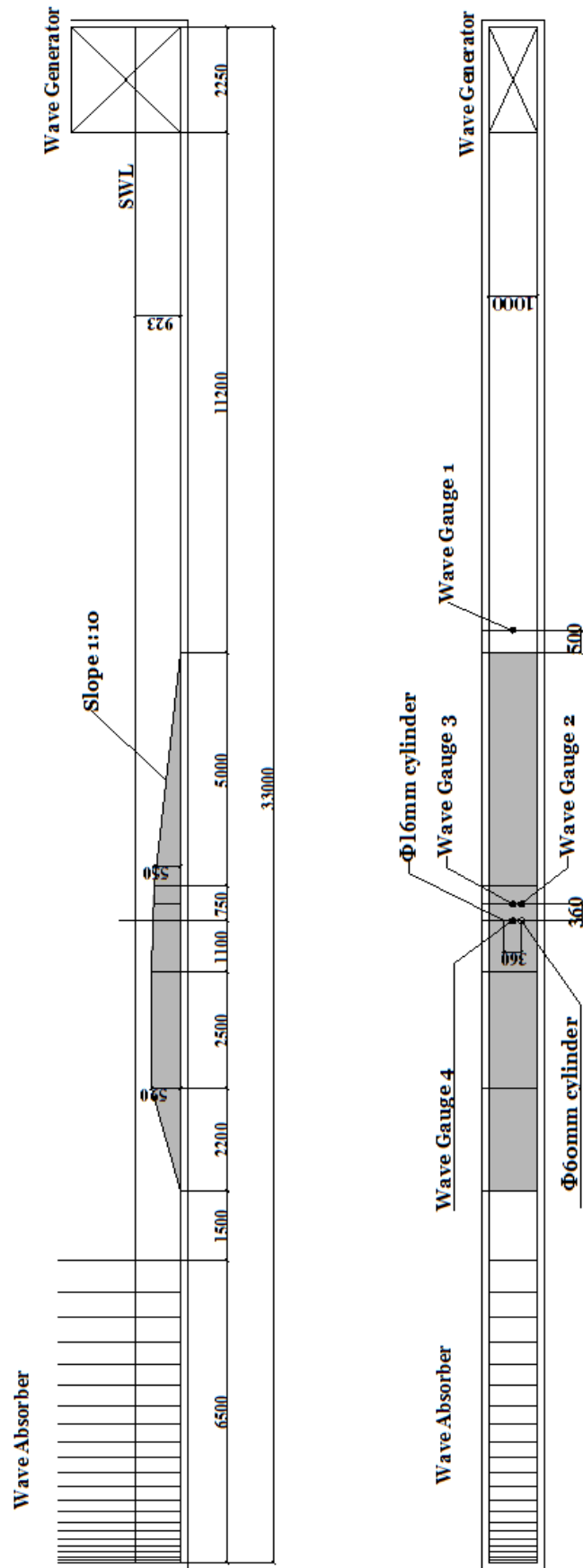
Figure 3.2: Cross-section and plan view of the wave flume [mm]
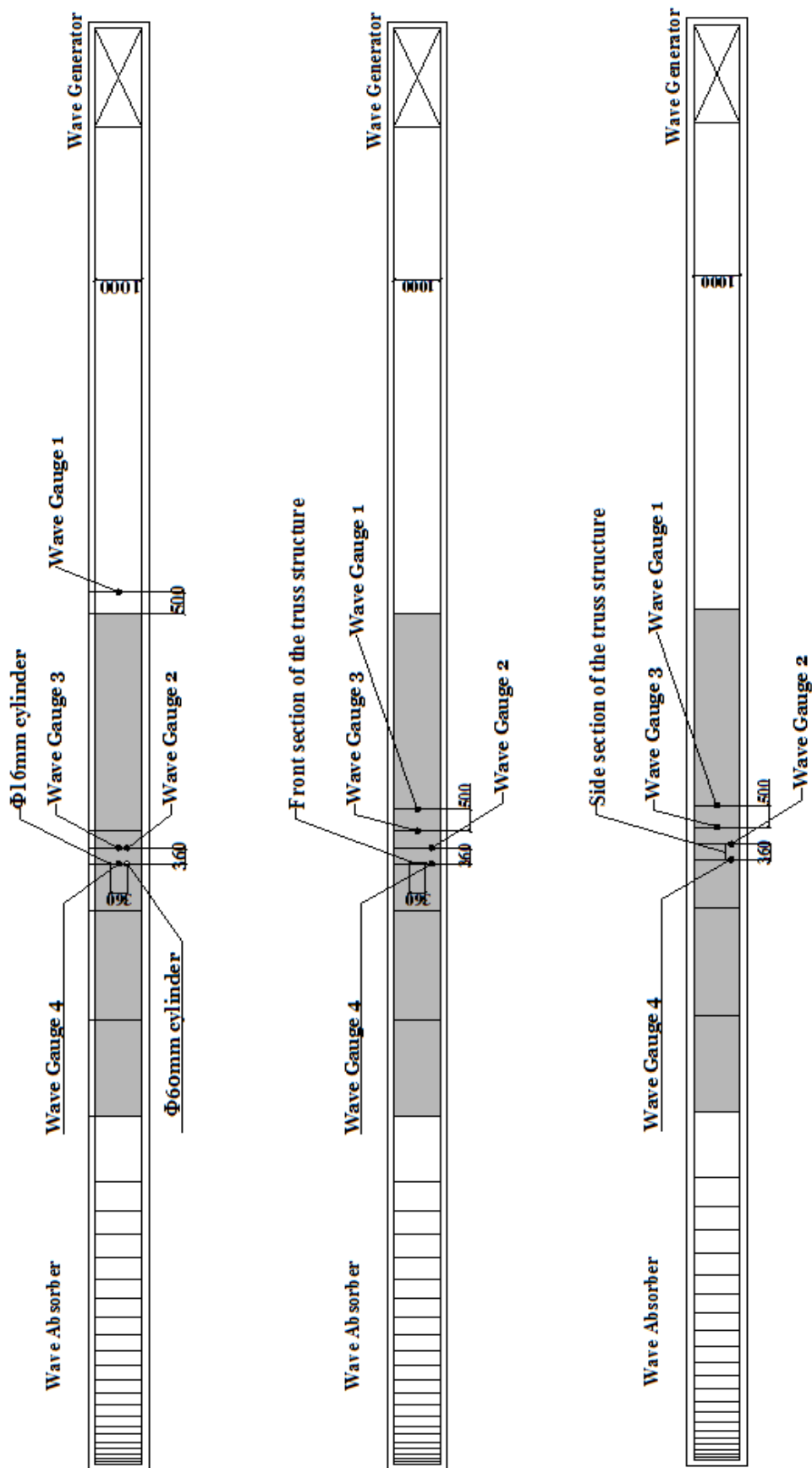
Figure 3.3: Wave gauge positions for different model structures [mm]

3.2 Wave Gauges

There were four wave gauges used throughout the experiments but their positions were changed according to the interest (Figure 3.3). These wave gauges are made out of steel tubes and it measures the water level as the immersed depth is proportional to the output voltage of the wave gauges. Normally theses wave gauges had to be calibrated before running the waves if the water level changed or refilled the wave flume.

Generally the calibration of the wave gauges were done by lifting or lowering the wave gauges and adjusting the voltages based on the heights so that 20cm of water level height corresponds to 10V (20cm = 10V). Since the maximum voltage that can be handled by the amplifier is 10V per channel, we had to be very careful with the height of the wave from the still water line so that it wouldn't exceed 20cm from the still water line. There were certain cases in the later part of the experiments where the level exceeded 20cm so it had to be again calibrated with a different gain factor, i.e. 20cm=5V (4cm/V). The Figure 3.4 shows one wave gauge that was used in the experiment.

Figure 3.4: A picture of a wave gauge used in the experiment

3.3 Force Transducers

There were four force transducers in operation throughout the tests. These transducers were used to measure the dynamic response forces of the structures; this response forces can be tensile or compressive forces. These are HBM S9M/500N transducers which are S-shaped and the maximum force that can be measured is 500N. Although they were calibrated in the factory, re-calibration was done with 3 different weights such as 0.5,1 and 2kgs. Figure 3.5 shows one of the force transducers used in this experiment.
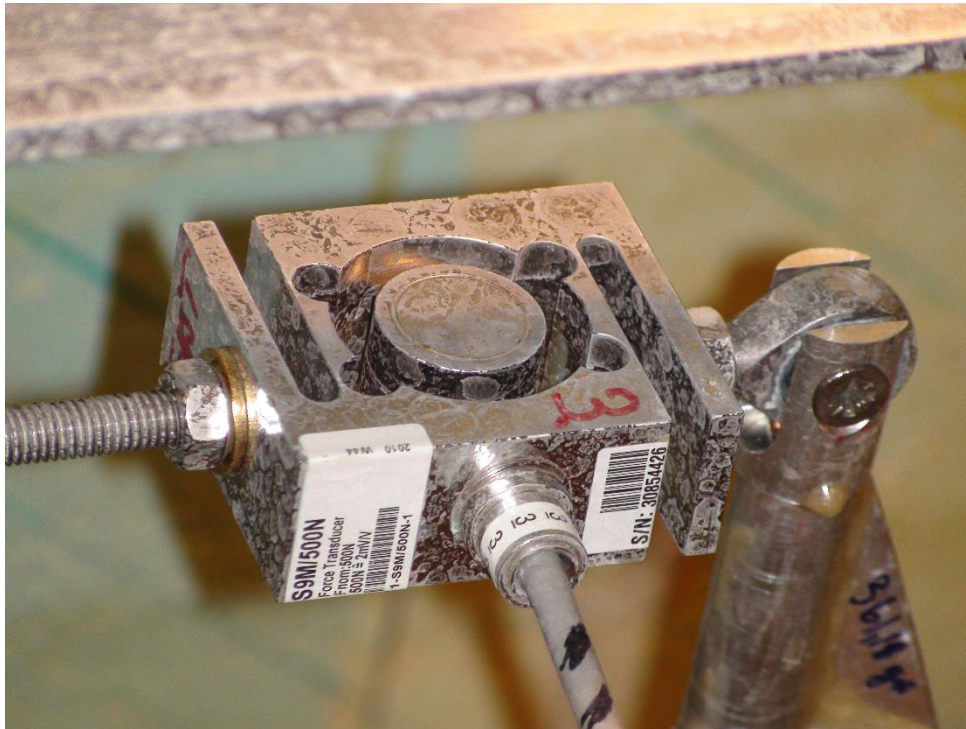
Figure 3.5: A picture of a force transducer used in the experiments

3.4 Impulse Hammer

An impulse hammer was used to find the natural frequency of the structure and importantly to formulate the transfer function in order to obtain the wave slamming force. This procedure will be described in detail in chapter 4.1. Figure 3.6 shows the physical appearance of this impulse hammer and its dimension drawing is shown in Figure 3.7. This hammer has three impacts tips which are made out of three different materials such as aluminium, plastic and soft plastic. Soft plastic tip was the one which was used in all the tests as it gives the clean impact signal for our structures. The maximum impact force that can be measured by this impulse hammer is about 453N (1000lbs).

Figure 3.6: A picture of an impulse hammer used in the experiments
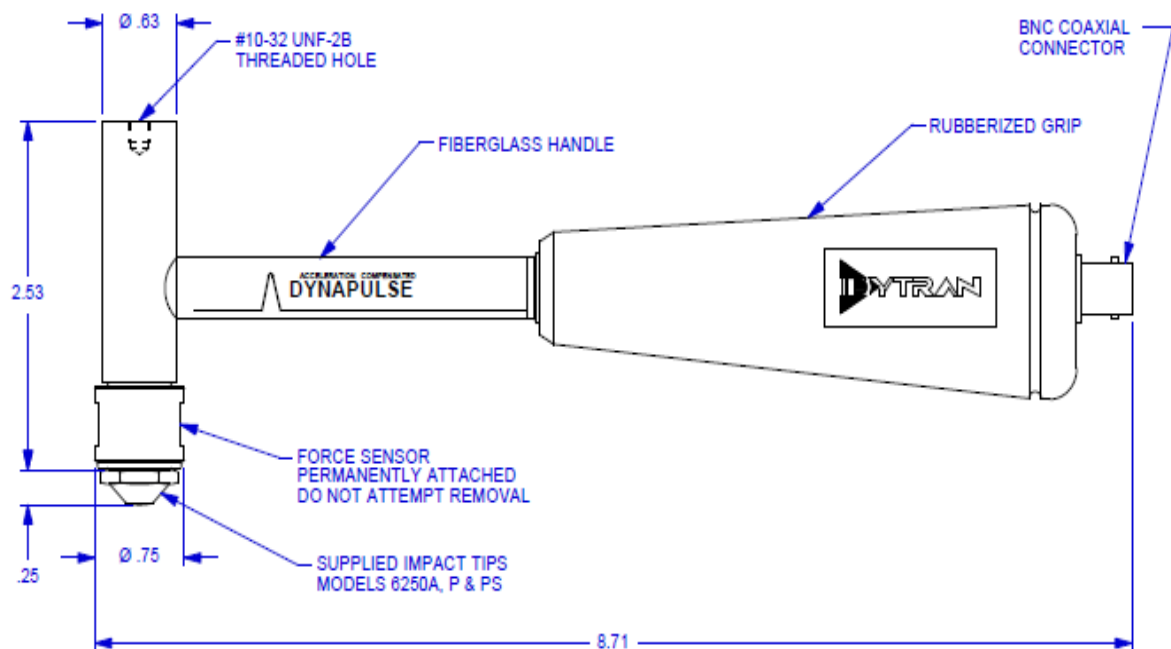
Figure 3.7: Physical dimensions of the impulse hammer [in] (Dytran, 2013)

3.5   Instrumented Structures

Four different types of structures have been used for this experiments; a 16mm diameter cylinder, a 60mm diameter cylinder, front panel of the truss structure and side panel of the truss structure. As shown in the Figure 3.9, both the cylinders and the side panel structures are instrumented with two force transducers each, one is on top and another one on bottom. The front panel of the truss structure has four transducers which are connected on the top and bottom of both the legs. All these model structures are made out of aluminium and they are hollow tubes. The vertical legs of the front and side panel of the truss structures are 16mm in diameter and cross bracings are 12mm in diameter.
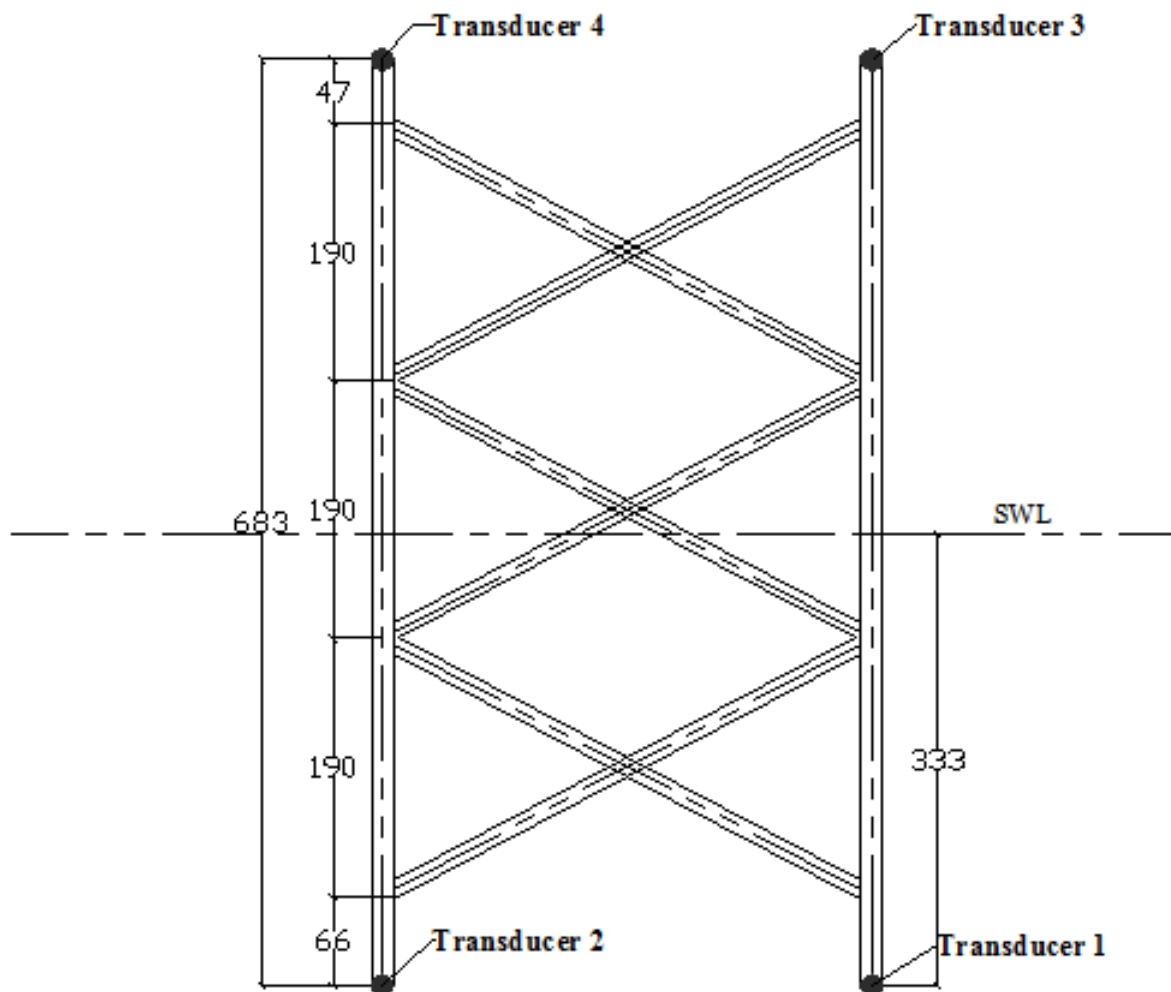
Figure 3.8: Truss structure with dimensions [mm]
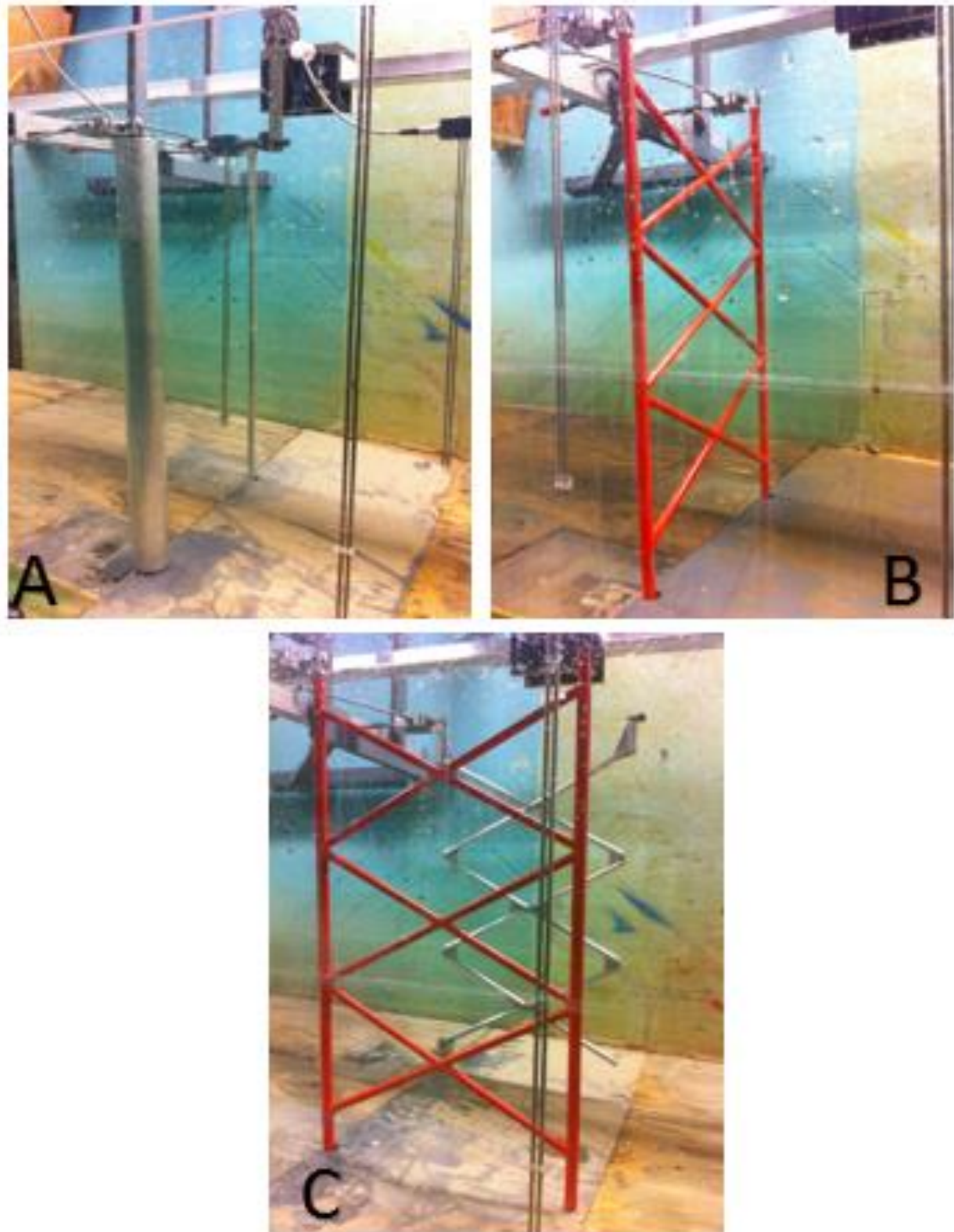
Figure 3.9: Two individual cylinders (A), front section of the truss structure (B) and side section of the truss structure (C)

3.6   Amplifier System

All the actions due to waves give analogue signals to relevant measuring instruments such as wave gauges and force transducers. These analogue signals have to be converted to digital signal in order to get required data. So, an amplifier system or an analogue-digital convertor must be employed; HBM MGCplus amplifier system (Figure 3.10) has been used throughout the tests. This amplifier system is not just for converting signals but also it plays an important role on DAQ (Data Acquisition). For the data acquisition, a software called 'Catman Easy' was used. This software is more user friendly and we can visualize the real time recordings with higher sampling rates.

Figure 3.10: HBM MGCplus amplifier system

3.7   Test Procedure

Large number of tests have been carried out in order to investigate the wave slamming effects. As the main objective this research study is to investigate the wave slamming forces on different parts of the truss structure, there were three different tests carried out with different part of structure as well as the impulse hammer tests on the different structures. These three type of tests are as follows,

- Tests with two different size (16mm and 60mm in diameter) cylinders placed at a distance which is exactly equal to the distance between the vertical legs of the truss structure used by Aashamar (2012).
- Tests with front section of the truss structure
- Tests with the side section of the truss structure

Each type consists of many tests for different wave period and eccentricity. APPENDIX A shows the details of tests that have been carried out with different test parameters for each different type of tests respectively.

The main steps involved in these experiments are given below,

- o Fill the wave flume to the required water level (33.3cm above the bed at the structure)
- o Turn on the wave generator system
- o Calibrate the wave gauges and analogue recorder
- o Set the desired eccentricity
- o Input wave parameters to the system
- o Run the waves
- o Record the data

As previously mentioned, another important test is the impulse hammer test. The impulse hammer test was done by hitting each structure at several points close to the area where the wave slamming would occur. Although the exact position of slamming is not known, according to Ros Collados (2011), the wave slamming occurs about 17cm above the still water line which is 33.3cm from the bed. These hammer plucking points for each structure are shown in Figure 3.11. It should be noted that the structure was plucked when it's in the water and the water level must be checked all the time before doing each tests. This is to incorporate the added mass and still water level damping in the tests (Tørum, 2013).
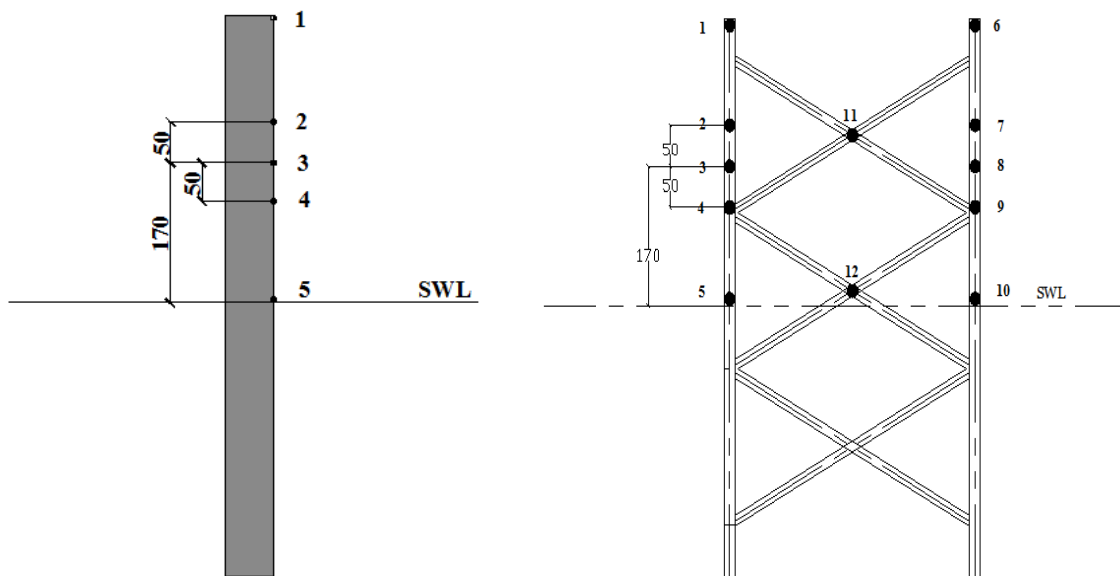
Figure 3.11: Hammer plucking points [mm]

3.7.1   Sampling Frequencies

Sampling frequency means the rate at which the data were recorded. Different sampling frequencies used for different measuring devices such as force transducers, wave gauges and impulse hammer. Table 3.1 shows the sampling frequencies of each devices which were used throughout the experiments.

Table 3.1: Sampling frequencies of different measuring devices

Device	Sampling Frequency [Hz]
Force transducers	19200
Wave gauges	9600
Impulse hammer	9600

Since the sampling frequency of the wave gauges and the impulse hammer are half of the sampling frequency of the force transducers, these both the data have been interpolated so that the sampling frequency of all the data would become 19200Hz.

3.8   Naming of data

Since there were many data recorded it is necessary to name them in an easily understandable way. The explanation of naming for different type of recorded data are mentioned below.

3.8.1   Wave force tests data

The data were named as, for example '*Ue440t185*'

U - Ushanth

e440– Eccentricity 'e'=4.40

t185- Wave period t=1.85s

3.8.2   Impulse hammer data

3.8.2.1   Two individual cylinders
The data were named as, for example '*Uham3*'

U – Ushanth

ham3- hammer point 3

3.8.2.2   Front panel of the truss structure
The data were named as, for example '*Uhamfp3*'

U – Ushanth

hamfp3- hammer point 3 for front panel

3.8.2.3   Side panel of the truss structure
The data were named as, for example '*Uhamsp3*'

U – Ushanth

hamsp3- hammer point 3 for side panel

3.9 Data Analysing Methods

A procedure used by Määtänen (1979) to resolve ice forces from measured response forces on structures subjected to moving ice is applicable for wave slamming loads as well (Tørum, 2013). The analysis method that Wienke and Oumeraci (2005) used was deconvolution method which is similar to Duhamel integral method that was used by Ros Collados (2011). These deconvolution and Duhamel integral approaches are more complex for truss structures and have not been used so far for truss structure. So, the method used by Määtänen (1979), Frequency Response Function method was used for both individual cylinders and truss structures. But, Duhamel integral method also used for only individual cylinders in order to compare and check the influence of the analysis methods.

The measured response force *f(t)* could be expanded into Fourier integral and in case of forced vibration will be,

$$f(t) = \frac{1}{2\pi} \int_{-\infty}^{\infty} H(\omega) S_F(\omega) e^{i\omega t} \, d\omega \tag{3.1}$$

Where, *H(ω)* is the frequency response function (FRF) and S(ω) is the linear spectrum of the forcing function. The frequency response function *H(ω)* or the transfer function is a calibration factor which is obtained by the pluck test by impulse hammer at several points as described in section 3.7.

The Fourier transform of equation (3.1) gives,

$$H(\omega) S_F(\omega) = \int_{-\infty}^{\infty} f(t) \, e^{-i\omega t} \, d\omega = S_f(\omega) \tag{3.2}$$

$S_f(\omega)$ is the linear spectrum of the measured signal *f(t)*. So, $S_f(\omega)$ can be solved from this above equation as,

$$S_F(\omega) = \frac{S_f(\omega)}{H(\omega)} \tag{3.3}$$

Finally, the Inverse Fourier Transform (IFFT) of the above equation gives the requested wave slamming force.

$$F(t) = \frac{1}{2\pi} \int_{-\infty}^{\infty} \frac{S_f(\omega)}{H(\omega)} \, e^{i\omega t} \, d\omega \tag{3.4}$$

The above equations can easily be solved by computer programs such as Matlab, although they look complicated. In this case Matlab has been used for the calculations and analyses.

3.9.1 Frequency Response Function (FRF)

As previously described, the frequency response function or transfer function was obtained by the pluck test using impulse hammer. Plucking points are shown in Figure 3.11 for each structure. The total response force due to an impact by the impulse hammer can be sum of all the force transducers connected to the structure assuming structure responding based on single degree of freedom (SDOF) which is explained in chapter 3.10 in detail. The impact force is directly measured by the impulse hammer. So, the ratio of the power spectrum of impulse force to the response forces gives the transfer function or the frequency response function.

So, frequency response function is now,

$$H(\omega) = \frac{S_{Total,hammer}(\omega)}{S_{Hammer}(\omega)} \tag{3.5}$$

Where, $S_{Total,hammer}(\omega)$ is the fast Fourier transform of the total response forces (power spectrum) obtained by summing up all the transducer forces due to the impact by the hammer and $S_{Hammer}(\omega)$ is the fast Fourier transform of the impact measurement obtained directly from hammer.

$$S_{Total,hammer}(\omega) = \int_{-\infty}^{\infty} f_{Total,hammer}(t)\, e^{-i\omega t}\, dt \tag{3.6}$$

And,

$$S_{Hammer}(\omega) = \int_{-\infty}^{\infty} f_{Hammer}(t)\, e^{-i\omega t}\, dt \tag{3.7}$$

The frequency response function $H(\omega)$ is counter checked by multiplying it by $S_{Hammer}(\omega)$, this should be equal to $S_{Total,hammer}(\omega)$. So both the spectrum were checked in order to make sure it has been done correctly.

3.9.2 Duhamel Integral Method

Duhamel integral approach has been used only for cylinder structures to compare with the results with the FRF method. The theoretical description of the Duhamel integral method is briefly described in this chapter. This method was used by Ros Collados (2011) in his master's thesis.
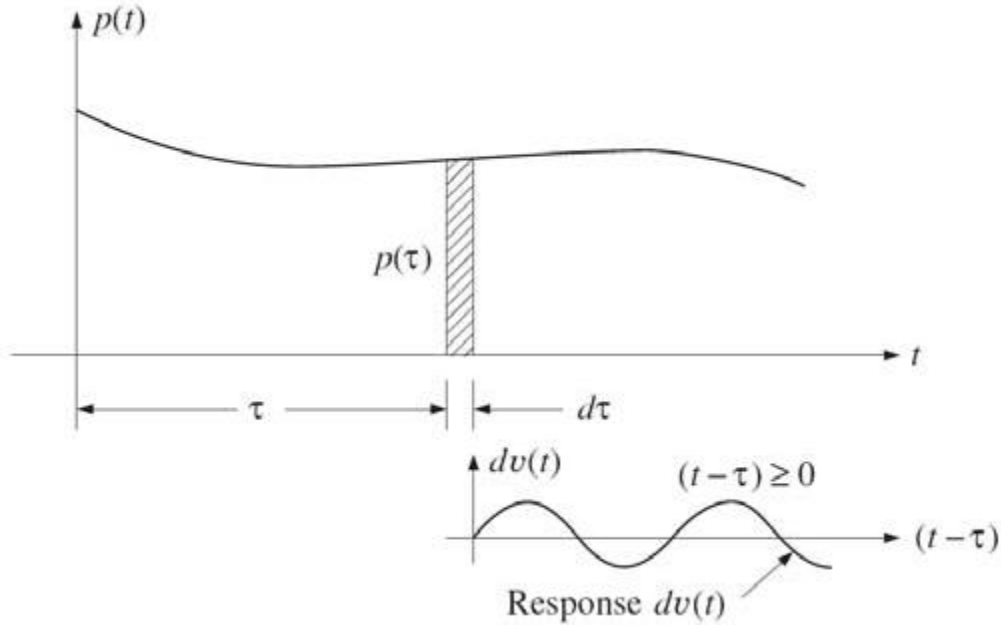
Figure 3.12: The derivation of the Duhamel integral (Ros Collados, 2011)

The above figure (Figure 3.12) shows the differential response for a given impact $p(\tau)$. The total calculated response can be obtained by integrating all the differential responses developed during the loading history (Ros Collados, 2011).

$$R_c(t) = \frac{k}{m\omega_d} \int_0^t p(\tau)sin\omega_d(t-\tau)e^{-\xi\omega(t-\tau)}d\tau \qquad (3.8)$$

Where, m is the oscillating mass, ω_d is the damped frequency of oscillation, $p(\tau)$ is the impact load applied for very short time τ and ξ is the damping coefficient and t is the time. It should be noticed that for small values of damping $\omega \approx \omega_d$. Equation (3.8) is called as Duhamel integral equation and this is being used to estimate the response of an undamped single degree of freedom (SDOF) system subject to any form of dynamic loading $p(\tau)$. This equation can be simplified and written as follows (Clough & Penzien, 1975)

$$R_c(t) = A(t) \sin \omega_d t - B(t) \cos \omega_d t \qquad (3.9)$$

where,

$$A(t) = \frac{k}{m\omega_d} \int_0^t p(\tau) \frac{e^{\xi\omega\tau}}{e^{\xi\omega t}} \cos \omega_d\tau \; d\tau \qquad (3.10)$$

$$B(t) = \frac{k}{m\omega_d} \int_0^t p(\tau) \frac{e^{\xi\omega\tau}}{e^{\xi\omega t}} \sin \omega_d\tau \; d\tau \qquad (3.11)$$

The incremental summation procedure can be used to evaluate the above given integral equations. The equation (3.10) can be written as below in order to describe the exponential decay behaviour caused by damping. This is an approximate recursive form using simple summation.

$$A_N \approx A_{N-1}e^{-\xi\omega\Delta\tau} + \frac{\Delta\tau\, k}{m\omega_d}y_{N-1}e^{-\xi\omega\Delta\tau} \quad, N = 1,2,3, \dots \tag{3.12}$$

where, $y_1 = p_1 \cos \omega_d t_1$, $y_2 = p_2 \cos \omega_d t_{2,}$ etc.

The same expressions will be applicable for B_N but, now y_N is in terms of $\sin \omega_d t_N$, i.e. $y_1 = p_1 \sin \omega_d t_1$, $y_2 = p_2 \sin \omega_d t_2$ and so on.

Finally, knowing all the calculated values of A_N and B_N for successive values of N, the corresponding ordinates of the response will be obtained by using equation (3.9).

$$R_{cN} = A_N \sin \omega_d t_N - B_N \cos \omega_d\, t_N \tag{3.13}$$

Although these expressions and procedure look more complex, it can be easy evaluated by the Matlab program. A Matlab code written by Ros Collados (2001) was modified according to the requirement. This code can be found in the APPENDIX B. The main steps involving in this Duhamel integral method is shown in the Figure 3.13. This method was only used for individual cylinders and was not used for truss structure sections.
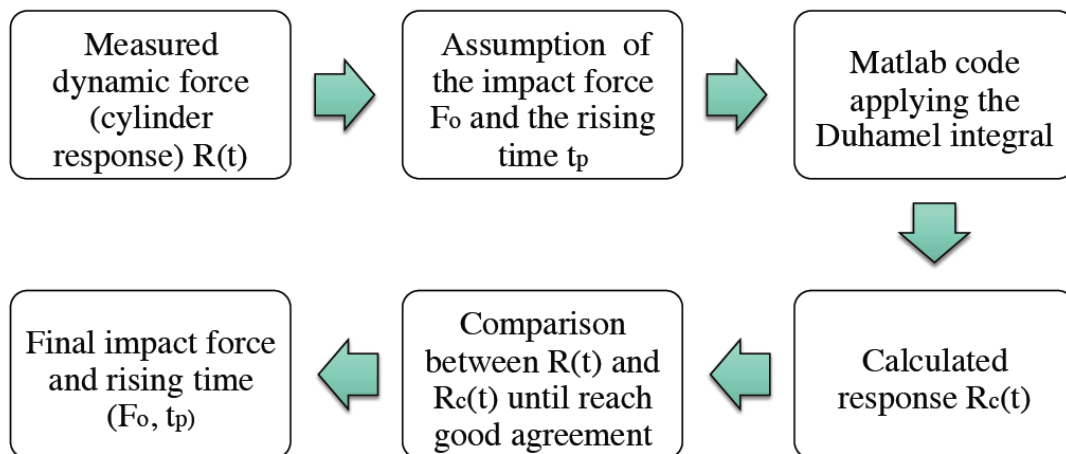
Figure 3.13: Main steps involving in the Duhamel integral approach (Ros Collados, 2011)

This is an iterative process as the assumed impact force and the measured responses should be in good agreement with each other. It means that the measures responses and calculated responses should be coincided with each other or almost geometrically fit on to another for a particular triangular impact force. Once these two responses are in agreement the impact force corresponds to that response will be the wave slamming force. This is illustrated in section 4.2.5 with some results.

3.10 Response Analyses

3.10.1 Single Degree of Freedom (SDOF)

The simplest oscillatory system is single degree of freedom, the motion of which can be described by a single coordinate or in other words vibration response can completely be described by one displacement variable (Naess, 2011). This SDOF system can be either free or forced vibration. The mass, elastic properties (stiffness) and energy loss mechanism or damping are the essential physical properties of linearly elastic structural or mechanic system subject to dynamic loadings. Figure 3.14 shows a principle sketch of a SDOF oscillator with linear damping in which m is the mass of the structure, k is the stiffness, c is the damping constant u is the displacement and $f(t)$ is the externally applied force.
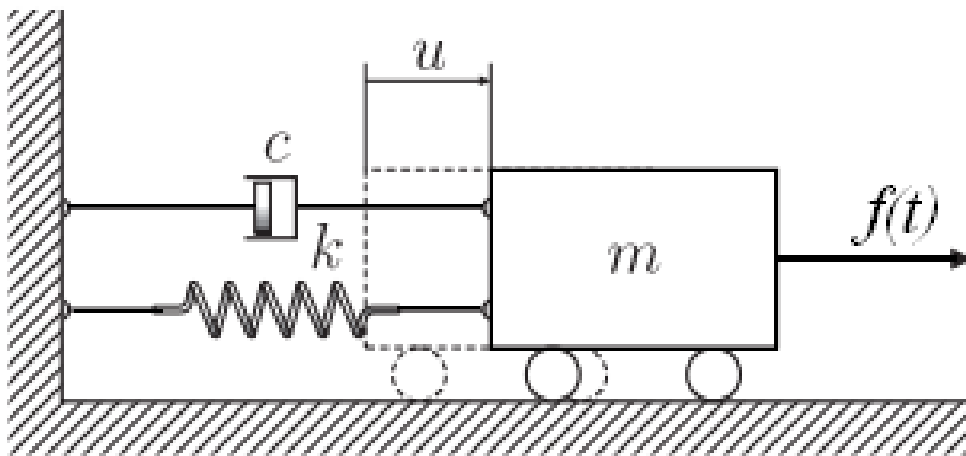
Figure 3.14: Principle sketch of a SDOF oscillator

If we apply the Newton's second law to this system for dynamic equilibrium,

$$m\ddot{u} + c\dot{u} + ku = f(t) \tag{3.14}$$

This is the most general and fundamental equation of the single degree of freedom oscillation. The response $u(t)$ can be obtained by integrating this equation for a particular time period with the applied force.

There are different type of impact loading which can be expressed by simple analytical functions. Some of these impulsive loading types and their behaviours are described in this chapter.

Figure 3.15 shows the maximum response ratio for a suddenly applied constant impact for a limited short time where, u_{max} is the maximum response, f_0 is the impulse load, k is the stiffness, t_* is the duration of impact and T_d is the natural period of oscillation. As it can be seen in this figure, the maximum response ratio increases and reaches a maximum value and this happens when $t_* \approx 0.5T_d$.
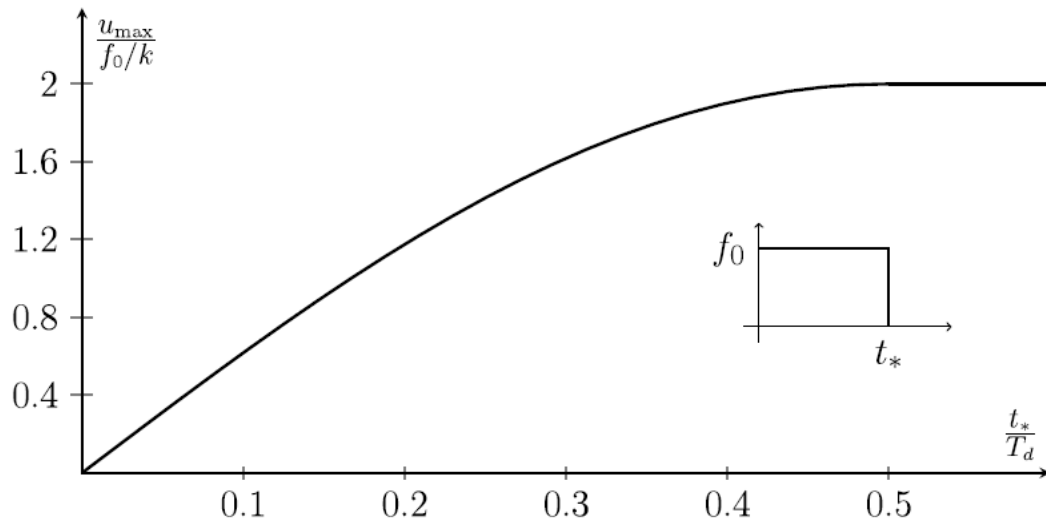
Figure 3.15: The maximum response to a suddenly applied constant force of limited time (Naess, 2011)

Figure 3.16 shows the maximum response for three simple impact force time histories for no damping. It's interesting to see that reduction in the maximum response ratio is insignificant compared to the situation with the previous case for suddenly applied load. Also the maximum response approaches the static value (ratio is about 1 or the maximum response becomes equal to static response f_0/k) when the rise time becomes too long.
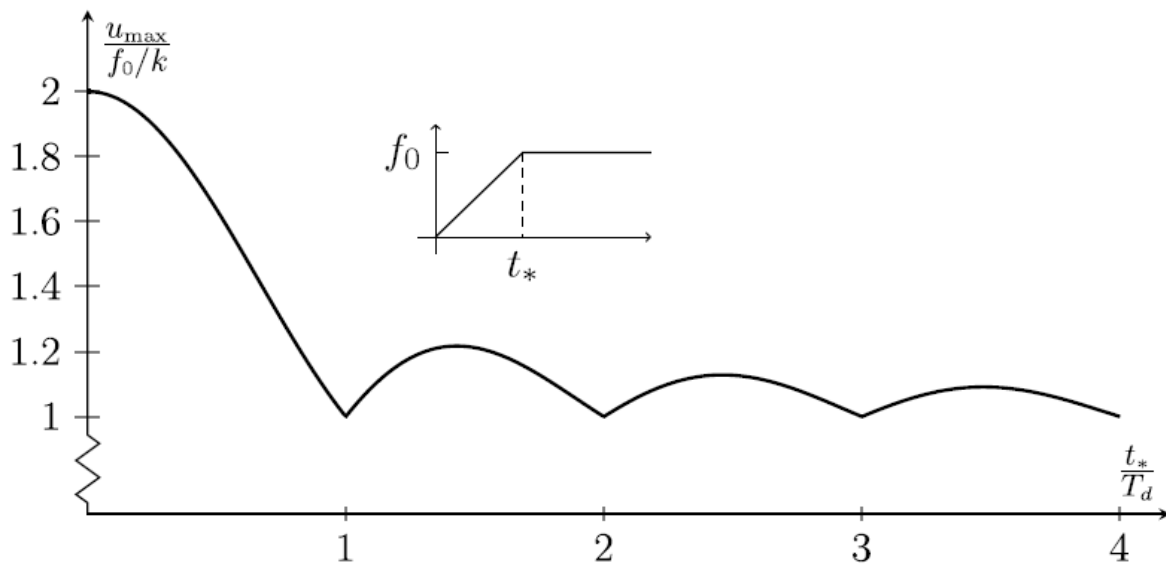
Figure 3.16: The maximum response to a constant force with a finite rise time (Naess, 2011)

The maximum response to a suddenly applied load that decreases linearly towards zero is shown in Figure 3.17. This is comparable with the situation of suddenly applied constant load for a limited period which is shown in Figure 3.15. Since the total triangular load is less than that of rectangular load, triangular load has lower maximum response than that for rectangular load. But, maximum responses to triangular load becomes larger only for larger t_*.

27
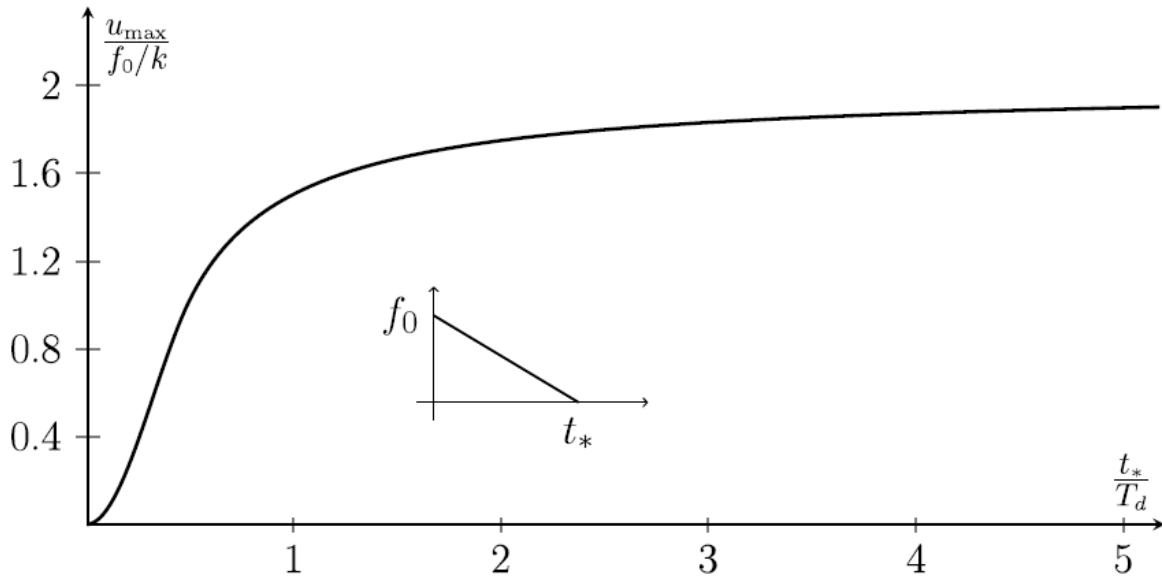
Figure 3.17: The maximum response to a suddenly applied triangular force time history (Naess, 2011)

The maximum response to a 'saw-tooth' pattern loading time history is shown in Figure 3.18. As it can easily be observed in the figure, the maximum response becomes largest when the impact duration is equal to the natural period of oscillation. The maximum response approaches the static value as the impact duration increases.
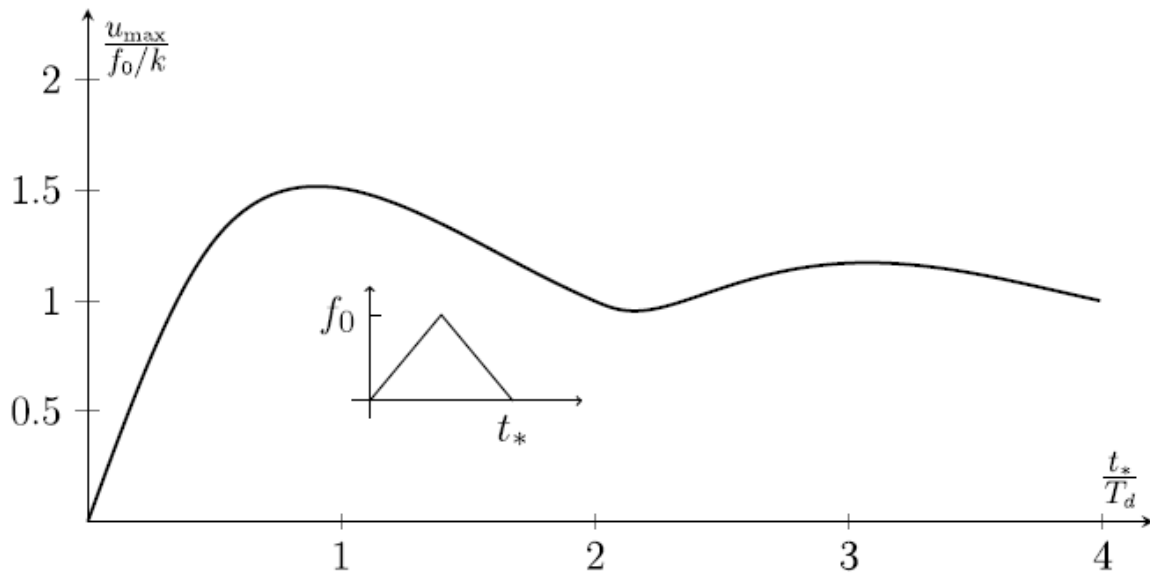
Figure 3.18: The maximum response to a 'saw-tooth' shape force time history (Naess, 2011)

As a summary, Figure 3.19 shows the maximum response ratios to different type of loadings such as rectangular, triangular and half-sinusoidal. Plunging breakers introduce very high

impulsive forces on slender structures in an extremely short duration and the time history of these forces has a clear triangular shape (Ros Collados, 2011).
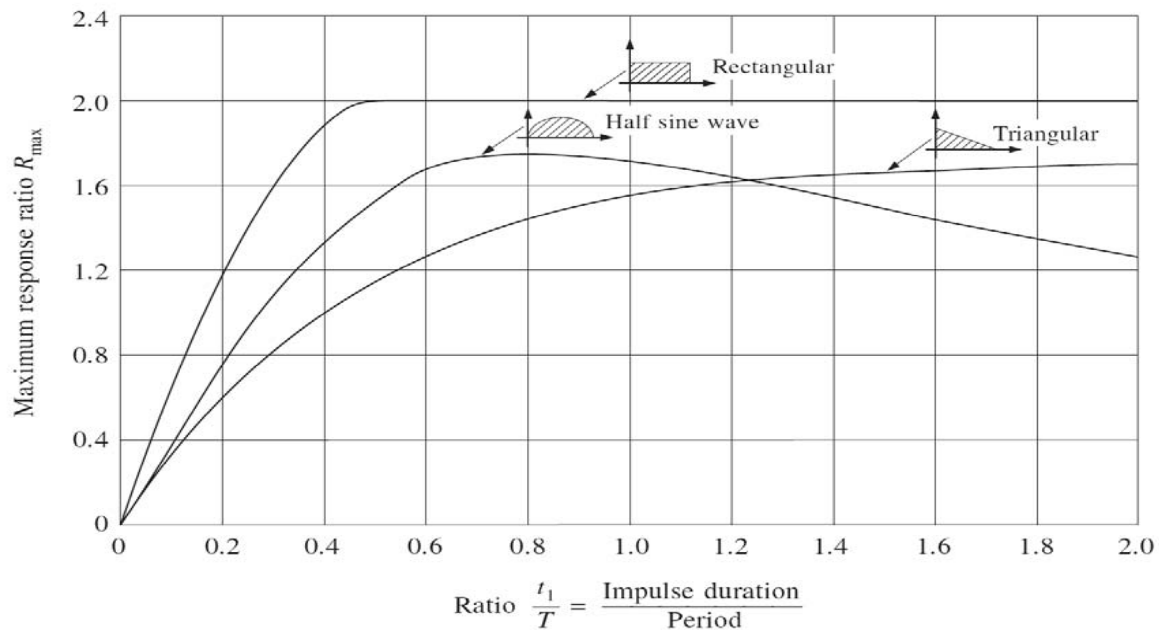
Figure 3.19: Displacement-response spectra (shock spectra) for different types of impulses (Clough & Penzien, 1975)

3.10.2　The Duration of Impact

The duration of impact is an important parameter to know in order to analyse the maximum response ratio. The duration of impact is set differently by different researchers this shown in Table 3.2.

Table 3.2: Duration of impact from different researches

Research Study	Duration of Impact, t_*
von Karman (1929)	$\dfrac{D}{2u}$
Wagner (1932)	$0.4\dfrac{D}{C_b}\ to\ 0.65\dfrac{D}{C_b}$
Goda et. al. (1966)	$\dfrac{1}{2}\dfrac{D}{C_b}$
Tanimoto et. al. (1986)	$\dfrac{1}{4}\dfrac{D}{C_b}\ to\ \dfrac{1}{2}\dfrac{D}{C_b}$
Wienke & Oumeraci (2005)	$\dfrac{13}{64}\dfrac{D}{C_b}$

According to the above table, it can be said that the duration of impact in a range as follows,

$$t_* = (0.25 \ to \ 0.5)\frac{D}{C_b} \tag{3.15}$$

It's advised always to look into the maximum response ratio by assuming a duration of impact and make sure that it follows one particular shape of loading i.e. triangular shape in our case.

4.0   ANALYSIS OF EXPERIMENTAL RESULTS

As mentioned in chapter 3.7, the experiments were carried out for three different types of structures such as two different size vertical piles, front section of the truss structure and side sections of the structure as well as the hammer test. In this chapter, experimental results are presented and they will be analysed.

4.1 Hammer Test and FRF

Hammer tests or the pluck tests were carried out on each structures in order to obtain the transfer function. This section describes well in detail how the obtained hammer test data were analysed and how the transfer function was developed in order to apply them on the wave slamming tests. In this section, only one test which was done for front section of the truss structure has been chosen and illustrate in detail.

As shown in Figure 3.11, pluck tests were performed on several points on the structure, here a test on point number 3 is considered. The time series of the results of the impulse test on point 3 is shown in Figure 4.1.
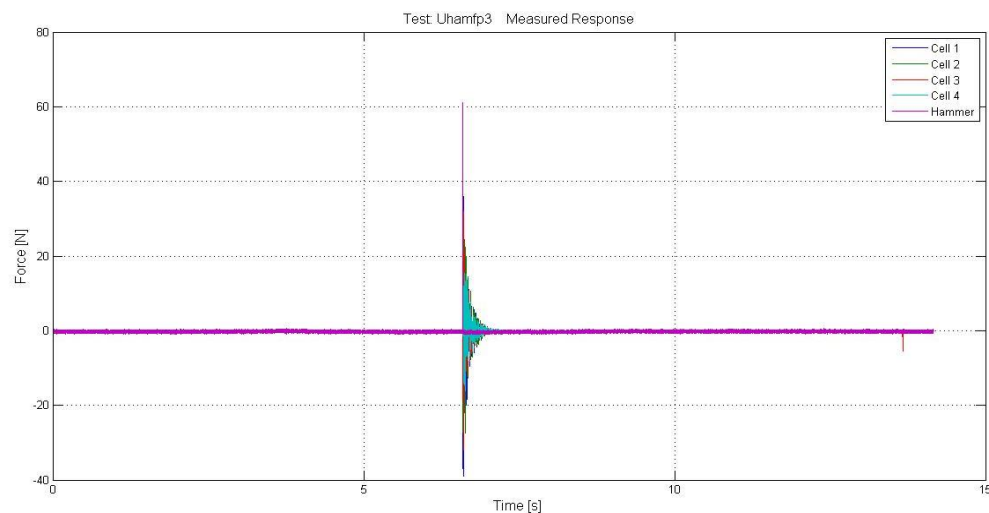
Figure 4.1: Time series of measured response and hammer impulse of 'Uhamfp3' (front section)

The data that will be required only has been extracted out from this series of data and the further analyses were done with this extracted data. In this case total responses will be the sum of all the forces from all four force transducers which were connected at top and bottom of each leg of the front section of the truss structure. Figure 4.2 shows the total responses to the given hammer impact. As it can be seen from this figure, the total response is very high at the time of impact and it decreases towards zero following a damping pattern. The natural period of oscillation is about 0.025s or the natural frequency of the structure is about 40Hz. The impact hammer force is very clean and single peak signal with very short time, this is clearly shown in Figure 4.3.
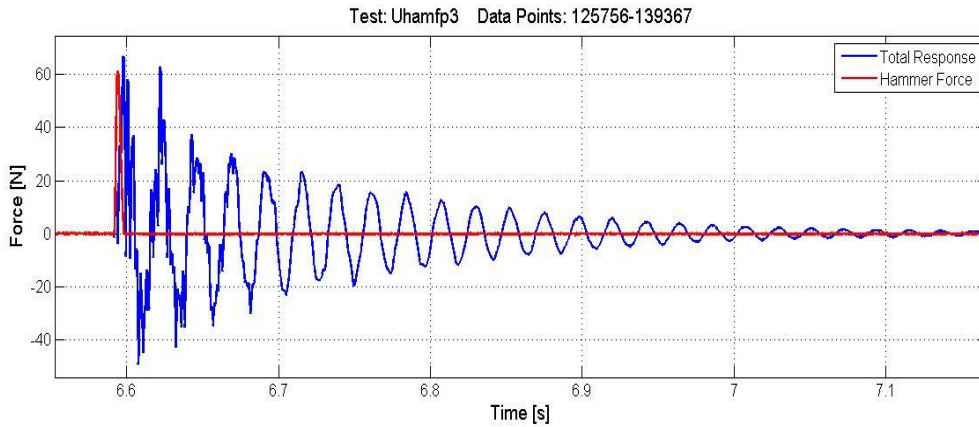
Figure 4.2: Total responses and hammer force of test Uhamfp3 (front section)
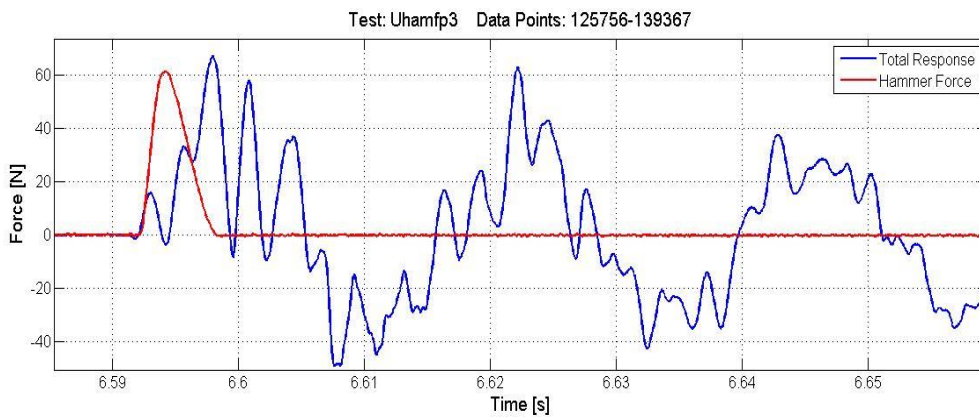
Figure 4.3: Expanded time view of total responses and hammer force of test Uhamfp3 (front section)

Now the power spectrum of both total responses and hammer force are obtained by performing fast Fourier transformations. As it can be seen in Figure 4.4, the peak power of the total response forces is concentrated at a frequency is about 40Hz; this is obviously the natural frequency of the structure. Finally the transfer function is obtained by dividing the spectrum of the total forces by the spectrum of the hammer force, as described by the equation (3.5), Figure 4.5 shows the squared linear transfer function in semi-log scale.
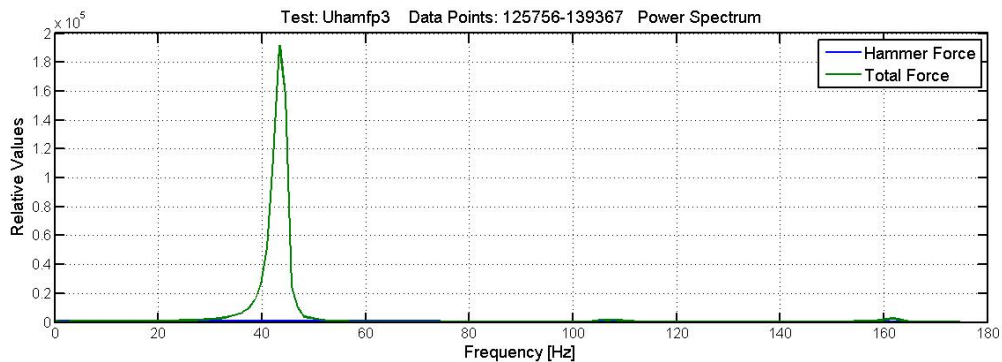
Figure 4.4: Power spectrum of total responses and hammer force of test Uhamfp3 (front section)
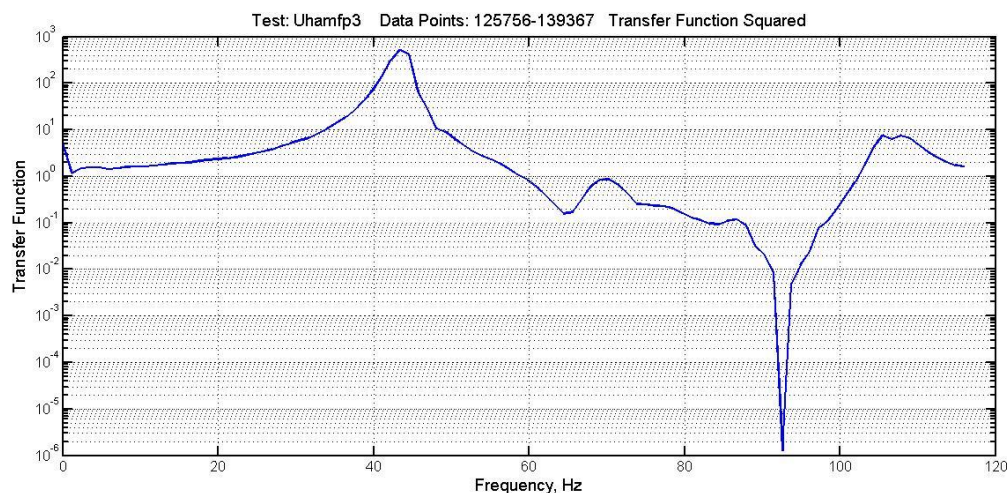
Figure 4.5: Squared linear transfer function in semi-log scale

4.2   Analysis of Wave Tests

4.2.1   Two Individual Cylinders

Two different size cylinders were placed at a distance exactly same as the distance between two vertical legs of the truss structure. The sizes of the individual cylinder are 60mm and 16 mm. Tests were carried out with different period of waves and different heights of waves as well. The test with maximum slamming forces that was obtained in each different period of waves is illustrated here and Table 4.1 shows the maximum slamming forces obtained for different wave period for large cylinder (60mm diameter).

Table 4.1: Maximum slamming forces on 60mm diameter cylinder for different wave periods

e	T [s], f [Hz]			
	1.85s (0.54Hz)	1.96s (0.51Hz)	2.08s (0.48Hz)	2.22s (0.45Hz)
4.6	19.41N			
4.6		25.18N		
4.9			16.2N	
4.9				26.39N

First we look into the test '*Ue460t185*' which gives the maximum slamming force for 1.85s period of waves and the eccentricity of 4.6. Figure 4.6 shows the whole time series of recorded total responses and the wave at the structure. The maximum response is selected for the further analysis and it should be noted that this is not always be the case as sometimes the first two or three waves give the maximum responses, because the data recording started just right after the wave paddles started moving, and the first few waves just break some distance away from the structure and cause much turbulences which results in very high responses.

So, it's always advised to select the maximum responses by looking at the wave which has a clean breaking pattern that has to be complied with the subsequent wave's pattern, because the

waves broken at some distances away from the structure will be very short in height and rather irregular pattern.
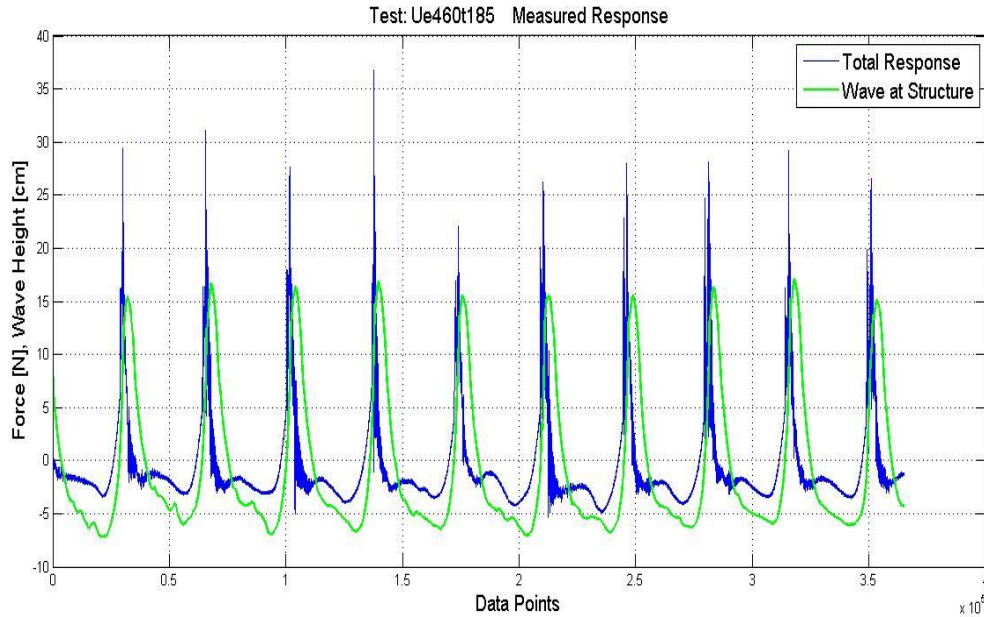
Figure 4.6: Time series of total measured responses and the wave at the structure-Test Ue460t185 (large cylinder)

In this case, the maximum response is obtained for the fourth wave in the recorded time series responses shown in Figure 4.6. This total response is the summation of the forces from top and bottom transducers that are connected to this large cylinder. The desired data are extracted from the whole time series Figure 4.7 shows the individual response forces from each transducers responsible for the maximum total responses. Top transducer give more forces than the bottom as slamming forces or the resultant of the wave forces acting more close to the top transducer than the bottom transducer.
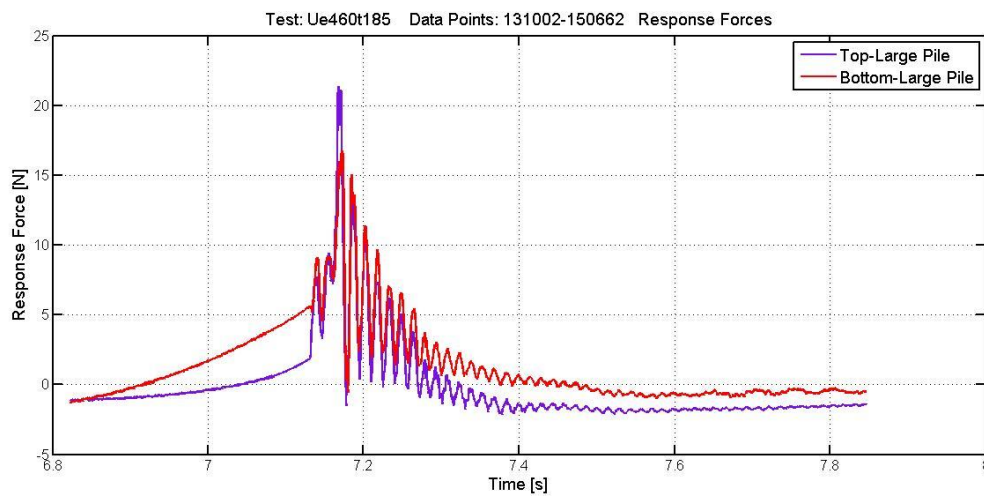
Figure 4.7: Individual response from top and bottom transducers – Test Ue460t185 (large cylinder)

As it can be seen in Figure 4.8, the total response has two small peaks before the highest peak that would probably cause the slamming force. These two small peaks could be because of the tongue of the plunging breakers that hits the structure first and subsequently the major part of the wave hits the structure and cause the highest response force. Also it should be noted in the same figure that there is a very small time lag between the peak response and the wave crest at the structure as this cylinder is large compared to the wave gauge in diameter so wave reaches the cylinder and hits before it reaches the wave gauge.
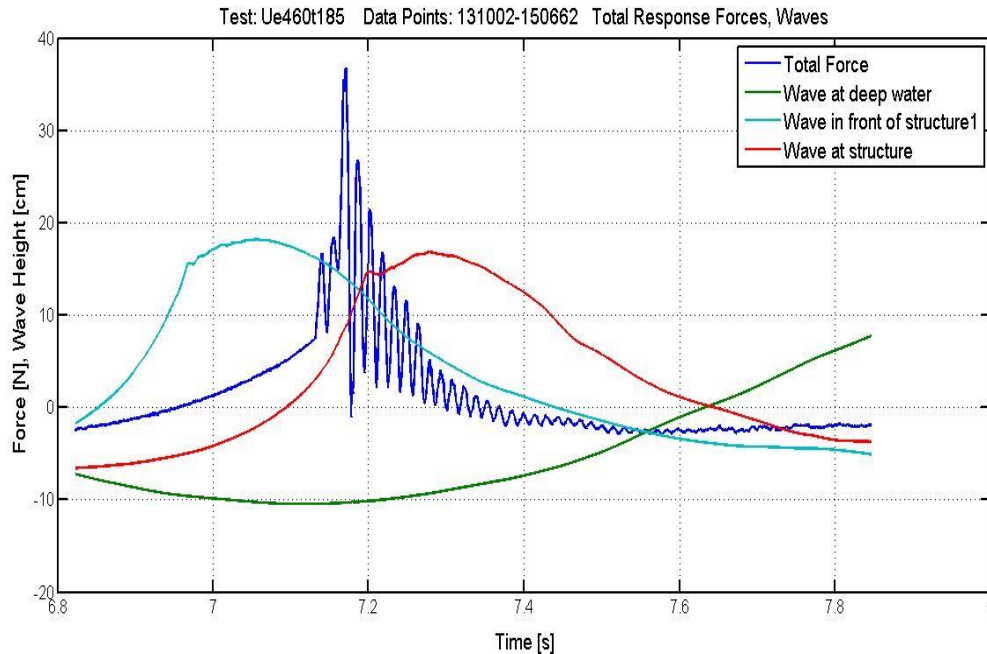
Figure 4.8: Total responses with waves at different points – Test Ue460t185 (large cylinder)

So, now we have the maximum total responses which consists of both hydrostatic and dynamic forces itself. This needs to be decomposed and the slamming forces will be found from the dynamic part of the responses. This can be done by filtering the total responses and the filtered signal is in form of quasi-static force distribution and this quasi static force will be subtracted from the total response forces. Matlab has a function called '*filtfilt*' that does zero phase filtering by filtering the data in forward and reverse direction. In fact this a low pass filtering process too. As it can be seen in Figure 4.9, green line shows the filtered signal of the total responses and that can be called as 'quasi static or hydro static forces'. The red colour line denotes the resultant signal after the subtraction of the quasi static force from the total response forces, which is called as dynamic forces. This dynamic component of the response contributes to the slamming forces.

Once the decomposition of the total forces has been done, we proceed with the dynamic signal and filter it one more time to get even more cleaned dynamic signal. This filtered dynamic signal is used for fast Fourier transform (FFT) to get the power spectrum $S_f(\omega)$ (Figure 4.10).
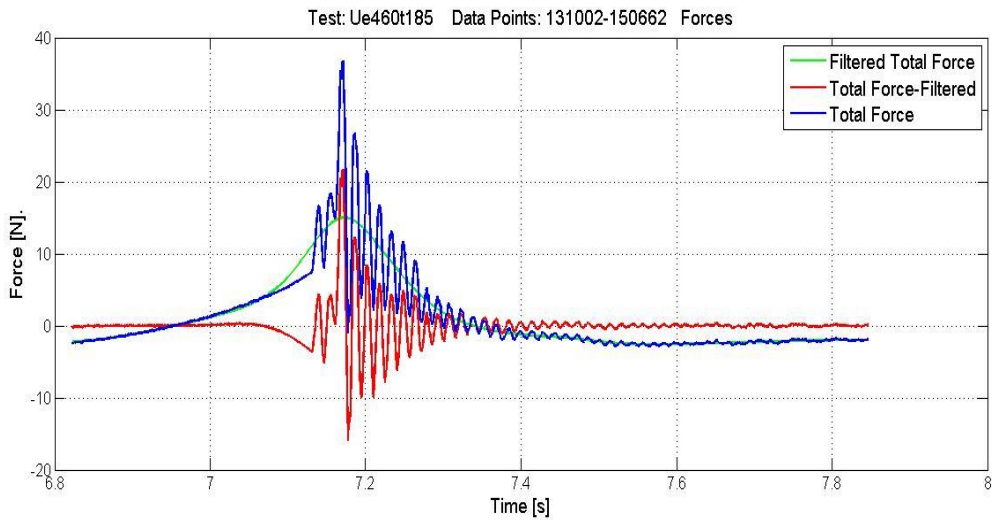
Figure 4.9: The decomposition of the total response forces – Test Ue460t185 (large cylinder)
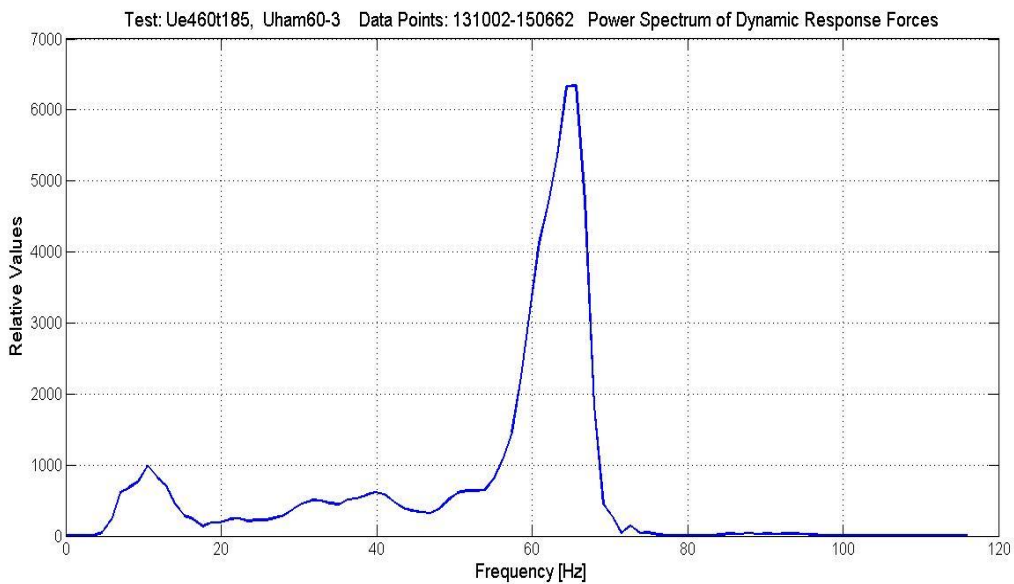
Figure 4.10: Power spectrum of the dynamic response forces – Test Ue460t185 (large cylinder)

The spectrum of the response forces then be divided by the transfer function or the frequency response function which was obtained previously for the same structure. Taking inverse fast Fourier transform (IFFT) and filtering it would give the slamming force according to the equation (3.4).
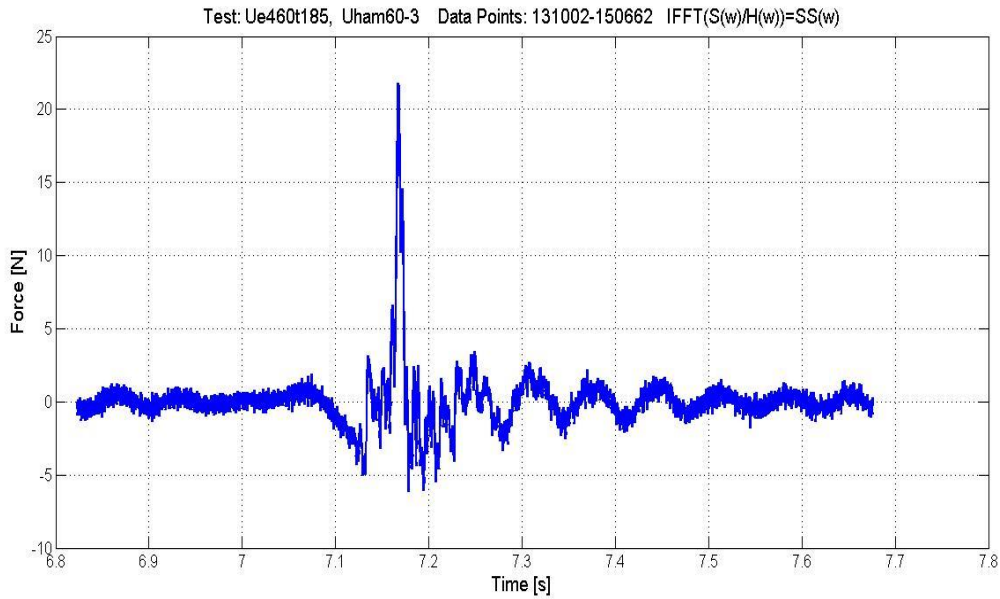
Figure 4.11: Inverse Fast Fourier Transform of $S_f(\omega)/H(\omega)$ – Test Ue460t185 and Uham60_3 (large cylinder)

The unfiltered signal after performing inverse fast Fourier transform is shown in Figure 4.11 and then this is low pass filtered and the final slamming force variation shown in Figure 4.12.
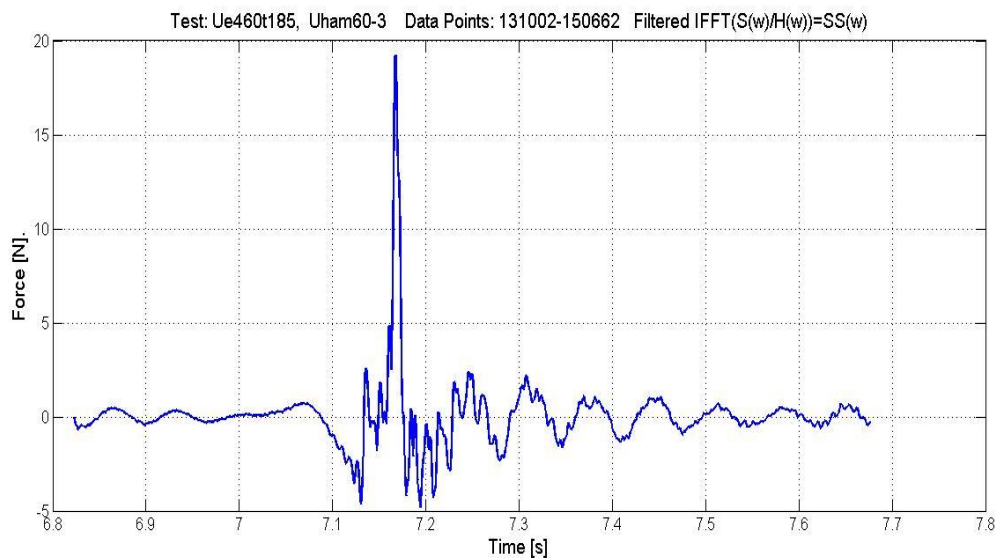
Figure 4.12: Low-pass filtered IFFT of $S_f(\omega)/H(\omega)$ - Test Ue460t185 and Uham60_3 (large cylinder)

4.2.1.1   The calculation of the slamming force

The calculation of the slamming force is based on the following equation,

$$F_s = 0.5\, C_S \rho_w D\, \lambda\, \eta_b C_b^2 \tag{4.1}$$

$$C_b = \sqrt{g(h + \eta_b)} \qquad (4.2)$$

where, , F_s	Total slamming force (*N*)
ρ_w	Density of the water (*1000kg/m³*)
D	Diameter of the vertical leg (*0.016m*)
λ	Curling factor (=0.46 according to Wienkie and Oumeraci, 2005 and 0.4 according to Goda (1966).
η_b	Crest height of the breaking wave
C_b	Celerity of the breaking wave (*m/s*)

The calculated slamming forces according to Wienke and Oumeraci (2005) and Goda, et. al. (1966) are compared with the measured slamming force in Chapter 5. But, here it's tabulated in Table 4.2.

Table 4.2: Measured and calculated slamming forces – Test Ue460t185 (large cylinder)

Maximum response force	**36.67 N**
Measured slamming force	**19.41 N**
Calculated slamming force based on Wienke & Oumeraci (2005)	**71.59 N**
Calculated slamming force based on Goda, et.al., (1966)	**31.13 N**

4.2.2   Front section of the truss structure

The front section or front panel of the model structure was undergone several tests with waves and hammer as we did for the large pile. The analysis method for the tests with the front panel is only frequency response function method.

The slamming forces for each wave period is given in APPENDIX A and the maximum slamming forces were taken out for the illustration. Table 4.3 gives the summary of the maximum wave slamming forces on the front section of the truss structure for different wave periods. Wave period of 2.08s test is chosen here for illustrative purpose. This is test *Ue440t208*.

Table 4.3: Maximum slamming forces on front section of truss structure for different wave periods

e	T [s], f [Hz]			
	1.85s (0.54Hz)	**1.96s (0.51Hz)**	**2.08s (0.48Hz)**	**2.22s (0.45Hz)**
4.4	10.03 N			
4.8		10.15 N		
4.4			13.46 N	
4.8				11.52 N

In this case the total responses will be the summation of all forces from all four transducers. The analysis method is the same as it's done for the large cylinder in the previous section.

Figure 4.13: Snapshot from test 'Ue440t208' (front section)

As it can be seen in the Figure 4.13, the wave breaks just in front of the structure and curling down and hits the structure. It seems that the curling factor must be smaller than what we used for the calculation of the slamming forces based on Wienke and Oumeraci (2005) and Goda (1966).
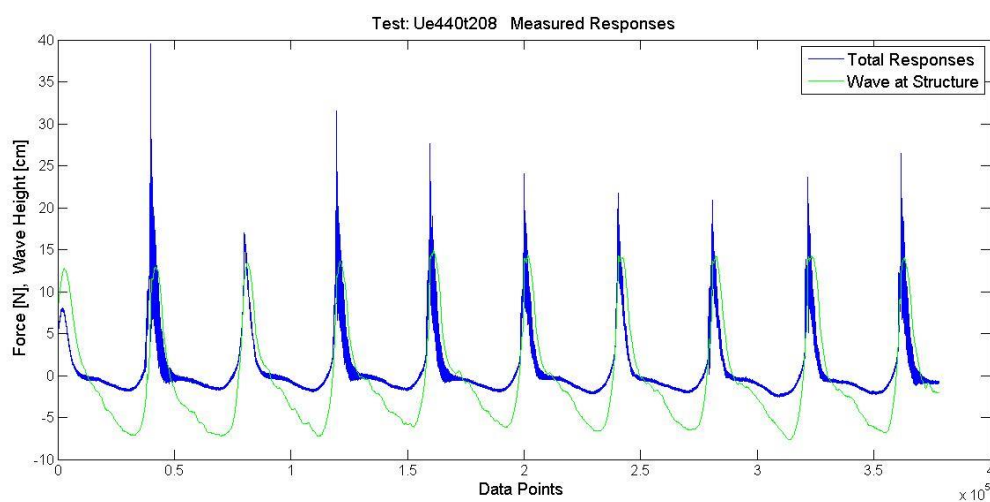
Figure 4.14: Time series of total measured responses and the wave at the structure-Test Ue440t208 (front section)

The desired portion of maximum responses is chosen and that will be analysed in the same way that was used for the large cylinder.
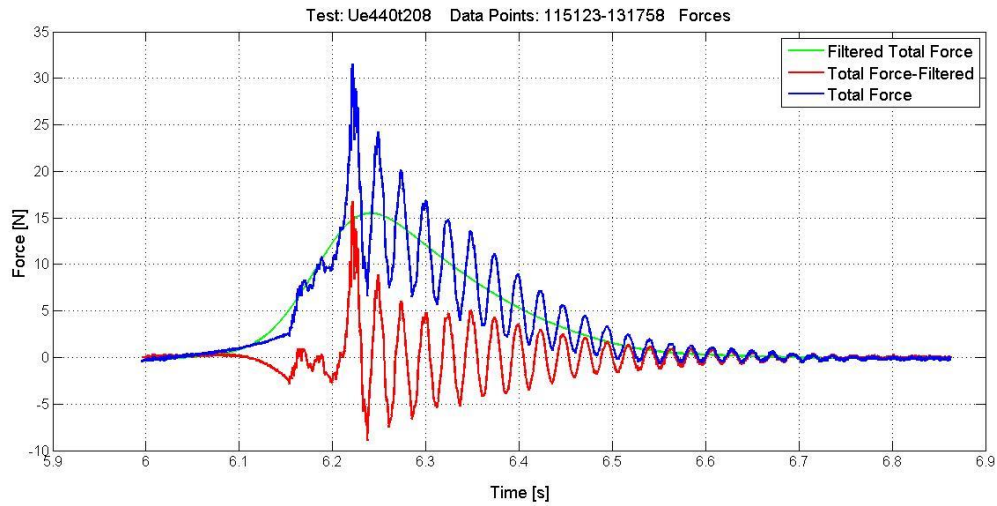
Figure 4.15: The decomposition of the total response forces – Test Ue440t208 (front section)
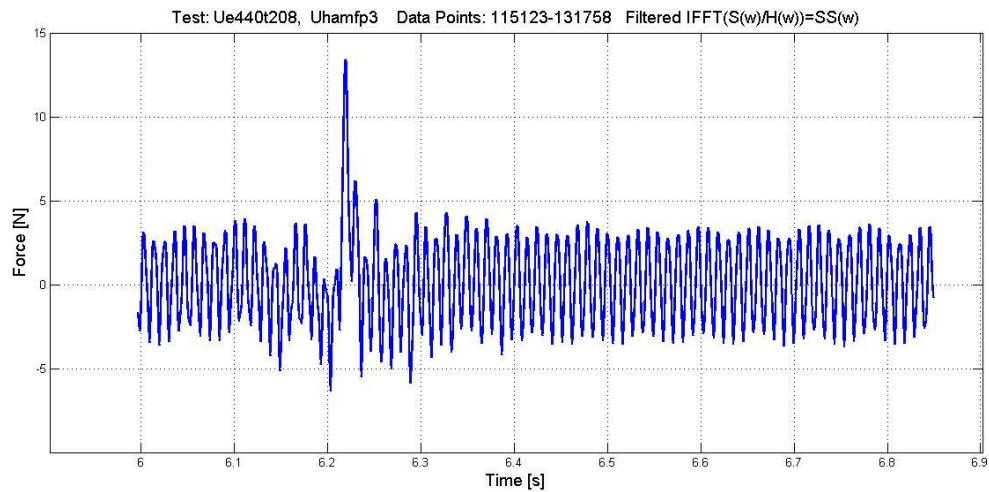
Figure 4.16: Low-pass filtered IFFT of $S_f(\omega)/H(\omega)$ - Test Ue440t185 and Uhamfp3 (front section)
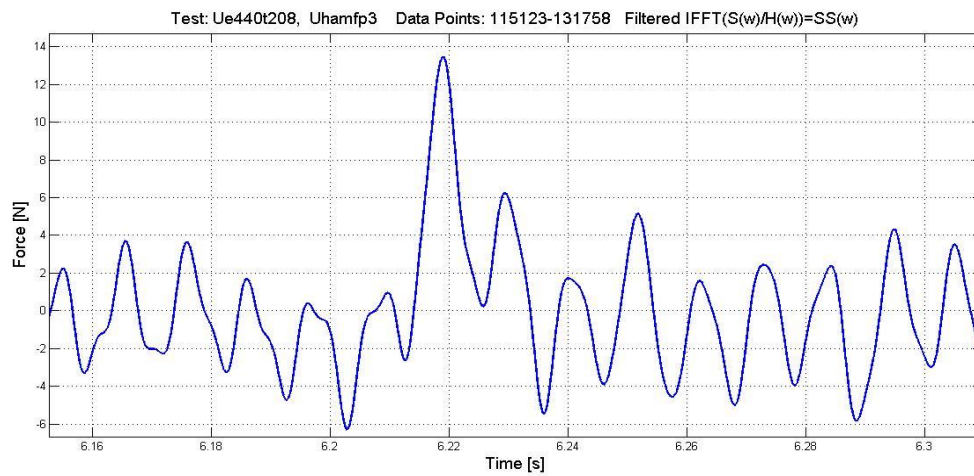
Figure 4.17: Time expanded view of the Low-pass filtered IFFT of $S_f(\omega)/H(\omega)$ - Test Ue440t208 and Uhamfp3 (front section)

4.2.2.1   The calculated slamming force of front section of the truss structure

Unlike the individual cylinder the front section of the truss structure is exposed to slamming forces on different parts of the structure such as vertical legs and cross bracings. So, it's important to take slamming forces on bracing into consideration as well.
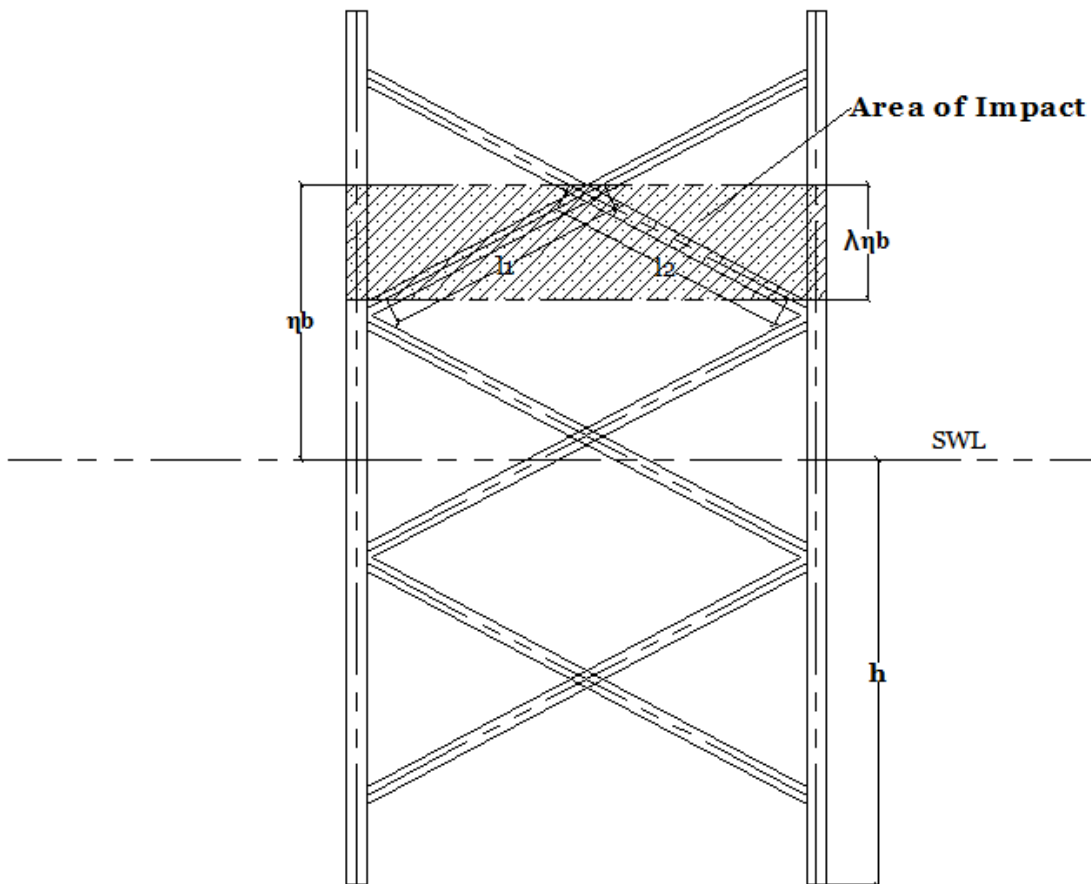
Figure 4.18: Definition sketch of the front section of the structure for slamming force calculation

As shown in Figure 4.18, the total length of the bracing within the impacted area has to be found and incorporated in the wave slamming equation.

$$F_s = 2[0.5\ C_S\rho_w D_1\ \lambda\ \eta_b C_b^2] + 0.5\ C_S\rho_w D_2\ \lambda\ \eta_b C_b^2 l \qquad (4.3)$$

where, F_s Total slamming force (*N*)

   ρ_w Density of the water (*1000kg/m³*)

   D_1 Diameter of the vertical leg (*0.016m*)

   D_1 Diameter of the cross-bracing (*0.012m*)

η_b	Crest height of the breaking wave
C_b	Celerity of the breaking wave (*m/s*)
$l=l_1+l_2$	Total length of the bracing within the area of impact
λ	Curling factor
	$\lambda=0.46$ [Wienke and Oumeraci (2005)]
	$\lambda=0.40$ [Goda, et. al., (1966)]
C_s	Slamming factor
	$C_s= 2\pi$ [Wienke and Oumeraci (2005)]
	$C_s= \pi$ [Goda, et. al., (1966)]

So, the calculated slamming forces for the test *Ue440t208* is tabulated in Table 4.4.

Table 4.4: Measured and calculated slamming forces – Test Ue440t208 (front section)

Maximum response force	**31.54 N**
Measured slamming force	**13.46 N**
Calculated slamming force based on Wienke & Oumeraci (2005)	**77.18 N**
Calculated slamming force based on Goda, et.al., (1966)	**33.56 N**

4.2.3   Side section of the truss structure

Several tests have been carried out on the side section of the truss structure as they done for other structures. This section also describes the analysed results as they have been illustrated for the other structures in the previous sections.

Referring to APPENDIX A, although tests *Ue550t185*, *Ue630t185* and *Ue630t222* give the larger slamming forces than that from test *Ue460t185* and *Ue570t222* from the respective wave periods, the test *Ue460t185* and *Ue570t185* are only taken into consideration here for the illustrative purpose as in other two tests the waves were breaking further away from the structure and caused large amount of turbulence. This will be discussed in the later chapters.

Table 4.5: Maximum slamming forces on side section of truss structure for different wave periods

e	T [s], f [Hz]			
	1.85s (0.54Hz)	**1.96s (0.51Hz)**	**2.08s (0.48Hz)**	**2.22s (0.45Hz)**
4.6	4.05 N			
4.8		3.86 N		
5.0			3.06 N	
5.7				3.91 N

4.2.3.1.1   Test Ue460t185 on Side Section
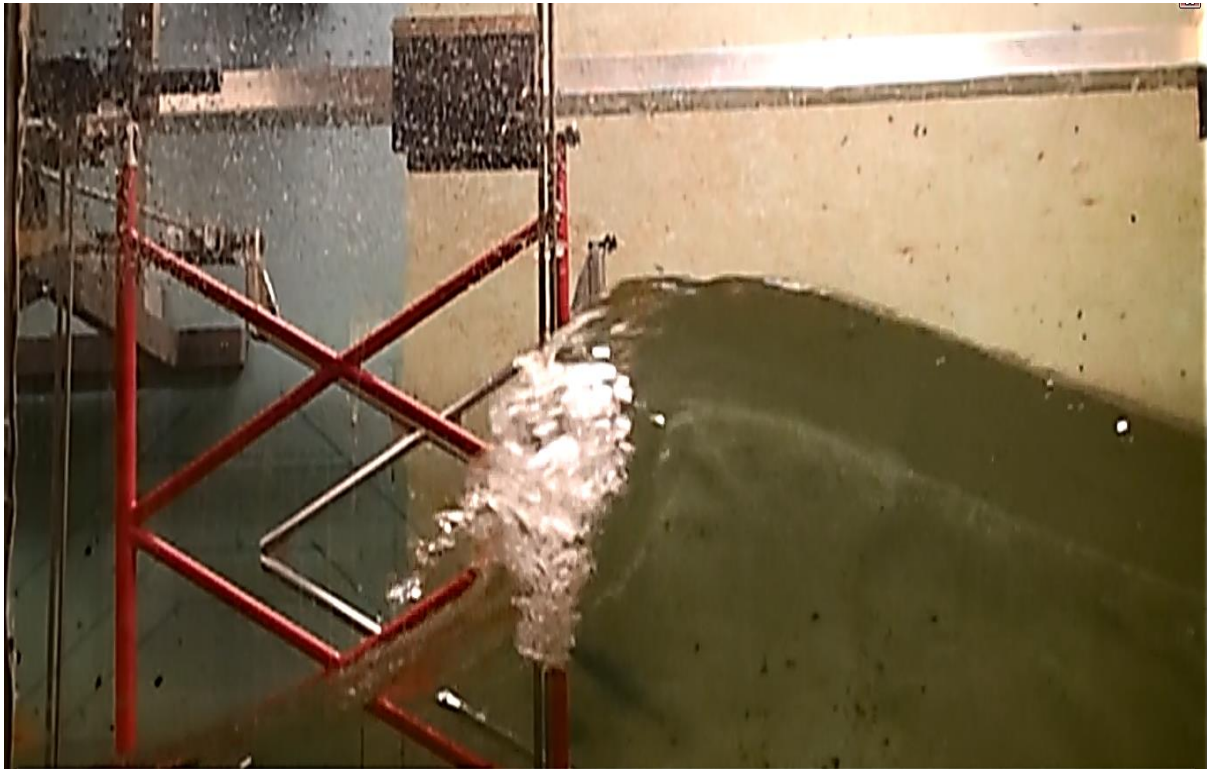
Figure 4.19: Snapshot from test 'Ue460t185' on side section of the truss structure
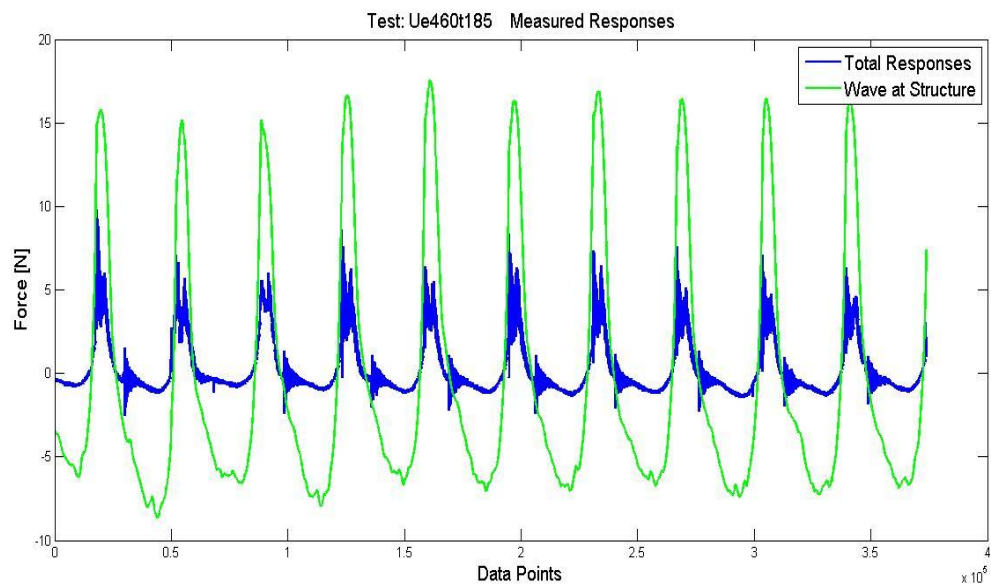
Figure 4.20: Time series of total measured responses and the wave at the structure-Test Ue460t185 (side section)
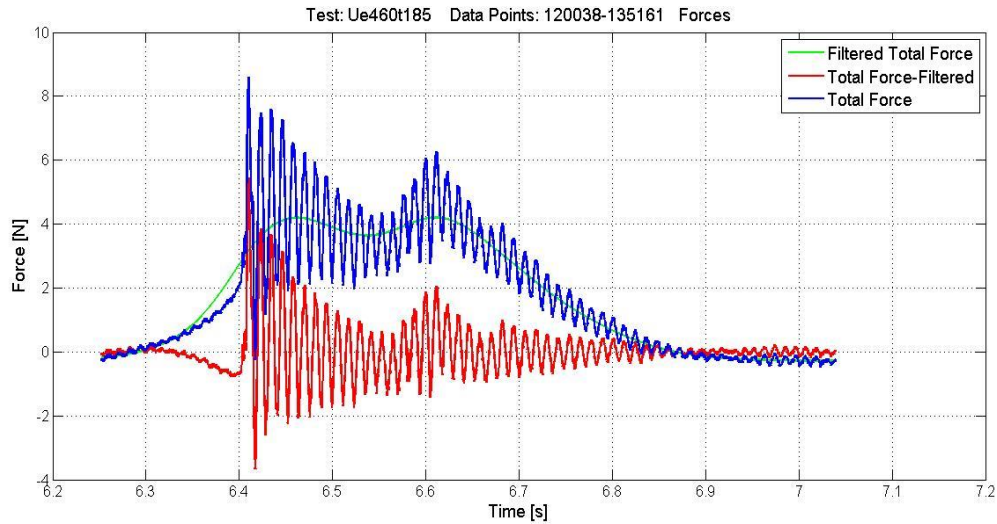
Figure 4.21: The decomposition of the total response forces – Test Ue460t185 (side section)
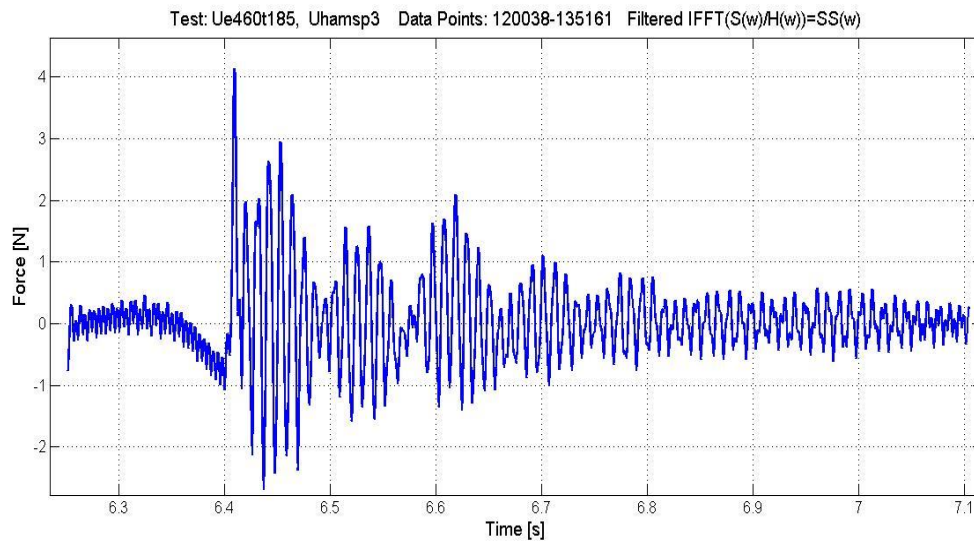
Figure 4.22: The measured slamming force- Test 'Ue460t185 (side section)

Table 4.6: Measured and calculated slamming forces – Test Ue460t185 (side section)

Maximum response force	**8.35 N**
Measured slamming force	**4.05 N**
Calculated slamming force based on Wienke & Oumeraci (2005)	**18.34 N**
Calculated slamming force based on Goda, et.al., (1966)	**7.97 N**

4.2.3.1.2   Test Ue480t196 on Side Section

Figure 4.23: Snapshot from test 'Ue480t196' on side section of the truss structure
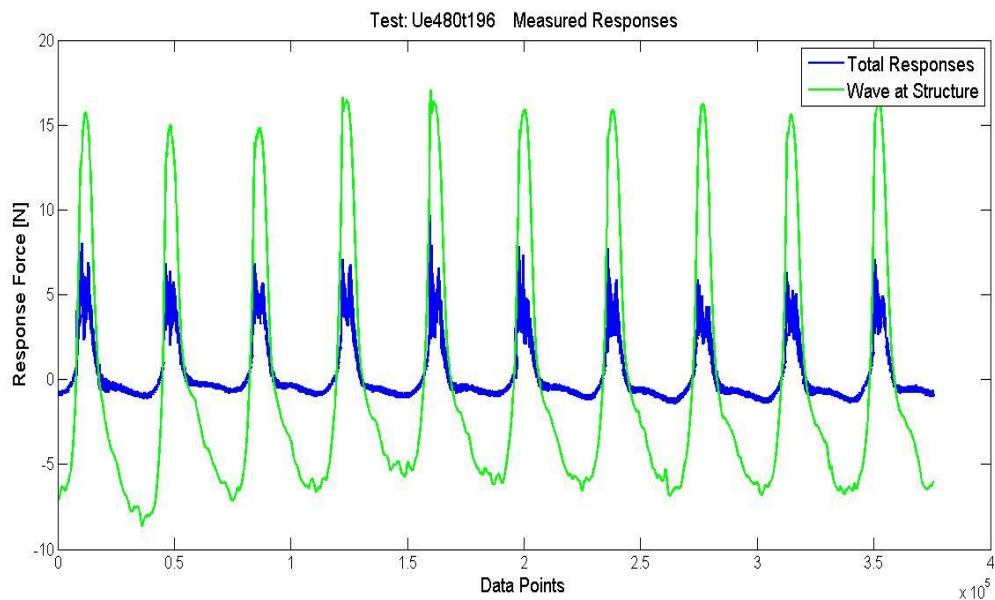
Figure 4.24: Time series of total measured responses and the wave at the structure-Test Ue480t196 (side section)
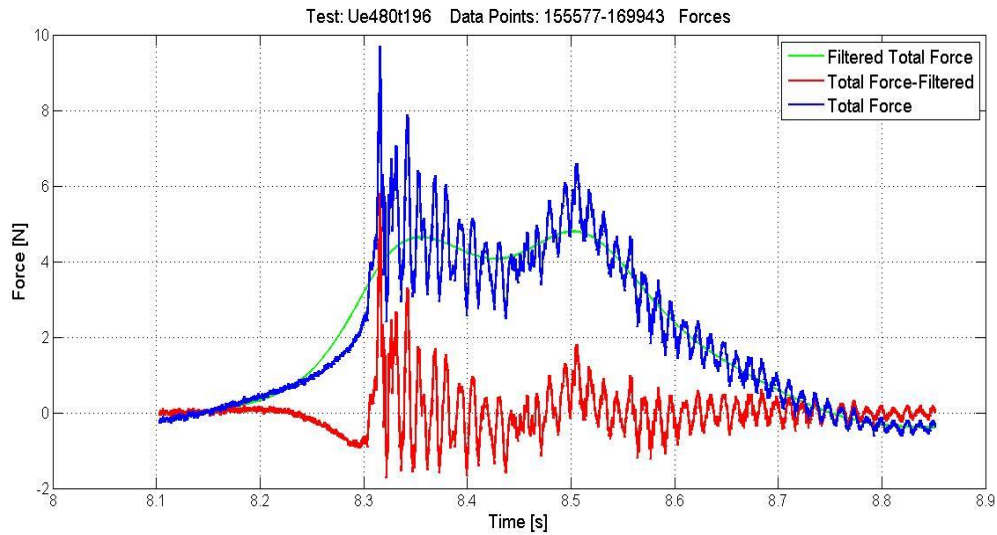
Figure 4.25: The decomposition of the total response forces – Test Ue480t196 (side section)
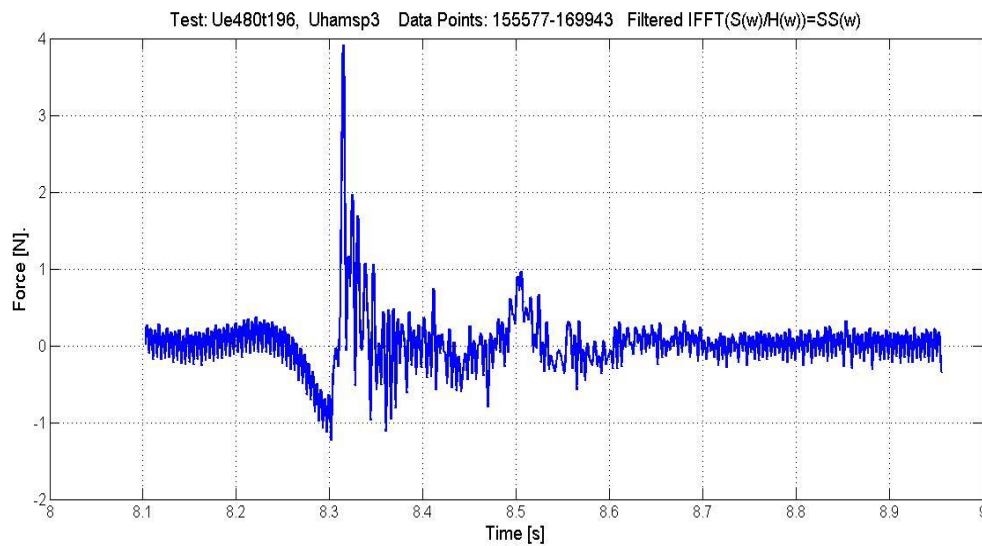
Figure 4.26: The measured slamming force- Test 'Ue480t196 (side section)

Table 4.7: Measured and calculated slamming forces – Test Ue480t196 (side section)

Maximum response force	**9.69 N**
Measured slamming force	**3.86 N**
Calculated slamming force based on Wienke & Oumeraci (2005)	**19.40 N**
Calculated slamming force based on Goda, et.al., (1966)	**8.43 N**

4.2.3.1.3   Test Ue500t208 on Side Section

Figure 4.27: Snapshot from test 'Ue500t208' on side section of the truss structure
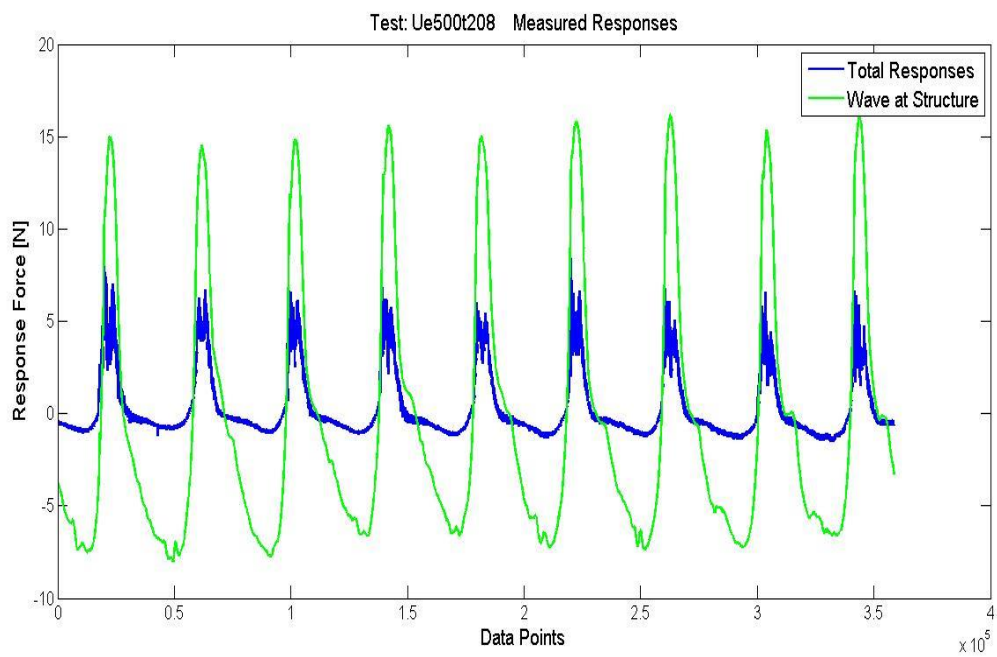
Figure 4.28: Time series of total measured responses and the wave at the structure-Test Ue500t208 (side section)
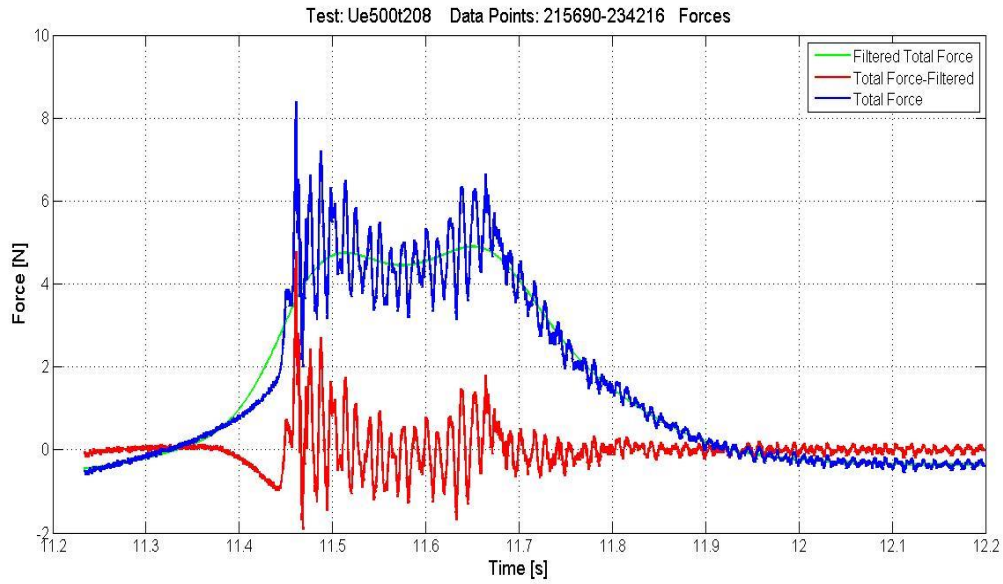
Figure 4.29: The decomposition of the total response forces – Test Ue500t208 (side section)
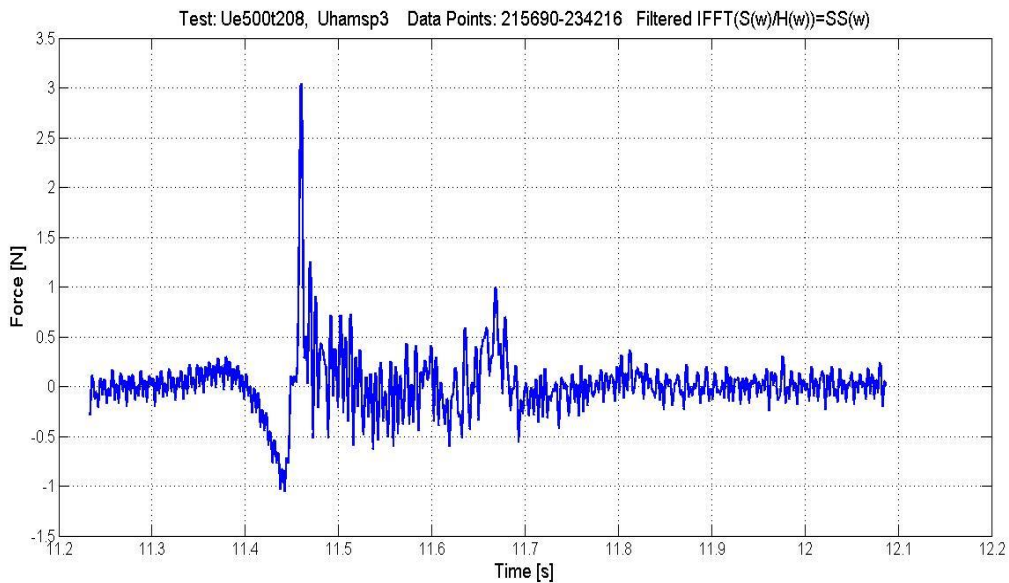
Figure 4.30: The measured slamming force- Test 'Ue500t208 (side section)

Table 4.8: Measured and calculated slamming forces – Test Ue500t208 (side section)

Maximum response force	**8.40 N**
Measured slamming force	**3.06 N**
Calculated slamming force based on Wienke & Oumeraci (2005)	**17.60 N**
Calculated slamming force based on Goda, et.al., (1966)	**7.65 N**

4.2.3.1.4 Test Ue570t222 on Side Section

Figure 4.31: Snapshot from test 'Ue570t222' on side section of the truss structure
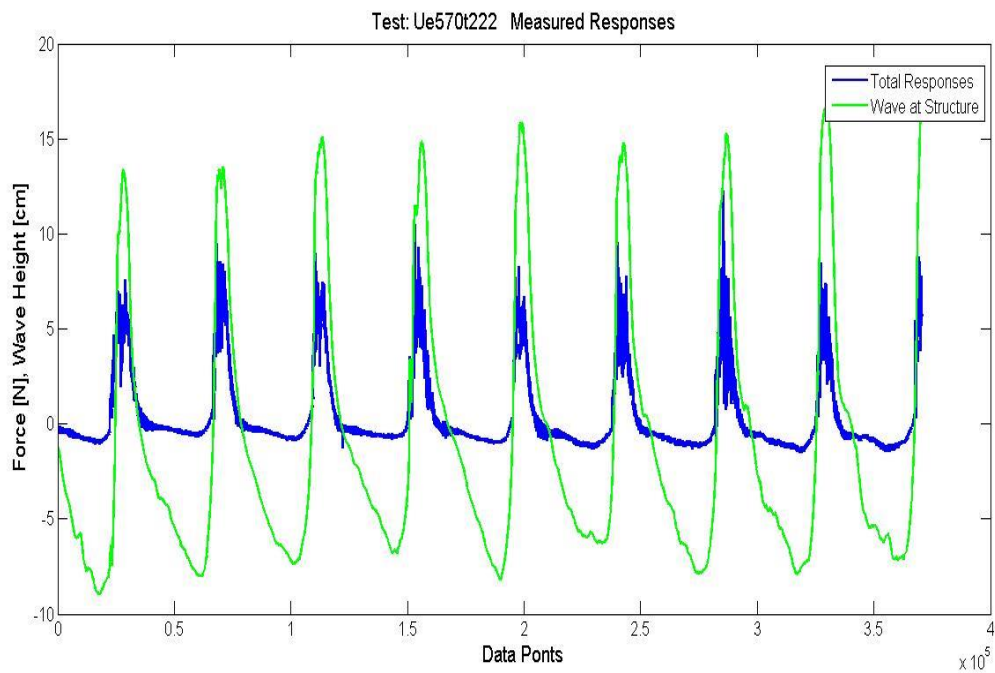
Figure 4.32: Time series of total measured responses and the wave at the structure-Test Ue570t222 (side section)
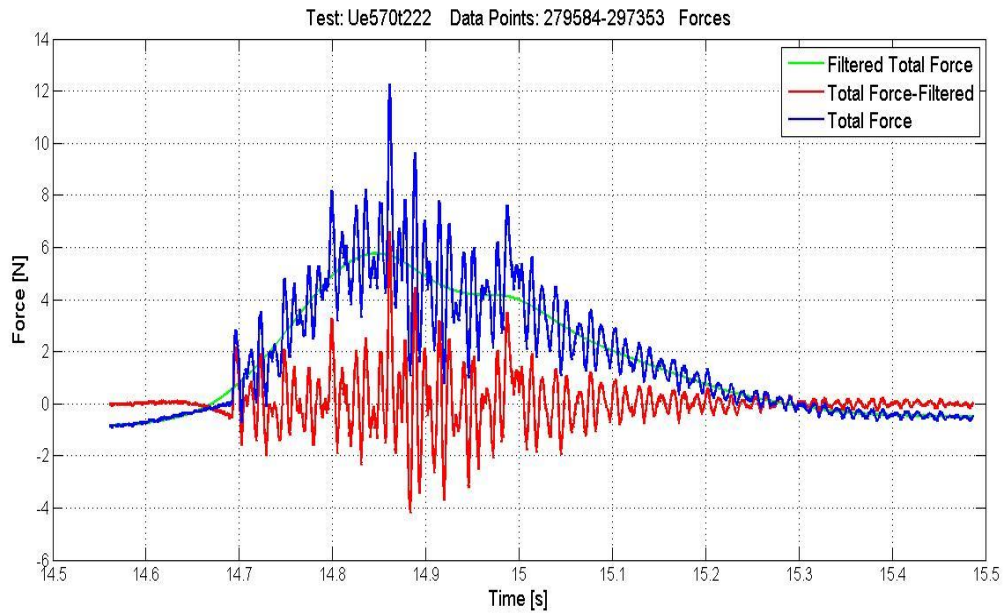
Figure 4.33: The decomposition of the total response forces – Test Ue570t222 (side section)
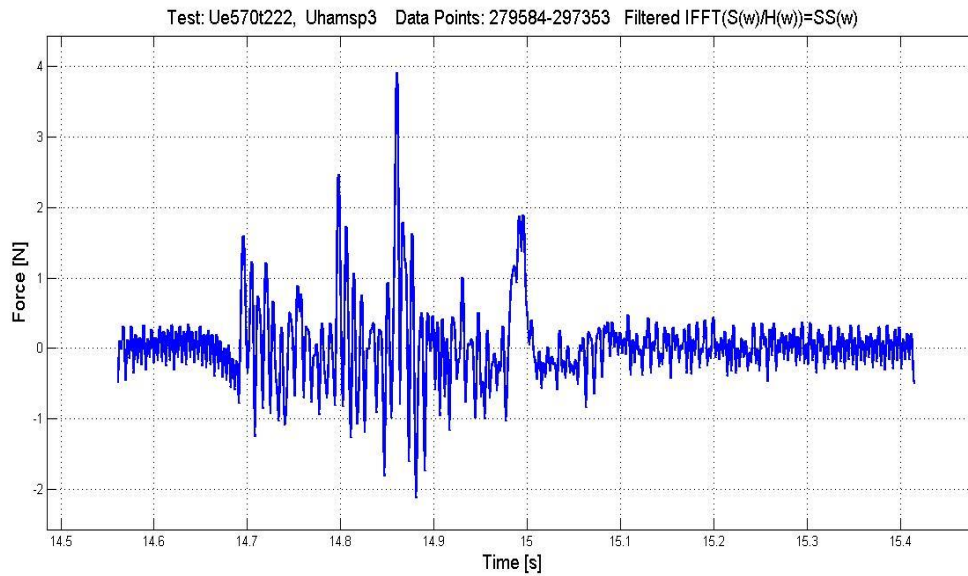
Figure 4.34: The measured slamming force- Test 'Ue570t222 (side section)

Table 4.9: Measured and calculated slamming forces – Test Ue570t222 (side section)

Maximum response force	**12.27 N**
Measured slamming force	**3.91 N**
Calculated slamming force based on Wienke & Oumeraci (2005)	**16.87 N**
Calculated slamming force based on Goda, et.al., (1966)	**7.33 N**

50

All the figures (i.e. Figure 4.21, Figure 4.25, Figure 4.29) containing total measured responses show that they have two peaks within a very short time. The first peak is higher than the following one. This is actually due to waves hitting on the front leg and rear leg respectively.

4.2.4   Tests with new slope of the bed (1:20)

The previous bed slope of 1:10 had been modified into 1:20 in order to obtain different pattern of waves (i.e. spilling breakers) and check whether any slamming forces occur. Few tests were carried out only for the side section of the truss structure. As it is given in APPENDIX A, the test that gave the maximum slamming force is chosen here for illustration. Figure 4.35 shows a snapshot of this test, as we see in this picture, wave is not breaking violently as they were breaking in the slope if 1:10. Although this looks like a plunging breaking it tends to spill, or it can be said that it's in the transition of plunging breakers and spilling breakers. Following figures show the results.

Figure 4.35: A snapshot from test 'Ue520t208' on side section with new slope
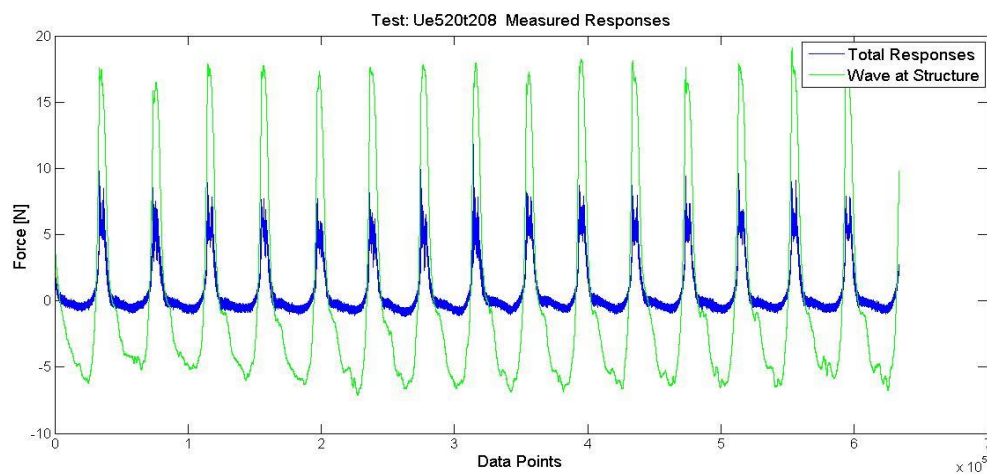
Figure 4.36: Time series of total measured responses and the wave at the structure-Test Ue520t208 (side section)

51
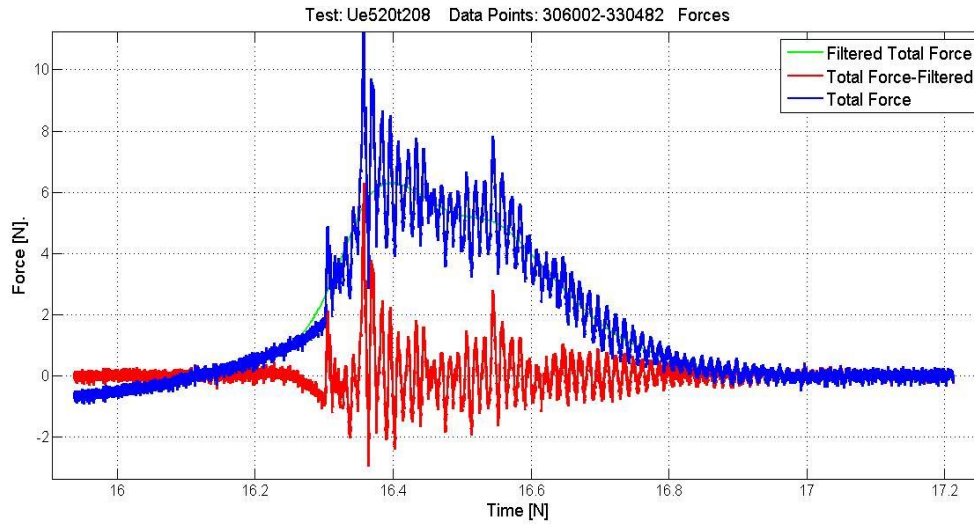
Figure 4.37: The decomposition of the total response forces – Test Ue520t208 (side section)
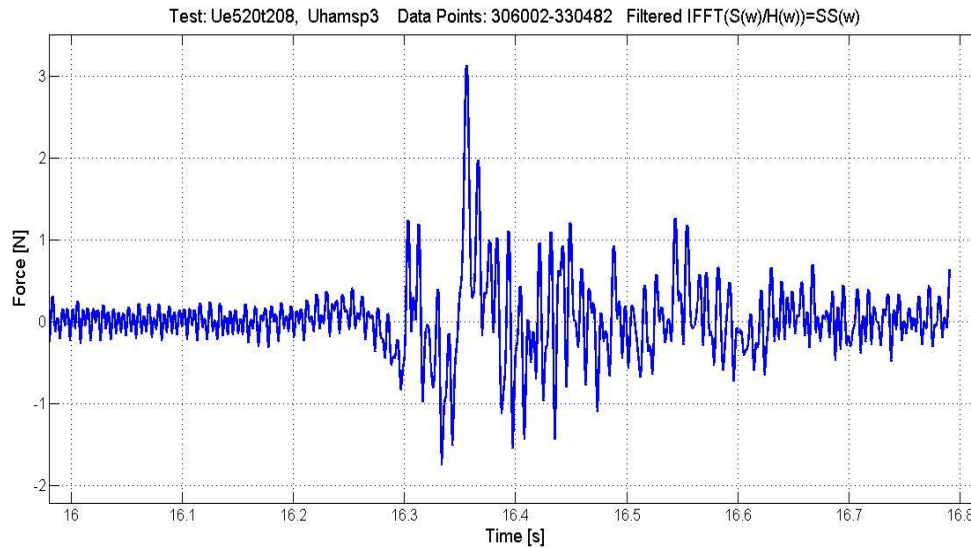
Figure 4.38: The final measured slamming force variation (side section)

Table 4.10: Measured and calculated slamming forces – Test Ue520t208 (side section)

Maximum response force	**11.84 N**
Measured slamming force	**3.12 N**
Calculated slamming force based on Wienke & Oumeraci	**20.95 N**
Calculated slamming force based on Goda	**9.12 N**

4.2.5   Duhamel Integral Method

Two individual cylinders were analysed by using Duhamel integral method as Ros Collados (2011) did in his master thesis. In this section, an analysis done for the large cylinder (60mm in diameter) is described in detail. For this case a test '*Ue460t185*' has been chosen for the detail illustration.

As it's shown in Figure 4.9, the dynamic part of the total response forces will be considered as an input for the Duhamel integral analysis. Figure 4.39 shows this decomposed dynamic part of the total response.
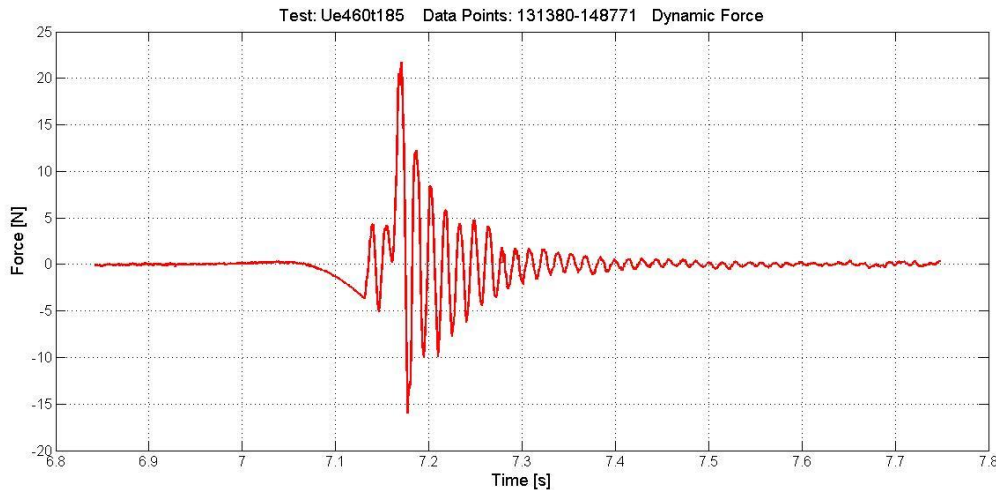
Figure 4.39: Dynamic part of the total responses – Test 460t185 (large cylinder)

A Matlab program used by Ros Collados (2011) has been modified and used for this analysis. Now this dynamic part of the total responses will be used as an input for this program. Before proceeding to the iterative process it's necessary to find the damping coefficient or the damping factor of structure as this will be used in the Duhamel integral. The damping factor is obtained through the logarithmic decrement (Tørum, 2013).

$$\delta = \frac{1}{n} ln \frac{x_i}{x_{i+n}} \tag{4.4}$$

where, δ is the logarithmic decrement, x_i is the amplitude of the i th oscillation and x_{i+n} is the amplitude of the $i+n$ th oscillation. Generally, the damping factor and the logarithmic decrement are related by the following equation,

$$\delta = \frac{2\pi\xi}{\sqrt{1-\xi^2}} \tag{4.5}$$

$\delta \approx 2\pi\xi$ is for small damping factors. So, damping factor is now,

$$\xi = \frac{1}{2\pi}\delta \tag{4.6}$$

From the above figure, damping coefficient is found to be about 0.055. Since this method is an iterative process first we assume an impact force and rise time so that the calculated response based on Duhamel integral should match the measured response. Figure 4.40 shows the final results after doing many trials by assuming different impact force and the rising time. Finally, the both calculated response (green) and the measured responses (red) are in agreement for an impact force of 21.5N and the rising time of 0.001s. It should be noted that the first peak of the measured response only adjusted with the calculated response as this is the response which caused by the slamming force and subsequent peaks follow the damping.

Figure 4.40: Duhamel integral method for test 'Ue460t185' (large cylinder)

So, the impact force or the slamming force obtained by Duhamel integral method is 21.5N and this is almost the same as what we obtained using frequency response function method (19.41N). Although this method looks simple, accuracy of this used method is a question and this will be discussed in the next chapter.

5.0   DISCUSSION ON THE RESULTS

Analysis of measured data and results are presented in the previous chapter. This chapter presents more detailed discussions and comments on several experimental results.

5.1   Eccentricity and Wave Height

Many tests were carried out changing eccentricity and the period of the waves. Since it is unknown that how the eccentricity changes the wave height, a brief analysis has been done by measuring the deep water wave height (from wave gauge 1 in Figure 3.2) for different eccentricity. This plotted in Figure 5.1.
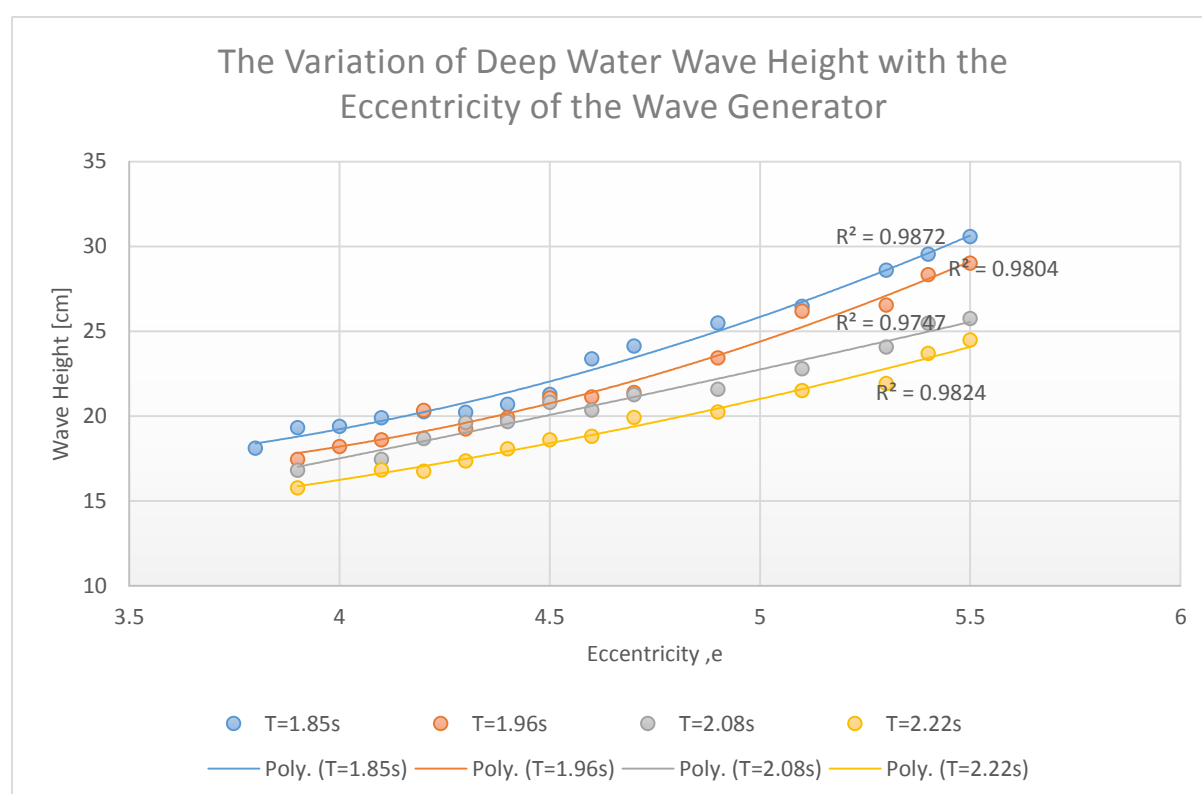
Figure 5.1: The variation of the wave height with the eccentricity for different wave periods

As it can be seen in the above figure, wave height increases with the increasing eccentricity for all wave periods. In the meantime short period waves have higher wave heights than that for the longer period waves, it means that wave heights decreases with the increasing wave periods.

5.2   Different Hammer Points

There were several hammer points used for testing, but the results shown in the previous chapter were for the hammer point exactly at the slamming height of about 17cm above the still water line (Ros Collados, 2011). But, it is necessary to check whether the hammer test data from the other points would affect the results. So, here the front section of the structure is taken for the comparison. There are 12 points were selected for the pluck tests. The figures shown

below is for only three different point such as 1, 2 and 5. But, Figure 5.5 shows the results for all 12 points.
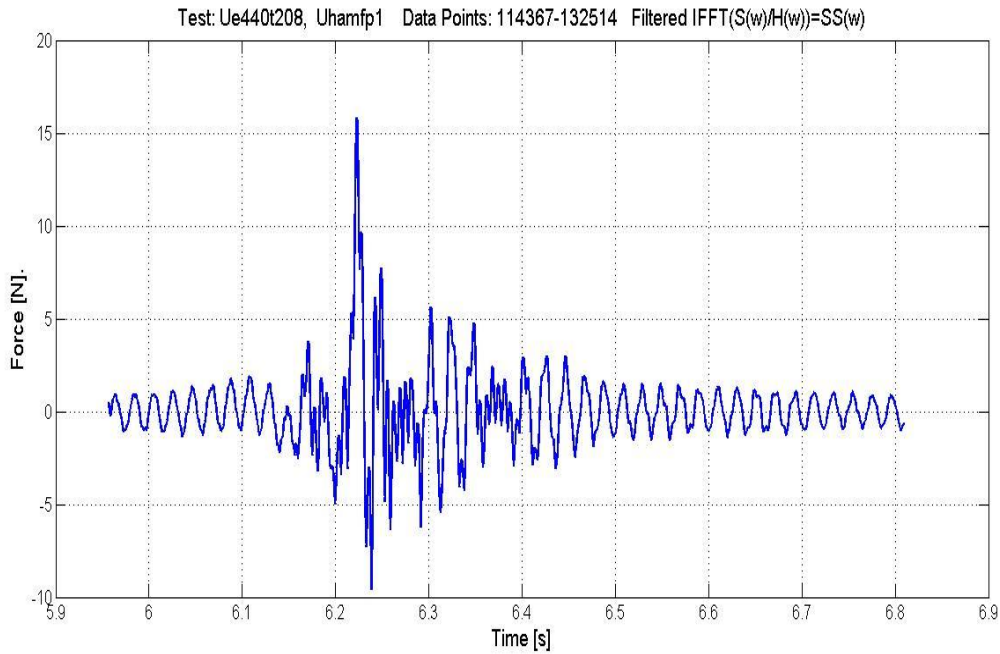
Figure 5.2: The measured slamming force – Tests Ue440t208 and Uhamfp1 (front section)
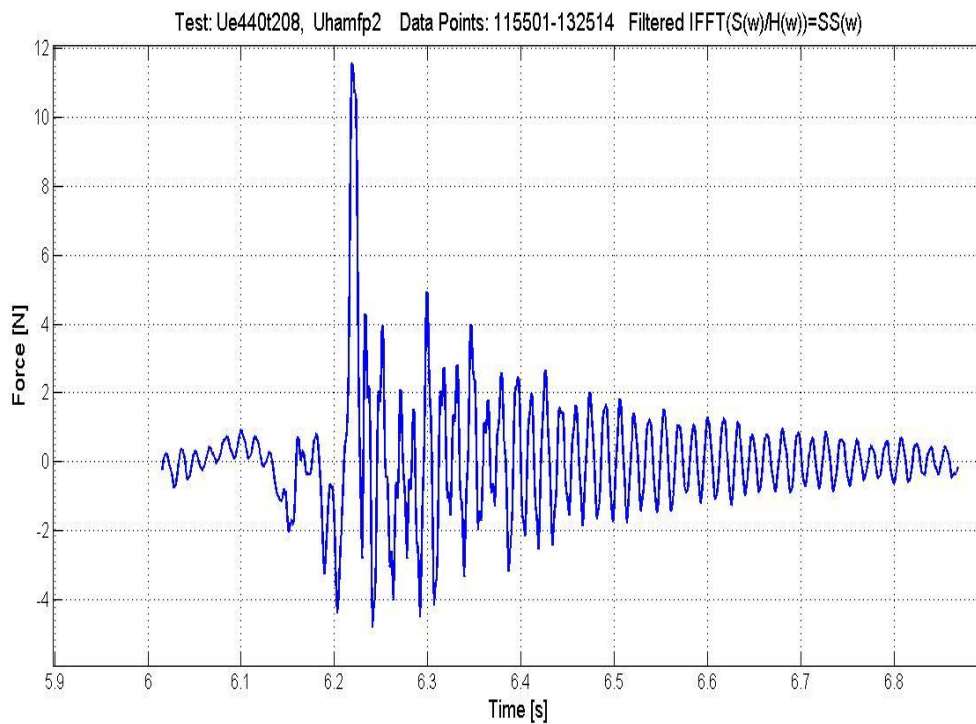
Figure 5.3: The measured slamming force – Tests Ue440t208 and Uhamfp2 (front section)
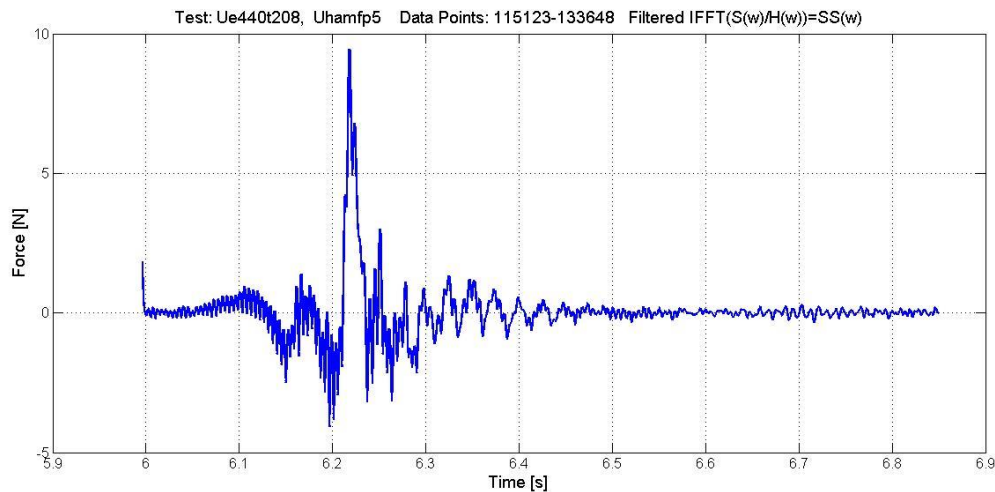
Figure 5.4: The measured slamming force – Tests Ue440t208 and Uhamfp5 (front section)
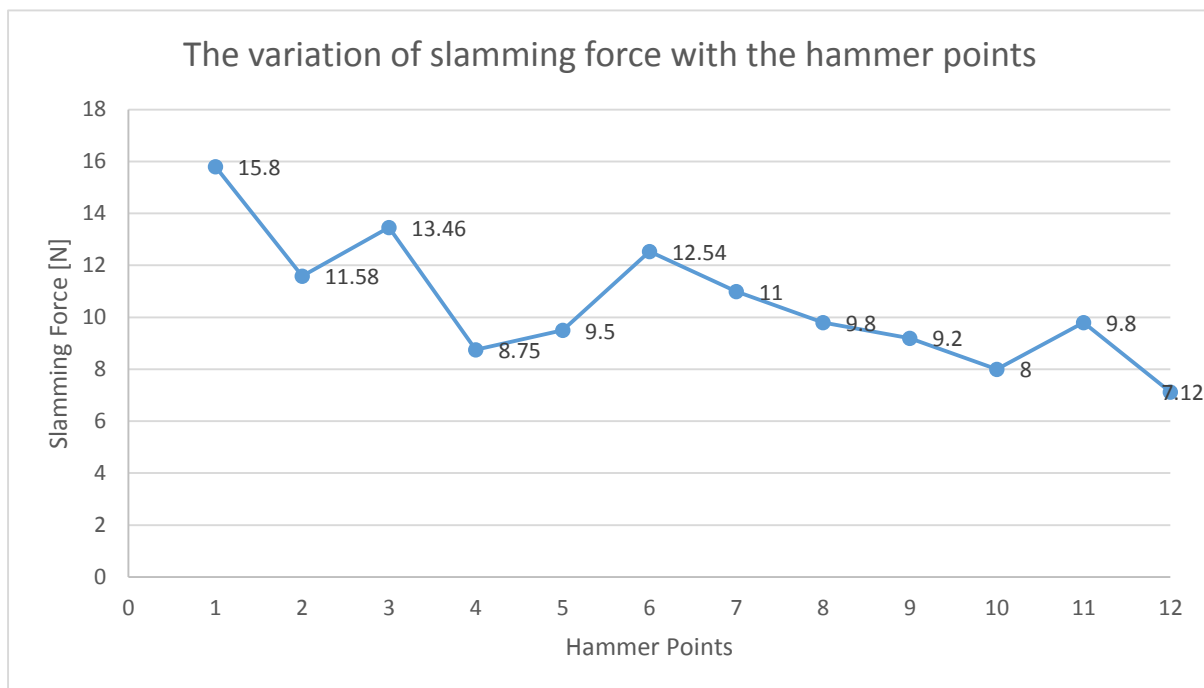
Figure 5.5: The variation of the slamming forces on front section of the truss structure with different hammer points

As it can be seen in Figure 5.5, the maximum slamming force of 15.8N occurs for the hammer pluck point of 1 which is at the top of the structure. One can observe that the points at top of the structure give the maximum slamming forces than that in the lower part or close to the still water line. This could be due to the different scenario of oscillating pattern of the structure when it's impacted at different positions. It means that here two types of damping such as structural damping and hydraulic damping could occur as this structure is partly in the water. However, in all the analysis the point exactly 17cm above the still water level was considered as they are about at the slamming area.

5.3 High Impact Forces

In some cases, for large value of eccentricities waves were breaking in front of the structure at some distance away from the structure. Most of the tests gave very high forces for this scenarios. Since it is known that they are not from wave impact, it's always interesting to investigate them. Few cases are chosen and they have been illustrated here.

First consider the test '*Ue610t196*' on the side section of the truss structure. As it's seen in APPENDIX A, this test gives a slamming force of 3.11N and a total response of 9.03N as well. These forces are very high compared to that with the results for the same wave period. Figure 5.6 shows a snap shot of this test. As it's shown in this figure, the wave is broken ahead of the structure and splashed on the structure. This may cause a lot of turbulence at the structure. If we look into the Figure 5.7, the time series of the measured response is not uniform as the measured total response (first peak) varies significantly. This could be due to the violent nature of the wave breaking ahead of the structure. The time expanded view of the maximum response force that resulted large impact force is shown in Figure 5.8. As it is shown in this figure, the maximum response is irrespective of the maximum wave crest height. In this case the wave height also small compared to the other cases as the wave already broken ahead of the structure.

Figure 5.6: Snapshot from test 'Ue610t196' on side section of the truss structure
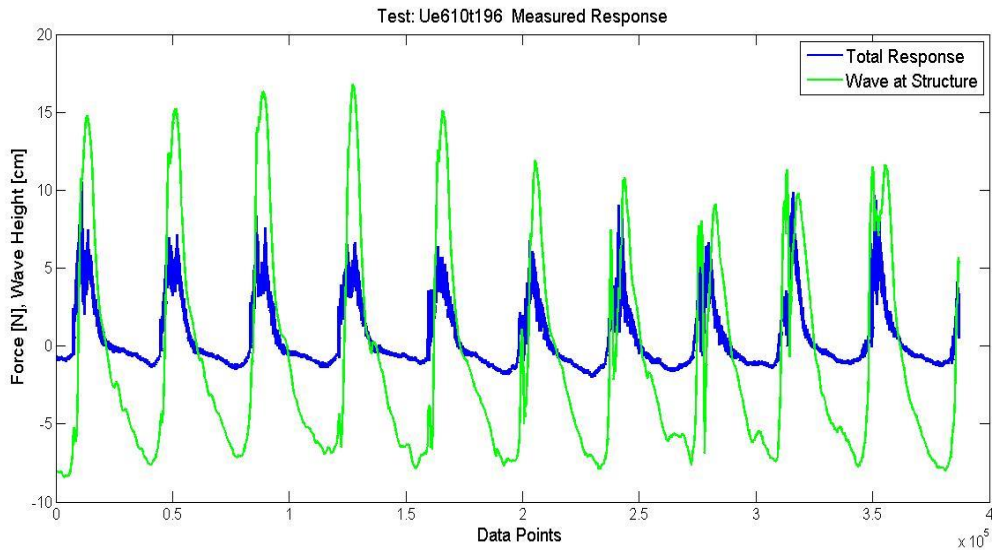
Figure 5.7: Total measured response – Test Ue610t196 on side section
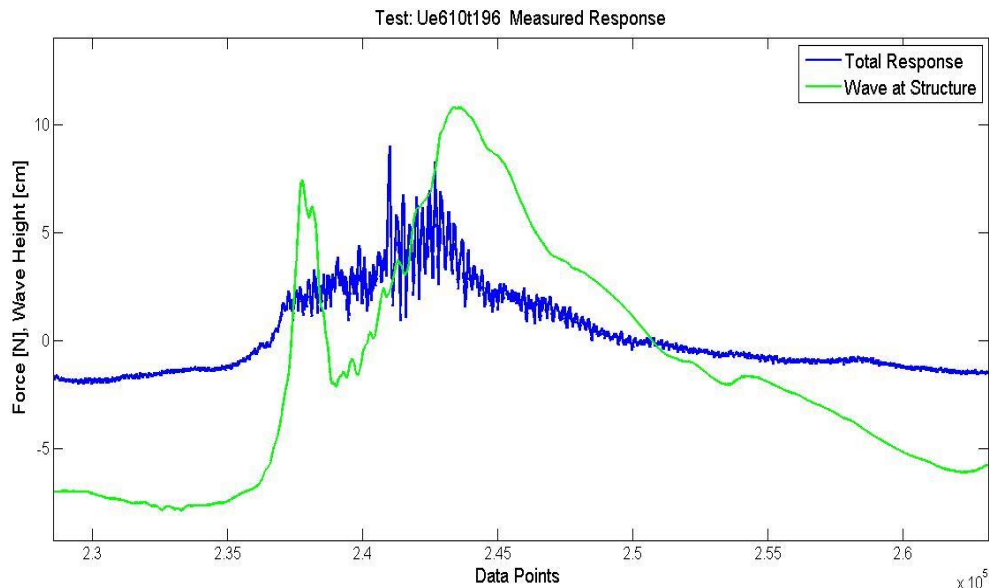
Figure 5.8: Time expanded view - Test Ue610t196 on side section

Endresen and Tørum (1992) investigated extremely high vertical forces on an elevated pipeline through surf zone. In this case pipeline was oriented almost normal to the coastline. They found that very high vertical forces acting on the pipeline was due to the large turbulence and eddies of water particles with high accelerations. The period of the turbulent variation is very short and the water particles accelerations become large. This would cause high inertia forces when it is broken in plunging pattern.

Figure 5.9: Snapshot from test 'Ue670t196' on side section of the truss structure

Another snapshot shown in Figure 5.9 was taken from a test 'Ue670t196', this resulted a force 2.52N. This one also broken even more ahead of the structure and cause much turbulence which led to such high forces.

5.4 Accuracy of Duhamel Integral Approach

Duhamel integral approach was used only for individual piles. As previously mentioned, the same method and the same Matlab program which was used by Ros Collados (2011) have been applied here too. Ros Collados (2011) investigated the breaking wave forces on a vertical cylinder and the cylinder instrumented with six ring type transducers placed at different elevation above the still water level. The natural frequency of the local transducers is very high compared to the natural frequency of the cylinder that we used in this research, or in other words, structure used by Ros Collados (2011) has very less natural period of oscillation.

Duhamel integral approach using Matlab is a curve fitting procedure such a way that the first peak of the measured response should almost match the calculated response. Since measured responses obtained by Ros Collados (2011) had many oscillations within the impact duration of 0.008s (Figure 5.10), it was easy to fit both the curves more accurately. But in our case, the natural period of oscillation is about 0.015s (Figure 4.40) and much larger than the impact duration, so it is hard to have even a cycle of oscillation within an impact duration time frame.
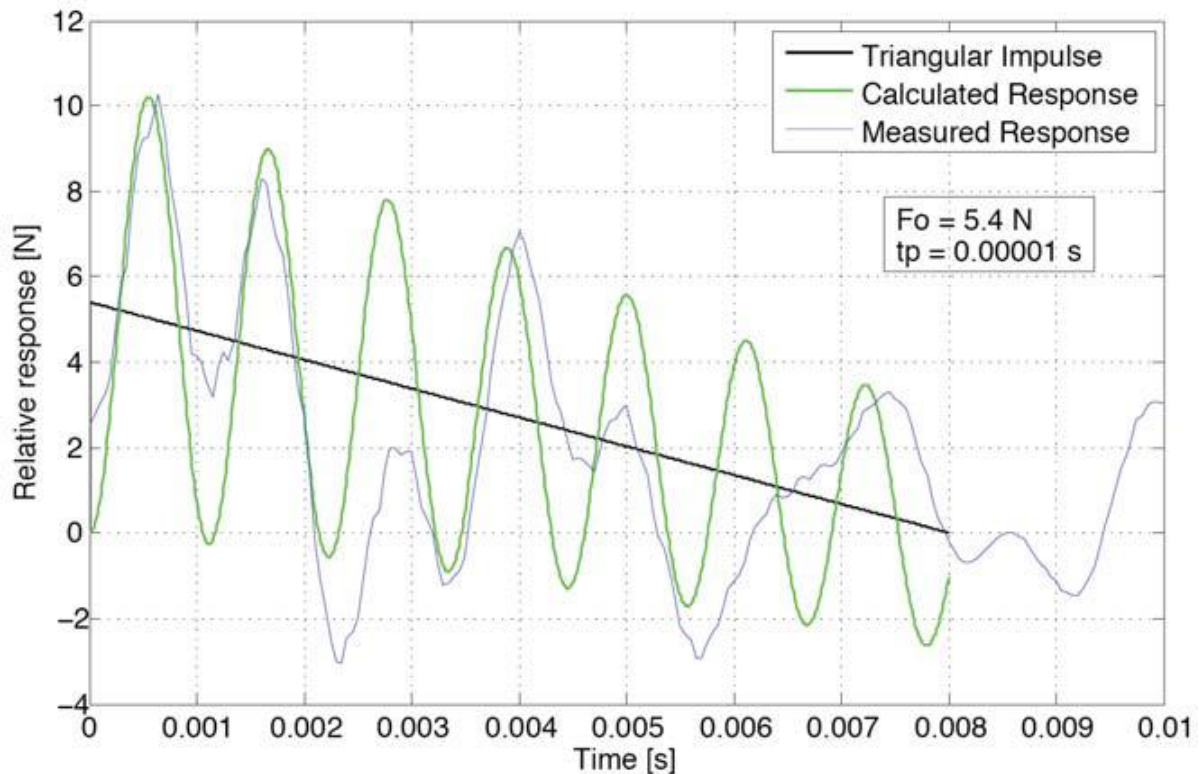
Figure 5.10: An example of getting the impact force using Duhamel integral approach (Ros Collados, 2011)

If we recall Figure 3.19, the variation of the maximum response ratio with the ratio of impulse duration to natural period of oscillation for different types of impulse loading, in our case the ratio between the impact duration and the natural period is about 0.5, so the maximum response ratio for all types of impulsive loading show an increasing pattern hence it is hard to predict the maximum response ratio. But, in Ros Collados (2011)'s case, the ratio between the impact duration and the natural period of oscillation is about more than 1, and the maximum response ratio for triangular and rectangular type impulsive loading have an uniform pattern and don't change much with the time ratio.

5.5 General Discussions

The two individual cylinders were tested simultaneously in order to compare the wave slamming forces on each of them. Here we choose a test 'Ue460t185' and compare the results of both the large cylinder and the small cylinder. According to APPENDIX A, large cylinder (60mm in diameter) resulted a slamming force of 19.41N whereas the small cylinder (16mm in diameter) resulted a slamming force of 3.23N. That means the slamming force on the large cylinder is about six time than that on the small cylinder.

According to the slamming equation (2.12), the slamming force is directly proportional to the diameter of the cylinder. The ratio between the diameter of the large and small cylinders is 3.75. So, the ratio of the measured slamming forces on large and small cylinder should be about

3.75 as other parameters in the equation (2.12) are the same for both the structures. Since, we got very large force on large cylinder or perhaps very small force on small cylinder, it can be confirmed that there must be size effects.

The realative cylinder diameter plays an important role on the wave impact forces on cylinders (Apelt & Piorewicz, 1987). The raltive cylinder diameter means, ratio of the diameter of the cylinder and the deepwater wave height (D/H_0). Apelt & Piorewicz (1987) investigated the wave impact forces for different D/H_0 values. They found that the maximum wave impact forces obatined for a relative cylinder diameter of 2 (i.e. $D/H_0 = 2$). Also they found that approximately 40-50% of the maximum slamming forces occurred for a D/H_0 value of 0.5. If we consider the small cylinder, the relative diameter in our case is about 0.064 as the average deep water wave height is about 25cm. So, this could be a reason for getting very small slamming force for small cylinders. Even in Wienke & Oumeraci's tests the minimum relative diameter was about 0.35 (0.7m/2m).

The result of the tests on small cylinder is comparable with the side section of the truss structure as they both the same in size. The results presented in APPENDIX A confirm that the slamming forces on the side section of the truss structure is approximately equal to the slamming forces acting on the small cylinder.

6.0 CONCLUSIONS AND RECOMMENDATIONS

There were totally more than hundred tests carried out on all the different structures such as two individual piles (16mm and 60mm in diameter), front section of the truss structure and the side section of the structure. All the data were analysed by using frequency response function method and only the data obtained from the two individual cylinders were analysed by using Duhamel integral method in addition to the frequency response function method. From the analysed data and the results the following conclusions have been made.

Maximum measured responses were not always the case to give the maximum slamming forces as they perhaps contained more quasi-static force than the dynamic forces.

The slamming forces obtained from all the test show that they were far lesser than the calculated slamming forces based on both Goda, et al. (1966) and Wienke & Oumeraci (2005). This could be due to the following reasons,

- o Size effects:
  This was confirmed from the results of the tests done on the two different size piles simultaneously. The compared calculated slamming forces based on Goda, et al. (1966) and Wienke & Oumeraci (2005) were obtained from tests with larger relative cylinder diameter (D/H_0) compared to the relative cylinder diameter in these experiments.
- o Scale effects:
  This was small scale test and theoretical results were based on large scale tests. The entrained air is different in small scale and in reality, generally entrapped air would reduce the impact pressure.
- o Unfavourable wave forms:
  Another important reason for getting lesser slamming forces is that the shape of the wave when it is hit the structure was not so vertical as the vertical shaped waves caused high slamming forces (Wienke & Oumeraci, 2005). This contributes to the curling factor as well. The position of the structure from the upper end of the slope also influences in the wave form, in our case structure was placed about 1m from the upper end of the slope whereas in Wienke & Oumeraci (2005)'s case it was placed exactly at the upper end of the slope.

Some test were carried out after modifying the bed slope from 1:10 to 1:20. These tests were performed on the side sections of the truss structure. It was observed that the waves were seem to be spilling type plunging breakers which means they were not typical pure, tongue shaped plunging breakers as they were spilling and not so violent like plunging breakers. The results show that the measured slamming forces were approximately the same in both the cases.

It was found that the impact duration in our case was larger than the impact duration that was derived by the previous researchers such as Wienke & Oumeraci (2005) and Goda et. al. (1966). This could be due to the wave might hit different parts of the truss structure at different times.

The applying analysing method (FRF method) was seem to be promising as it was compared with the Duhamel integral approach and found that they both gave almost the same result for vertical piles.

Based on the above conclusions, it is recommended to perform a large scale experimental study on a truss structure in order to overcome such short comings in the small scale tests. Since there are different impact forces on different part of the truss structure (bracings), it is also recommended to do the large scale test to measure the slamming forces on each member locally.

REFERENCES

Aashamar, M. (2012). *Wave slamming forces on truss support structures for wind turbines.* NTNU, Department of Civil and Transport Engineering. Trondheim: Norwegian University of Science and Technology.

Apelt, C., & Piorewicz, J. (1987). Laboratory Studies of Breaking Wave Forces Acting on Vertical Cylinders in Shallow Water. *Coastal Engineering, 11*, 263-282.

Aune, L. (2011). *Bølgjeslag mot jacket på grunt vatn (Wave slamming forces on jacket in shallow water).* Trondheim: Department of Structural Engineering.

Battjes, J. (1974). Surf similarity. *Proceedings of 14th International Conference on Coastal Engineering*, *1*, pp. 467-479. Copenhagen.

Chella, M., Tørum, A., & Myrhaug, D. (2012). An Overview of Wave Impact Forces on Offshore Wind. *Energy Procedia, 20*, 217 – 226.

Clough, R., & Penzien, J. (1975). *Dyanamics of structure* (2nd ed.). International Editions. Retrieved 1993

Dytran. (2013, June 15). *Dytran Instruments Inc. - Product Details*. Retrieved from Dytran Instruments Inc. : http://www.dytran.com/img/products/5800B.pdf

Endresen, H., & Tørum, A. (1992). Wave forces on a pipeline through the surf zone. *Coastal Engineering, 18*, 267-281.

Goda, Y., Haranka, S., & Kitahata, M. (1966). Study of impulsive breaking wave forces on piles. *Port and Harbour Research Institute, 5*(6), 1-30.

Innogy, R. (2013, June 20). *Thornton Bank - RWE Innogy*. Retrieved June 20, 2013, from RWE-The Energy to lead: http://www.rwe.com/web/cms/en/248922/rwe-innogy/sites/wind-offshore/in-operation/thornton-bank/

Irschik, K., Sparboom, U., & Oumeraci, H. (2002). Breaking wave characteristics for the loading of a slender pile. Cardiff: ASCE.

Judith, B., & Marcel, S. J. (2012). *Coastal Dynamics I.* Delft: VSSD, Delft University of Technology.

Morison, J., O'brien , M., Johnson, J., & Schaaf, S. (1950). The forces exerted by surface waves on piles. *Jounal of Petroleum Technology, Petroleum transactions, AMIE, 189*, 149-154.

Naess, A. (2011). *An introduction to random vibrations.* Trondheim: Centre for Ships and Ocean Structures, NTNU.

Ros Collados, X. (2011). *Impact forces on a vertical pile from plunging breaking waves.* Trondheim: Norwegian University of Science and Technology.

Tanimoto, K., Takahashi, S., Kaneko, T., & Shiota, K. (1986). Impulsive breaking wave forces on an inclined pile exerted by random waves. *Proceedings of 20th International Conference on Coastal Engineering*, (pp. 2288-2302).

Tørum, A. (2013). *Analysis of force response data from tests on a model of a truss structure subjected to plunging breaking waves.* Department of Civil and Transport Engineering. Trondheim, Norway: Norwegian University of Science and Technology.

von Karman, T. (1929). *The impact on seaplane floats during landing.* Washington: National Advisory Committee for Aeronautics.

Wagner, H. (1932). Über stoss-und gleitvorgänge an der oberfläche von flüssigkeiten. *Zeitshrift für Angewandte Mathmatik und Mechanik, 12*(4), 193-215.

Wienke, J., & Oumeraci, H. (2005). Breaking wave impact force on a vertical and inclined slender pile—theoretical and large-scale model investigations. *Coastal Engineering , 52*, 435 − 462.

Wind Energy-IFE. (2013, 06 20). Retrieved from Institute for Energy Technology: http://www.ife.no/en/ife/main_subjects_new/energy_environment/windenergy

LIST OF SYMBOLS

$f(t)$ = Line force
f_0 = Impulse load
k = Stiffness
l = Total length of the bracing within the area of impact
m = Oscillating mass
t = Time
t_* = Duration of impact
u = Water particle velocity
u_{max} = Maximum response

C_b = Breaking wave celerity
C_D = Drag coefficient
C_M = Inertia coefficient
C_s = Slamming factor
D = Diameter of the pile
F_D = Drag force
F_M = Inertia force
F_S = Slamming force
H_0 = Deep water wave height
$H(\omega)$ = Frequency response function
L_0 = Deep water wave length
R = Radius of the pile
$S_f(\omega)$ = Linear spectrum of applied force
T_d = Natural period of oscillation
V = Voltage

ρ_w = Density of water
λ = Curling factor
η_b = Breaking crest height
ξ_0 = Iribarren parameter
ξ = Damping factor
ω_d = Damped frequency
τ = Duration of impact

APPENDICES

APPENDIX A

Results of all the experiments are tabulated in this appendix.

Table A.1: The measured and calculated slamming forces- Large cylinder [wave period 1.85s]

Test	e	T (s)	Total Response (N)	Measured Slamming Force (N)	η_b (m)	H_b (m)	$\lambda\eta_b$ (m) W & O	$\lambda\eta_b$ (m) Goda	C_b (m/s)	τ (s) W & O	τ (s) Goda	Calculated Slamming Force (N) W & O	Calculated Slamming Force (N) Goda
Ue410t185	4.1	1.85	34.04	17.43	0.156	0.21	0.072	0.062	2.190	0.006	0.014	64.888	28.212
Ue420t185	4.2	1.85	29.71	12	0.204	0.218	0.094	0.082	2.295	0.005	0.013	93.182	40.514
Ue430t185	4.3	1.85	31.05	14.25	0.158	0.221	0.073	0.063	2.195	0.006	0.014	65.988	28.691
Ue440t185	4.4	1.85	32.67	14.29	0.163	0.232	0.075	0.065	2.206	0.006	0.014	68.770	29.900
Ue450t185	4.5	1.85	29.2	13.65	0.17	0.239	0.078	0.068	2.221	0.005	0.014	72.735	31.624
Ue460t185	4.6	1.85	36.67	19.41	0.168	0.234	0.077	0.067	2.217	0.005	0.014	71.594	31.128
Ue470t185	4.7	1.85	35.79	15.45	0.165	0.232	0.076	0.066	2.210	0.006	0.014	69.894	30.389
Ue490t185	4.9	1.85	37.16	13	0.172	0.233	0.079	0.069	2.226	0.005	0.013	73.884	32.123
Ue510t185	5.1	1.85	36.88	14.77	0.156	0.223	0.072	0.062	2.190	0.006	0.014	64.888	28.212
Ue530t185	5.3	1.85	33.95	13.36	0.139	0.209	0.064	0.056	2.152	0.006	0.014	55.806	24.264
Ue540t185	5.4	1.85	31.56	11.84	0.152	0.219	0.070	0.061	2.181	0.006	0.014	62.707	27.264
Ue550t185	5.5	1.85	41.59	23.9	0.131	0.197	0.060	0.052	2.134	0.006	0.014	51.703	22.480

Table A.2: The measured and calculated slamming forces- Large cylinder [wave period 1.96s]

Test	e	T (s)	Total Response (N)	Measured Slamming Force (N)	η_b (m)	H_b (m)	$\lambda\eta_b$ (m) W & O	$\lambda\eta_b$ (m) Goda	C_b (m/s)	τ (s) W & O	τ (s) Goda	Calculated Slamming Force (N) W & O	Calculated Slamming Force (N) Goda
Ue410t185	4.1	1.85	34.04	17.43	0.156	0.21	0.072	0.062	2.190	0.006	0.014	64.888	28.212
Ue410t196	4.1	1.96	18.46	6.76	0.172	0.227	0.079	0.069	2.226	0.005	0.013	73.884	32.123
Ue420t196	4.2	1.96	25.99	10.41	0.16	0.221	0.074	0.064	2.199	0.006	0.014	67.096	29.172
Ue430t196	4.3	1.96	26.05	12.47	0.149	0.217	0.069	0.060	2.174	0.006	0.014	61.089	26.560
Ue440t196	4.4	1.96	30	16.21	0.154	0.218	0.071	0.062	2.186	0.006	0.014	63.794	27.736
Ue450t196	4.5	1.96	38.06	19.23	0.152	0.223	0.070	0.061	2.181	0.006	0.014	62.707	27.264
Ue460t196	4.6	1.96	39.08	25.18	0.153	0.217	0.070	0.061	2.183	0.006	0.014	63.249	27.500
Ue470t196	4.7	1.96	33.59	14.87	0.168	0.224	0.077	0.067	2.217	0.005	0.014	71.594	31.128
Ue490t196	4.9	1.96	39.75	23.1	0.119	0.181	0.055	0.048	2.106	0.006	0.014	45.752	19.892
Ue510t196	5.1	1.96	36.01	11.51	0.119	0.191	0.055	0.048	2.106	0.006	0.014	45.752	19.892
Ue530t196	5.3	1.96	47.41	26.29	0.123	0.179	0.057	0.049	2.115	0.006	0.014	47.709	20.743
Ue540t196	5.4	1.96	30.75	12.5	0.093	0.145	0.043	0.037	2.044	0.006	0.015	33.699	14.652
Ue550t196	5.5	1.96	46.59	19.59	0.111	0.175	0.051	0.044	2.087	0.006	0.014	41.921	18.227

Table A.3: The measured and calculated slamming forces- Large cylinder [wave period 2.08s]

Test	e	T (s)	Total Response (N)	Measured Slamming Force (N)	ηb (m)	Hb (m)	ληb (m) W & O	ληb (m) Goda	Cb (m/s)	τ (s) W & O	τ (s) Goda	Calculated Slamming Force (N) W & O	Calculated Slamming Force (N) Goda
Ue410t208	4.1	2.08	26.35	11.71	0.153	0.209	0.070	0.061	2.183	0.006	0.014	63.249	27.500
Ue420t208	4.2	2.08	26.12	8.51	0.146	0.207	0.067	0.058	2.168	0.006	0.014	59.486	25.864
Ue430t208	4.3	2.08	24.29	9.2	0.144	0.211	0.066	0.058	2.163	0.006	0.014	58.426	25.403
Ue440t208	4.4	2.08	26.36	8.54	0.146	0.214	0.067	0.058	2.168	0.006	0.014	59.486	25.864
Ue450t208	4.5	2.08	30.39	11	0.148	0.208	0.068	0.059	2.172	0.006	0.014	60.553	26.327
Ue460t208	4.6	2.08	29.6	9.44	0.146	0.224	0.067	0.058	2.168	0.006	0.014	59.486	25.864
Ue470t208	4.7	2.08	30.03	13.5	0.144	0.204	0.066	0.058	2.163	0.006	0.014	58.426	25.403
Ue490t208	4.9	2.08	32.65	16.2	0.132	0.216	0.061	0.053	2.136	0.006	0.014	52.210	22.700
Ue510t208	5.1	2.08	32.01	14.57	0.153	0.225	0.070	0.061	2.183	0.006	0.014	63.249	27.500
Ue530t208	5.3	2.08	32.89	13.05	0.13	0.21	0.060	0.052	2.131	0.006	0.014	51.198	22.260
Ue540t208	5.4	2.08	41.32	16.65	0.165	0.238	0.076	0.066	2.210	0.006	0.014	69.894	30.389
Ue550t208	5.5	2.08	35.3	14.34	0.16	0.231	0.074	0.064	2.199	0.006	0.014	67.096	29.172

Table A.4: The measured and calculated slamming forces- Large cylinder [wave period 2.22s]

Test	e	T (s)	Total Response (N)	Measured Slamming Force (N)	η_b (m)	H_b (m)	$\lambda\eta_b$ (m) W & O	$\lambda\eta_b$ (m) Goda	C_b (m/s)	τ (s) W & O	τ (s) Goda	Calculated Slamming Force (N) W & O	Calculated Slamming Force (N) Goda
Ue440t222	4.4	2.22	20.02	7.84	0.16	0.232	0.074	0.064	2.199	0.006	0.014	67.096	29.172
Ue450t222	4.5	2.22	28.91	16.46	0.158	0.231	0.073	0.063	2.195	0.006	0.014	65.988	28.691
Ue460t222	4.6	2.22	40.74	19.89	0.159	0.22	0.073	0.064	2.197	0.006	0.014	66.541	28.931
Ue470t222	4.7	2.22	35.98	20.09	0.161	0.224	0.074	0.064	2.201	0.006	0.014	67.652	29.414
Ue490t222	4.9	2.22	49.46	26.39	0.148	0.218	0.068	0.059	2.172	0.006	0.014	60.553	26.327
Ue510t222	5.1	2.22	35.1	14.06	0.171	0.244	0.079	0.068	2.224	0.005	0.013	73.309	31.873
Ue530t222	5.3	2.22	37.97	19.23	0.179	0.242	0.082	0.072	2.241	0.005	0.013	77.956	33.894
Ue540t222	5.4	2.22	47.19	24.94	0.165	0.229	0.076	0.066	2.210	0.006	0.014	69.894	30.389
Ue550t222	5.5	2.22	44.6	23.13	0.142	0.215	0.065	0.057	2.159	0.006	0.014	57.373	24.945

Table A.5: The measured and calculated slamming forces- Small cylinder [wave period 1.85s]

Test	e	T (s)	Total Response (N)	Measured Slamming Force (N)	η_b (m)	H_b (m)	$\lambda\eta_b$ (m) W & O	$\lambda\eta_b$ (m) Goda	C_b (m/s)	τ (s) W & O	τ (s) Goda	Calculated Slamming Force (N) W & O	Calculated Slamming Force (N) Goda
Ue410t185	4.1	1.85	6.16	2.35	0.156	0.21	0.072	0.062	2.190	0.001	0.004	17.303	7.523
Ue420t185	4.2	1.85	6.69	3.52	0.204	0.218	0.094	0.082	2.295	0.001	0.003	24.849	10.804
Ue430t185	4.3	1.85	6.27	3.3	0.158	0.221	0.073	0.063	2.195	0.001	0.004	17.597	7.651
Ue440t185	4.4	1.85	5.52	2.1	0.163	0.232	0.075	0.065	2.206	0.001	0.004	18.339	7.973
Ue450t185	4.5	1.85	5.54	3.26	0.17	0.239	0.078	0.068	2.221	0.001	0.004	19.396	8.433
Ue460t185	4.6	1.85	6.34	3.23	0.168	0.234	0.077	0.067	2.217	0.001	0.004	19.092	8.301
Ue470t185	4.7	1.85	5.89	5.52	0.165	0.232	0.076	0.066	2.210	0.001	0.004	18.638	8.104
Ue490t185	4.9	1.85	7.07	5.05	0.172	0.233	0.079	0.069	2.226	0.001	0.004	19.702	8.566
Ue510t185	5.1	1.85	7.29	4.48	0.156	0.223	0.072	0.062	2.190	0.001	0.004	17.303	7.523
Ue530t185	5.3	1.85	8.79	8.22	0.139	0.209	0.064	0.056	2.152	0.002	0.004	14.882	6.470
Ue540t185	5.4	1.85	8.29	10.75	0.152	0.219	0.070	0.061	2.181	0.001	0.004	16.722	7.270
Ue550t185	5.5	1.85	9.45	10.47	0.131	0.197	0.060	0.052	2.134	0.002	0.004	13.788	5.995

Table A.6: The measured and calculated slamming forces- Small cylinder [wave period 1.96s]

Test	e	T (s)	Total Response (N)	Measured Slamming Force (N)	η_b (m)	H_b (m)	$\lambda\eta_b$ (m)		C_b (m/s)	τ (s)		Calculated Slamming Force (N)	
							W & O	Goda		W & O	Goda	W & O	Goda
Ue410t196	4.1	1.96	4.95	2.47	0.172	0.227	0.079	0.069	2.226	0.001	0.004	19.702	8.566
Ue420t196	4.2	1.96	5.98	2.95	0.16	0.221	0.074	0.064	2.199	0.001	0.004	17.892	7.779
Ue430t196	4.3	1.96	5.87	3.64	0.149	0.217	0.069	0.060	2.174	0.001	0.004	16.290	7.083
Ue440t196	4.4	1.96	6.67	5.57	0.154	0.218	0.071	0.062	2.186	0.001	0.004	17.012	7.396
Ue450t196	4.5	1.96	6.67	3.47	0.152	0.223	0.070	0.061	2.181	0.001	0.004	16.722	7.270
Ue460t196	4.6	1.96	6.38	4.85	0.153	0.217	0.070	0.061	2.183	0.001	0.004	16.866	7.333
Ue470t196	4.7	1.96	6.88	2.37	0.168	0.224	0.077	0.067	2.217	0.001	0.004	19.092	8.301
Ue490t196	4.9	1.96	7.4	4.96	0.119	0.181	0.055	0.048	2.106	0.002	0.004	12.201	5.305
Ue510t196	5.1	1.96	6.85	5.02	0.119	0.191	0.055	0.048	2.106	0.002	0.004	12.201	5.305

Table A.7: The measured and calculated slamming forces- Small cylinder [wave period 2.08s]

Test	e	T (s)	Total Response (N)	Measured Slamming Force (N)	η_b (m)	H_b (m)	$\lambda\eta_b$ (m) W & O	$\lambda\eta_b$ (m) Goda	C_b (m/s)	τ (s) W & O	τ (s) Goda	Calculated Slamming Force (N) W & O	Calculated Slamming Force (N) Goda
Ue410t208	4.1	2.08	6.56	3.16	0.153	0.209	0.070	0.061	2.183	0.001	0.004	16.866	7.333
Ue420t208	4.2	2.08	5.99	2.38	0.146	0.207	0.067	0.058	2.168	0.001	0.004	15.863	6.897
Ue430t208	4.3	2.08	5.68	1.55	0.144	0.211	0.066	0.058	2.163	0.002	0.004	15.580	6.774
Ue440t208	4.4	2.08	6.39	2.97	0.146	0.214	0.067	0.058	2.168	0.001	0.004	15.863	6.897
Ue450t208	4.5	2.08	6.56	2.9	0.148	0.208	0.068	0.059	2.172	0.001	0.004	16.147	7.021
Ue460t208	4.6	2.08	6.32	2.77	0.146	0.224	0.067	0.058	2.168	0.001	0.004	15.863	6.897
Ue470t208	4.7	2.08	6.22	1.95	0.144	0.204	0.066	0.058	2.163	0.002	0.004	15.580	6.774
Ue490t208	4.9	2.08	5.03	3.08	0.132	0.216	0.061	0.053	2.136	0.002	0.004	13.923	6.053
Ue510t208	5.1	2.08	8.91	6.91	0.153	0.225	0.070	0.061	2.183	0.001	0.004	16.866	7.333
Ue530t208	5.3	2.08	6.98	8.28	0.13	0.21	0.060	0.052	2.131	0.002	0.004	13.653	5.936
Ue540t208	5.4	2.08	6.56	5.2	0.165	0.238	0.076	0.066	2.210	0.001	0.004	18.638	8.104
Ue550t208	5.5	2.08	8.74	10.21	0.16	0.231	0.074	0.064	2.199	0.001	0.004	17.892	7.779

Table A.8: The measured and calculated slamming forces- Small cylinder [wave period2.22s]

Test	e	T (s)	Total Response (N)	Measured Slamming Force (N)	η_b (m)	H_b (m)	λ_{nb} (m)		C_b (m/s)	τ (s)		Calculated Slamming Force (N)	
							W & O	Goda		W & O	Goda	W & O	Goda
Ue430t222	4.3	2.22	6	2.15	0.151	0.219	0.069	0.060	2.179	0.001	0.004	16.577	7.208
Ue440t222	4.4	2.22	6.16	2.47	0.16	0.232	0.074	0.064	2.199	0.001	0.004	17.892	7.779
Ue450t222	4.5	2.22	6.31	2.88	0.158	0.231	0.073	0.063	2.195	0.001	0.004	17.597	7.651
Ue460t222	4.6	2.22	7.12	3.26	0.159	0.22	0.073	0.064	2.197	0.001	0.004	17.744	7.715
Ue470t222	4.7	2.22	7.98	2.96	0.161	0.224	0.074	0.064	2.201	0.001	0.004	18.041	7.844
Ue490t222	4.9	2.22	7.95	3.05	0.148	0.218	0.068	0.059	2.172	0.001	0.004	16.147	7.021
Ue510t222	5.1	2.22	7.8	3.32	0.171	0.244	0.079	0.068	2.224	0.001	0.004	19.549	8.500
Ue530t222	5.3	2.22	7.91	3.08	0.179	0.242	0.082	0.072	2.241	0.001	0.004	20.788	9.038
Ue540t222	5.4	2.22	7.53	4.5	0.165	0.229	0.076	0.066	2.210	0.001	0.004	18.638	8.104
Ue550t222	5.5	2.22	7.24	3.08	0.142	0.215	0.065	0.057	2.159	0.002	0.004	15.300	6.652

Table A.9: The measured and calculated slamming forces- Front section [wave period 1.85s]

Test	e	T (s)	Total Response (N)	Measured Slamming Force (N)	η_b (m)	H_b (m)	$\lambda\eta_b$ (m) W & O	$\lambda\eta_b$ (m) Goda	C_b (m/s)	τ (s) W & O	τ (s) Goda	I (m) W & O	I (m) Goda	Calculated Slamming Force (N) W & O	Calculated Slamming Force (N) Goda
Ue360t185	3.6	1.85	14.2	2.57	0.154	0.204	0.071	0.062	2.186	0.001	0.004	0.310	0.270	89.891	39.083
Ue370t185	3.7	1.85	22.31	6.49	0.146	0.212	0.067	0.058	2.168	0.001	0.004	0.294	0.256	83.822	36.444
Ue380t185	3.8	1.85	22.81	7.89	0.158	0.211	0.073	0.063	2.195	0.001	0.004	0.318	0.277	92.984	40.428
Ue390t185	3.9	1.85	22.37	6.22	0.163	0.223	0.075	0.065	2.206	0.001	0.004	0.328	0.285	96.903	42.132
Ue400t185	4	1.85	26.15	6.2	0.143	0.206	0.066	0.057	2.161	0.002	0.004	0.288	0.250	81.585	35.472
Ue410t185	4.1	1.85	23.83	5.23	0.15	0.213	0.069	0.060	2.177	0.001	0.004	0.302	0.263	86.837	37.755
Ue420t185	4.2	1.85	24.34	6.6	0.16	0.22	0.074	0.064	2.199	0.001	0.004	0.322	0.280	94.544	41.106
Ue430t185	4.3	1.85	24.3	7.08	0.151	0.2	0.069	0.060	2.179	0.001	0.004	0.304	0.264	87.597	38.086
Ue440t185	4.4	1.85	26.29	10.03	0.157	0.22	0.072	0.063	2.192	0.001	0.004	0.316	0.275	92.207	40.090
Ue450t185	4.5	1.85	30.8	9.12	0.15	0.213	0.069	0.060	2.177	0.001	0.004	0.302	0.263	86.837	37.755
Ue460t185	4.6	1.85	32.03	9.91	0.153	0.22	0.070	0.061	2.183	0.001	0.004	0.308	0.268	89.124	38.750
Ue480t185	4.8	1.85	32.29	8.68	0.161	0.227	0.074	0.064	2.201	0.001	0.004	0.324	0.282	95.328	41.447
Ue500t185	5	1.85	32.03	7.87	0.181	0.245	0.083	0.072	2.246	0.001	0.004	0.365	0.317	111.509	48.482
Ue520t185	5.2	1.85	33.63	7.53	0.169	0.237	0.078	0.068	2.219	0.001	0.004	0.340	0.296	101.685	44.211

Table A.10: The measured and calculated slamming forces- Front section [wave period 1.96s]

Test	e	T (s)	Total Response (N)	Measured Slamming Force (N)	η_b (m)	H_b (m)	$\lambda\eta_b$ (m)		C_b (m/s)	τ (s)		l (m)		Calculated Slamming Force (N)	
							W & O	Goda		W & O	Goda	W & O	Goda	W & O	Goda
Ue380t196	3.8	1.96	12	0.97	0.161	0.215	0.074	0.064	2.201	0.001	0.004	0.324	0.282	95.328	41.447
Ue390t196	3.9	1.96	14.31	2.09	0.174	0.235	0.080	0.070	2.230	0.001	0.004	0.350	0.305	105.737	45.972
Ue410t196	4.1	1.96	18.02	2.61	0.168	0.223	0.077	0.067	2.217	0.001	0.004	0.338	0.294	100.882	43.862
Ue420t196	4.2	1.96	21.42	6.33	0.159	0.212	0.073	0.064	2.197	0.001	0.004	0.320	0.278	93.763	40.766
Ue430t196	4.3	1.96	21.86	3.45	0.158	0.217	0.073	0.063	2.195	0.001	0.004	0.318	0.277	92.984	40.428
Ue440t196	4.4	1.96	24.17	6.55	0.166	0.227	0.076	0.066	2.213	0.001	0.004	0.334	0.291	99.283	43.167
Ue450t196	4.5	1.96	26.91	7.27	0.172	0.225	0.079	0.069	2.226	0.001	0.004	0.346	0.301	104.109	45.265
Ue460t196	4.6	1.96	27.65	6.95	0.163	0.23	0.075	0.065	2.206	0.001	0.004	0.328	0.285	96.903	42.132
Ue480t196	4.8	1.96	29.45	10.15	0.177	0.236	0.081	0.071	2.237	0.001	0.004	0.357	0.310	108.196	47.042

Table A.11: The measured and calculated slamming forces- Front Section [wave period 2.08s]

Test	e	T (s)	Total Response (N)	Measured Slamming Force (N)	η_b (m)	H_b (m)	$\lambda\eta_b$ (m)		C_b (m/s)	τ (s)		l (m)		Calculated Slamming Force (N)	
							W & O	Goda		W & O	Goda	W & O	Goda	W & O	Goda
Ue380t208	3.8	2.08	19.44	10.09	0.153	0.215	0.070	0.061	2.183	0.001	0.004	0.308	0.268	89.124	38.750
Ue390t208	3.9	2.08	22.75	6.14	0.145	0.208	0.067	0.058	2.165	0.002	0.004	0.292	0.254	83.074	36.119
Ue400t208	4	2.08	23.94	6.29	0.159	0.223	0.073	0.064	2.197	0.001	0.004	0.320	0.278	93.763	40.766
Ue410t208	4.1	2.08	24.59	7.75	0.136	0.203	0.063	0.054	2.145	0.002	0.004	0.274	0.238	76.450	33.239
Ue420t208	4.2	2.08	24.35	6.04	0.148	0.216	0.068	0.059	2.172	0.001	0.004	0.298	0.259	85.325	37.098
Ue430t208	4.3	2.08	27.28	6.68	0.132	0.204	0.061	0.053	2.136	0.002	0.004	0.266	0.231	73.569	31.987
Ue440t208	4.4	2.08	31.54	13.46	0.137	0.208	0.063	0.055	2.147	0.002	0.004	0.276	0.240	77.177	33.555
Ue450t208	4.5	2.08	24.94	4.88	0.159	0.222	0.073	0.064	2.197	0.001	0.004	0.320	0.278	93.763	40.766
Ue460t208	4.6	2.08	27.17	10.5	0.157	0.23	0.072	0.063	2.192	0.001	0.004	0.316	0.275	92.207	40.090
Ue480t208	4.7	2.08	31.22	12.04	0.146	0.215	0.067	0.058	2.168	0.001	0.004	0.294	0.256	83.822	36.444
Ue520t208	5.2	2.08	34.33	15.1	0.158	0.231	0.073	0.063	2.195	0.001	0.004	0.318	0.277	92.984	40.428
Ue540t208	5.4	2.08	34.49	11.69	0.147	0.23	0.068	0.059	2.170	0.001	0.004	0.296	0.257	84.572	36.770

Table A.12: The measured and calculated slamming forces- Front Section [wave period 2.22s]

Test	e	T (s)	Total Response (N)	Measured Slamming Force (N)	η_b (m)	H_b (m)	$\lambda\eta_b$ (m) W & O	$\lambda\eta_b$ (m) Goda	C_b (m/s)	τ (s) W & O	τ (s) Goda	l (m) W & O	l (m) Goda	Calculated Slamming Force (N) W & O	Calculated Slamming Force (N) Goda
Ue420t222	4.2	2.22	17.28	3.04	0.164	0.228	0.075	0.066	2.208	0.001	0.004	0.330	0.287	97.694	42.476
Ue430t222	4.3	2.22	20.86	8.87	0.152	0.218	0.070	0.061	2.181	0.001	0.004	0.306	0.266	88.359	38.417
Ue440t222	4.4	2.22	24.07	6.68	0.167	0.232	0.077	0.067	2.215	0.001	0.004	0.336	0.293	100.082	43.514
Ue450t222	4.5	2.22	27.94	9.35	0.152	0.216	0.070	0.061	2.181	0.001	0.004	0.306	0.266	88.359	38.417
Ue460t222	4.6	2.22	28.89	8.29	0.162	0.234	0.075	0.065	2.204	0.001	0.004	0.326	0.284	96.114	41.789
Ue480t222	4.8	2.22	37.48	11.52	0.157	0.232	0.072	0.063	2.192	0.001	0.004	0.316	0.275	92.207	40.090
Ue500t222	5	2.22	32.97	11.06	0.17	0.239	0.078	0.068	2.221	0.001	0.004	0.342	0.298	102.491	44.561
Ue520t222	5.2	2.22	36.08	10.28	0.15	0.219	0.069	0.060	2.177	0.001	0.004	0.302	0.263	86.837	37.755
Ue525t222	5.25	2.22	35.79	9.6	0.165	0.238	0.076	0.066	2.210	0.001	0.004	0.332	0.289	98.487	42.821
Ue530t222	5.3	2.22	31.32	8.61	0.175	0.238	0.081	0.070	2.232	0.001	0.004	0.352	0.307	106.554	46.328
Ue540t222	5.4	2.22	35.75	8.22	0.164	0.243	0.075	0.066	2.208	0.001	0.004	0.330	0.287	97.694	42.476

Table A.13: The measured and calculated slamming forces- Side Section [wave period 1.85s]

Test	e	T (s)	Total Response (N)	Measured Slamming Force (N)	η_b (m)	H_b (m)	$\lambda\eta_b$ (m)		C_b (m/s)	τ (s)		Calculated Slamming Force (N)	
							W & O	Goda		W & O	Goda	W & O	Goda
Ue420t185	4.2	1.85	8.86	3.92	0.169	0.222	0.078	0.068	2.219	0.001	0.004	19.244	8.367
Ue440t185	4.4	1.85	5.7	1.43	0.157	0.227	0.072	0.063	2.192	0.001	0.004	17.450	7.587
Ue460t185	4.6	1.85	8.35	4.05	0.163	0.233	0.075	0.065	2.206	0.001	0.004	18.339	7.973
Ue480t185	4.8	1.85	7.07	2.44	0.164	0.232	0.075	0.066	2.208	0.001	0.004	18.488	8.038
Ue490t185	4.9	1.85	8.7	2.82	0.166	0.235	0.076	0.066	2.213	0.001	0.004	18.789	8.169
Ue500t185	5	1.85	8.36	2.6	0.187	0.258	0.086	0.075	2.259	0.001	0.004	22.057	9.590
Ue510t185	5.1	1.85	8.48	3.02	0.168	0.237	0.077	0.067	2.217	0.001	0.004	19.092	8.301
Ue530t185	5.3	1.85	8.65	3.64	0.163	0.231	0.075	0.065	2.206	0.001	0.004	18.339	7.973
Ue550t185	5.5	1.85	8.65	6.27	0.111	0.177	0.051	0.044	2.087	0.002	0.004	11.179	4.860
Ue610t185	6.1	1.85	9.02	4.25	0.111	0.177	0.051	0.044	2.087	0.002	0.004	11.179	4.860

Table A.14: The measured and calculated slamming forces- Side Section [wave period 1.96s]

Test	e	T (s)	Total Response (N)	Measured Slamming Force (N)	η_b (m)	H_b (m)	$\lambda\eta_b$ (m) W & O	$\lambda\eta_b$ (m) Goda	C_b (m/s)	τ (s) W & O	τ (s) Goda	Calculated Slamming Force (N) W & O	Calculated Slamming Force (N) Goda
Ue460t196	4.6	1.96	7.8	2.38	0.16	0.219	0.074	0.064	2.199	0.001	0.004	17.892	7.779
Ue480t196	4.8	1.96	9.69	3.86	0.17	0.224	0.078	0.068	2.221	0.001	0.004	19.396	8.433
Ue490t196	4.9	1.96	8.17	3.23	0.17	0.225	0.078	0.068	2.221	0.001	0.004	19.396	8.433
Ue500t196	5	1.96	8.21	1.85	0.164	0.225	0.075	0.066	2.208	0.001	0.004	18.488	8.038
Ue510t196	5.1	1.96	8.07	1.6	0.16	0.213	0.074	0.064	2.199	0.001	0.004	17.892	7.779
Ue530t196	5.3	1.96	5.62	3.32	0.162	0.228	0.075	0.065	2.204	0.001	0.004	18.189	7.908
Ue550t196	5.5	1.96	9.27	2.89	0.137	0.2	0.063	0.055	2.147	0.002	0.004	14.605	6.350
Ue610t196	6.1	1.96	9.03	3.11	0.108	0.186	0.050	0.043	2.080	0.002	0.004	10.803	4.697
Ue650t196	6.5	1.96	13.22	5.77	0.168	0.26	0.077	0.067	2.217	0.001	0.004	19.092	8.301
Ue670t196	6.7	1.96	9.54	2.52	0.17	0.248	0.078	0.068	2.221	0.001	0.004	19.396	8.433

Table A.15: The measured and calculated slamming forces- Side Section [wave period 2.08s]

Test	e	T (s)	Total Response (N)	Measured Slamming Force (N)	η_b (m)	H_b (m)	$\lambda\eta_b$ (m)		C_b (m/s)	τ (s)		Calculated Slamming Force (N)	
							W & O	Goda		W & O	Goda	W & O	Goda
Ue460t208	4.6	2.08	7.1	2.42	0.162	0.223	0.075	0.065	2.204	0.001	0.004	18.189	7.908
Ue480t208	4.8	2.08	7.11	2.27	0.158	0.227	0.073	0.063	2.195	0.001	0.004	17.597	7.651
Ue490t208	4.9	2.08	6.68	2.3	0.161	0.231	0.074	0.064	2.201	0.001	0.004	18.041	7.844
Ue500t208	5	2.08	8.4	3.06	0.158	0.23	0.073	0.063	2.195	0.001	0.004	17.597	7.651
Ue510t208	5.1	2.08	7.31	2.1	0.147	0.215	0.068	0.059	2.170	0.001	0.004	16.005	6.959
Ue530t208	5.3	2.08	7.52	2.42	0.159	0.23	0.073	0.064	2.197	0.001	0.004	17.744	7.715
Ue550t208	5.5	2.08	8.2	2.75	0.164	0.236	0.075	0.066	2.208	0.001	0.004	18.488	8.038
Ue610t208	6.1	2.08	10.16	2.86	0.153	0.224	0.070	0.061	2.183	0.001	0.004	16.866	7.333

Table A.16: The measured and calculated slamming forces- Side Section [wave period 2.22s]

Test	e	T (s)	Total Response (N)	Measured Slamming Force (N)	η_b (m)	H_b (m)	$\lambda \eta_b$ (m)		C_b (m/s)	τ (s)		Calculated Slamming Force (N)	
							W & O	Goda		W & O	Goda	W & O	Goda
Ue460t222	4.6	2.22	7.4	1.93	0.154	0.214	0.071	0.062	2.186	0.001	0.004	17.012	7.396
Ue480t222	4.8	2.22	7.74	2.13	0.161	0.223	0.074	0.064	2.201	0.001	0.004	18.041	7.844
Ue490t222	4.9	2.22	7.65	2.33	0.158	0.218	0.073	0.063	2.195	0.001	0.004	17.597	7.651
Ue500t222	5	2.22	9.21	2.6	0.197	0.265	0.091	0.079	2.280	0.001	0.004	23.683	10.297
Ue510t222	5.1	2.22	8.54	1.75	0.154	0.23	0.071	0.062	2.186	0.001	0.004	17.012	7.396
Ue530t222	5.3	2.22	8.82	2.05	0.155	0.222	0.071	0.062	2.188	0.001	0.004	17.157	7.460
Ue550t222	5.5	2.22	8.86	2.3	0.149	0.222	0.069	0.060	2.174	0.001	0.004	16.290	7.083
Ue570t222	5.7	2.22	12.27	3.91	0.153	0.231	0.070	0.061	2.183	0.001	0.004	16.866	7.333
Ue610t222	6.1	2.22	10.61	3.07	0.147	0.226	0.068	0.059	2.170	0.001	0.004	16.005	6.959
Ue630t222	6.3	2.22	12.73	5.69	0.114	0.199	0.052	0.046	2.094	0.002	0.004	11.559	5.026

Table A.17: The measured and calculated slamming forces- Side Section [for new slope 1:20]

Test	e	T (s)	Total Response (N)	Measured Slamming Force (N)	η_b (m)	H_b (m)	$\lambda\eta_b$ (m) W & O	$\lambda\eta_b$ (m) Goda	C_b (m/s)	τ (s) W & O	τ (s) Goda	Calculated Slamming Force (N) W & O	Calculated Slamming Force (N) Goda
Ue490t185	4.9	1.85	8.52	2.14	0.166	0.226	0.076	0.066	2.213	0.001	0.004	18.789	8.169
Ue490t196	4.9	1.96	8.39	1.66	0.168	0.228	0.077	0.067	2.217	0.001	0.004	19.092	8.301
Ue490t208	4.9	2.08	8.45	2.59	0.182	0.247	0.084	0.073	2.248	0.001	0.004	21.261	9.244
Ue500t185	5	1.85	8.85	2.82	0.172	0.232	0.079	0.069	2.226	0.001	0.004	19.702	8.566
Ue500t196	5	1.96	7.36	1.35	0.151	0.217	0.069	0.060	2.179	0.001	0.004	16.577	7.208
Ue500t208	5	2.08	9.43	2.16	0.177	0.239	0.081	0.071	2.237	0.001	0.004	20.476	8.903
Ue500t222	5	2.22	10.05	2.39	0.163	0.218	0.075	0.065	2.206	0.001	0.004	18.339	7.973
Ue510t196	5.1	1.96	8.78	1.99	0.167	0.22	0.077	0.067	2.215	0.001	0.004	18.940	8.235
Ue510t208	5.1	2.08	9.96	2.72	0.18	0.253	0.083	0.072	2.243	0.001	0.004	20.945	9.107
Ue510t222	5.1	2.22	9.3	2.32	0.158	0.218	0.073	0.063	2.195	0.001	0.004	17.597	7.651
Ue520t185	5.2	1.85	7.8	2.71	0.162	0.221	0.075	0.065	2.204	0.001	0.004	18.189	7.908
Ue520t196	5.2	1.96	9.46	2.95	0.15	0.215	0.069	0.060	2.177	0.001	0.004	16.434	7.145
Ue520t208	5.2	2.08	11.84	3.12	0.18	0.244	0.083	0.072	2.243	0.001	0.004	20.945	9.107
Ue520t222	5.2	2.22	10.56	2.62	0.153	0.211	0.070	0.061	2.183	0.001	0.004	16.866	7.333

APPENDIX B

There are two sample Matlab codes that used for the data analysis are given in this appendix, one is FRF method for side section and another is Duhamel integral approach for large cylinder.

Matlab code for analysis of data based on FRF method for side section of the truss is given below.

```matlab
close all
clear all
load('Sidepanel_hammer1.mat','Uhamsp3');
Data=Uhamsp3;
U='Uhamsp3';
t1=1/19200:1/19200:length(Data)*1/19200;
T=t1';
D=1:length(Data);
fst=Data(:,3); fsb=Data(:,1); flt=Data(:,4); flb=Data(:,2);
fstot=fsb+fst; fltot=flb+flt;
Fham=Data(:,5); %Hammer Force

figure
plot(Data);
[Dmin,yy1]=ginput(1);
[Dmax,yy2]=ginput(1);

t=T(Dmin:Dmax);
dd=Dmax-Dmin;
d=2^nextpow2(dd);
Tmin=Dmin/19200;
Tmax=Dmax/19200;

% Extracted portion of data
Ftotl=fltot(Dmin:Dmax);
Ftots=fstot(Dmin:Dmax);Fst=fst(Dmin:Dmax); Fsb=fsb(Dmin:Dmax);
Flt=flt(Dmin:Dmax); Flb=flb(Dmin:Dmax);

hammer=Fham(Dmin:Dmax);
m=mean(Fham(1:50000));
offset=m;
Hammer=hammer-offset;
figure
h=plot(t,Ftotl,'-',t,Hammer,':');
set(h,'linewidth',2);
%axis([7.2 7.4 -60 100]);
xlabel('Time [s]','fontsize',12);ylabel('Force [N]','fontsize',12);
title(['Test: ',U,'    ','Data Points: ',num2str(round(Dmin)),'-
',num2str(round(Dmax))],'fontsize',12);
legend('Total','Hammer');
grid

figure
h=plot(t,Flt,'-',t,Flb,':',t,Hammer,'-');
xlabel('Time [s]','fontsize',12); ylabel('Force [N]','fontsize',12);
title(['Test: ',U,'    ','Data Points: ',num2str(round(Dmin)),'-
',num2str(round(Dmax))],'fontsize',12);
legend('Top-Large','Bottom-Large','Hammer');
set(h,'linewidth',2);
grid

y1=fft(Hammer,d);
yham=y1.*conj(y1)/d;

y2=fft(Ftotl,d);
yftotl=y2.*conj(y2)/d;
```

```
ytotl=ifft(y2);
f=19200.*(0:d/2)/d;
ff=f./19200;

figure
h=plot(f(1:100),yftotl(1:100));
set(h,'linewidth',2);
xlabel('Frequency, Hz','fontsize',12); ylabel('Relative
Values','fontsize',12);
title(['Test: ',U,'    ','Data Points: ',num2str(round(Dmin)),'-
',num2str(round(Dmax)),'    ','Power Spectrum-Total Forces'],'fontsize',12);
set(gca,'fontsize',12,'linewidth',2);
grid


H=yftotl./yham;
HH=y2./y1;
PHH=2*HH.*conj(HH);


SFF=y2./HH;
FFF=ifft(SFF);

figure
h=plot(f(1:150),yham(1:150),'-',f(1:150),yftotl(1:150),':');
set(h,'linewidth',2);
xlabel('Frequency, Hz','fontsize',12); ylabel('Relative
Values','fontsize',12);
title(['Test: ',U,'    ','Data Points: ',num2str(round(Dmin)),'-
',num2str(round(Dmax)),'    ','Power Spectrum'],'fontsize',12);
legend('Hammer Force','Total Force');
set(gca,'fontsize',12,'linewidth',2)
grid


figure
h=plot(f(1:100),y1(1:100),'-',f(1:100),y2(1:100),':');
set(h,'linewidth',2);
xlabel('Frequency, Hz','fontsize',12);
ylabel('Force, N','fontsize',12);
title(['Test: ',U,'    ','Data Points: ',num2str(round(Dmin)),'-
',num2str(round(Dmax)),'    '],'fontsize',12);
legend('Hammer Force','Total Force');
set(gca,'fontsize',12,'linewidth',2)
grid


figure
h=semilogy(f(1:100),PHH(1:100));
set(h,'linewidth',2);
xlabel('Frequency, Hz','fontsize',12);
ylabel('Transfer Function','fontsize',12);
title(['Test: ',U,'    ','Data Points: ',num2str(round(Dmin)),'-
',num2str(round(Dmax)),'    ','Transfer Function Squared'],'fontsize',12);
set(gca,'fontsize',12,'linewidth',2)
grid
```

```matlab
%%% Wave Data Analysis

load('Sidepanel_waves.mat','Ue610t196');
wdata=Ue610t196;
W='Ue610t196';

wt=1/19200*(1:length(wdata));
wftl=wdata(:,4); wfbl=wdata(:,2); wfts=wdata(:,3); wfbs=wdata(:,1);
wftotl=wftl+wfbl; wftots=wfts+wfbs;
figure
plot(wftotl);
w1=wdata(:,5); w2=wdata(:,6); w3=wdata(:,7); w4=wdata(:,8);

plot(wftotl); hold on
plot(w2,'g');
[wdmin,wyyy1]=ginput(1);
[wdmax,wyyy2]=ginput(1);
wdif=wdmax-wdmin;

if wdif<=dd;
    wdif;
else wdif=dd;
end

wd=2^nextpow2(wdif);
wtmin=wdmin/19200;
wtmax=wdmax/19200;
wtt=wt(wdmin:wdmax);
wtopl=wftl(wdmin:wdmax); wbotl=wfbl(wdmin:wdmax); wtops=wfts(wdmin:wdmax);
wbots=wfbs(wdmin:wdmax);
wtotl=wftotl(wdmin:wdmax); wtots=wftots(wdmin:wdmax);

wave1=w1(wdmin:wdmax); wave2=w2(wdmin:wdmax); wave3=w3(wdmin:wdmax);
wave4=w4(wdmin:wdmax);

figure
h=plot(wtt,wtopl,'-',wtt,wbotl,':');
set(h,'linewidth',2);
xlabel('Time, s','fontsize',12);
ylabel('Response Force, N','fontsize',12);
title(['Test: ',W,'    ','Data Points: ',num2str(round(wdmin)),'-
',num2str(round(wdmax)),'    ','Response Forces'],'fontsize',12);
legend('Top','Bottom','fontsize',12);
set(gca,'fontsize',12,'linewidth',2)
grid

figure
h=plot(wtt,wave1,'-',wtt,wave2,':',wtt,wave3,'-',wtt,wave4,':');
set(h,'linewidth',2);
xlabel('Time, s','fontsize',12);
ylabel('Wave Height, cm','fontsize',12);
title(['Test: ',W,'    ','Data Points: ',num2str(round(wdmin)),'-
',num2str(round(wdmax)),'    ','Waves'],'fontsize',12);
legend('Wave at deep water','Wave in front of structure1','Wave in front of
structure2','Wave at structure','fontsize',12);
set(gca,'fontsize',12,'linewidth',2)
grid

figure
```

```matlab
h=plot(wtt,wtotl,'-',wtt,wave1,':',wtt,wave3,'-',wtt,wave4,':');
set(h,'linewidth',2);
xlabel('Time, s','fontsize',12);
ylabel('Force, N. Wave Height, cm,','fontsize',12);
title(['Test: ',W,'    ','Data Points: ',num2str(round(wdmin)),'-
',num2str(round(wdmax)),'   ','Total Response Forces,
Waves'],'fontsize',12);
legend('Total Force','Wave at deep water','Wave in front of
structure1','Wave at structure','fontsize',12);
set(gca,'fontsize',12,'linewidth',2)
grid

[b,a]=butter(2,6/9600,'low');
wy=filtfilt(b,a,wtotl);
wye=wtotl-wy;

figure
plot(wtt,wy,'g',wtt,wye,'r',wtt,wtotl,'b');
xlabel('Time,sec','fontsize',12)
ylabel('Force, N.','fontsize',12);
title(['Test: ',W,'    ','Data Points: ',num2str(round(wdmin)),'-
',num2str(round(wdmax)),'   ','Forces'],'fontsize',12);
legend('Filtered Total Force','Total Force-Filtered','Total Force');
grid on;

wyy=filtfilt(b,a,wye);
wyye=wye-wyy;

wff=fft(wyye,wd);
wp=wff.*conj(wff)/wd;
wifft=ifft(wff,wd);
wpff=wyye.*conj(wyye)/wd;




figure
plot(f(1:100),wp(1:100));
xlabel('Frequency, Hz','fontsize',12); ylabel('Relative
Values','fontsize',12);
title(['Test: ',W,'  ',U,'    ','Data Points: ',num2str(round(wdmin)),'-
',num2str(round(wdmax)),'   ','Power Spectrum of Response
Forces'],'fontsize',12);
grid

f1=19200.*(0:wd/2)/wd;

sf=wff./HH;
pff=sf.*conj(sf)/wd;
fff=ifft(sf,wd);

tx=(wtt(end)+1/19200:1/19200:(wd-length(wtt))/19200+wtt(end));

if length(wtt)>=wd;
    wtt1=wtt(:,1:wd);
else wtt1=[wtt,tx];
end

figure
plot(wtt1,fff);
xlabel('Time,sec','fontsize',12); ylabel('Force, N.','fontsize',12);
```

```matlab
title(['Test: ',W,'   ',U,'    ','Data Points: ',num2str(round(wdmin)),'-
',num2str(round(wdmax)),'   ','IFFT(S(w)/H(w))=SS(w)'],'fontsize',12);
grid;


[b1,a1]=butter(2,200/9600,'low');
wdfilter=filtfilt(b1,a1,fff);


figure
plot(wtt1,wdfilter,'-');
xlabel('Time,sec','fontsize',12); ylabel('Force, N.','fontsize',12);
title(['Test: ',W,'   ',U,'    ','Data Points: ',num2str(round(wdmin)),'-
',num2str(round(wdmax)),'   ','Filtered
IFFT(S(w)/H(w))=SS(w)'],'fontsize',12);
grid;


Rmax=max(wtotl)
Fsm=max(wdfilter)
ncrest=max(wave2)/100
Hb=min(wave2)*(-1/100)+ncrest
disp('Thank You')
```

The matlab code for the Duhamel integral approach is given below.

```matlab
clear all
close all

load('Wye440185.mat');
wdmin=1350;
wdmax=1700;
tmin=wdmin/19200;
tmax=wdmax/19200;
tdif=tmax-tmin;
wdif=wdmax-wdmin;


Fo=9.5;
Tp=0.00001;
Td=0.006;
tr=20.474;
Tn=0.0025;
ten=0.009;%Varighet (Duration)
time1=(0:1/19200:Tp);
X1=Fo*(time1./Tp);
time=(0:1/19200:Td);
time2=(0:1/19200:tdif);


X2=(Fo/(Td-Tp))*(Td-time);
X=[X1,X2(Tp/(1/19200)+1:Td/(1/19200))];
f6=(tr*20000:(tr+0.01)*20000);


%Rnew is the response measured at the instant t
%po is the breaking wave force that we assume for the evaluated instant t
freq=2*pi*60;
chi=0.035;
m=0.012016;
k=m*(freq)^2;
Tstep=1/19200;
j=[1:(Tstep*(Td*19200)/Td):length(X)];
Rob=[];
Rnew=[];
yA=[0];
yB=[0];
A=[0];
B=[0];
for i=1:(Td/Tstep)
%Duhamel Integral
yA(i)=X(j(i))*cos(freq*time(j(i)));
yB(i)=X(j(i))*sin(freq*time(j(i)));
A(i+1)=A(i)*exp(-chi*freq*Tstep)+((Tstep*k)/(m*freq))*yA(i)*exp(-
chi*freq*Tstep);
B(i+1)=B(i)*exp(-chi*freq*Tstep)+((Tstep*k)/(m*freq))*yB(i)*exp(-
chi*freq*Tstep);
Rob(i)=A(i)*sin(freq*time(j(i)))-B(i)*cos(freq*time(j(i)));
Rob=[Rob];
Rnew=[Rnew];
end
tx=length(X(1,:));

F1=plot(time(:,1:tx),X);
%F1=plot(time,X);
set(F1,'Color','black','LineWidth',1.1);
hold on
```

```matlab
p=plot(linspace(0,Td,length(Rob)),Rob,'-');
set(p,'Color','green','LineWidth',1.1);
hold on
plot(time2,wtotl(1:length(time2)),'-');

%plot(linspace(0,0.01,201),f5*2)
%Axis([0 0.01 -4 12])
xlabel('Time [s]','fontsize',14)
ylabel('Relative response [N]','fontsize',14)
grid
h = legend('Triangular Impulse','Calculated Response','Measured
Response',2);
set(h,'Interpreter','none','location','NorthEast','fontsize',14)
```

APPENDIX C

Some snap-shots are shown in this appendix. These snaps compare the wave breaking pattern on different bed slopes (1:10 and 1:20) for same wave characteristics (wave period and eccentricity of the wave paddle)

Figure C.1: Test Ue500t185 , Slope 1:10

Figure C.2: Test Ue500t185 , Slope 1:20

Figure C.3: Test Ue500t196 , Slope 1:10

Figure C.4: Test Ue500t196 , Slope 1:20

Figure C.5: Ue500t208 , Slope 1:10

Figure C.6: Ue500t208 , Slope 1:20

Figure C.7: Ue500t222 , Slope 1:10

Figure C.8: Ue500t222 , Slope 1:20

C.6

APPENDIX D

The test sheet or the manufacturer calibration sheet of all four force transducers that were used in the experiments are given in this appendix.

1

Hottinger Baldwin Messtechnik GmbH

Im Tiefen See 45
D-64293 Darmstadt

Zertifiziert nach ISO 9001 und ISO 14001
ISO 9001 and ISO 14001 certified / Certification selon ISO9001 et ISO 14001

Prüfprotokoll/Test certificate/Protocole d'essai

Typ: S9M/500N   **Auftrag:** 4500337542
Type / Type   Order no. / Commission

Justiermessbereich: 500N   **Prüfer:** Wuchunxia
Adjusted range / Étendue d'essai   Examiner / Vérifieur

Seriennummer: 30854411   **Datum:** 08.11.10
Serial number / No-. de série   Test date / Date d'essai

Prüfergebnisse:
Test results / Résultats d'essai

Eingangsgröße [kN]   **Ausgangsgröße [mV/V]**
Input quantity / Grandeur d'entrée   Output quantity / Grandeur de sortie

          0   0.00415
          500N   2.00378

Aus den Prüfergebnissen berechnete messtechnische Kenngrößen:
Metrological characteristic quantities calculated from the test results
Grandeurs caractéristiques de mesure calculées à partir des résultats d'essai

Kennwert C [mV/V]   1.99963
Sensitivity / Sensibilité

Allgemeine Zusatzinformationen:
General information / Informations complémentaires

Alle weiteren messtechnischen Eigenschaften des Aufnehmers sind durch Typprüfungen und laufende Produktaudits des
Qualitätswesens garantiert.
All other metrological characteristics of the transducer are verified by type testing and regular product audits of the quality department.
Toutes les autres caractéristiques techniques du capteur sont garanties par le Service Qualité, au moyen d'essais et d'audits suivis sur
le produit.

Figure D.1: Calibration sheet of force transducer 1

2

HBM

Hottinger Baldwin Messtechnik GmbH

Im Tiefen See 45
D-64293 Darmstadt

Zertifiziert nach ISO 9001 und ISO 14001
ISO 9001 and ISO 14001 certified / Certification selon ISO9001 et ISO 14001

Prüfprotokoll/Test certificate/Protocole d'essai

Typ: S9M/500N   Auftrag: 4500337542
Type / Type   Order no. / Commission

Justiermessbereich: 500N   Prüfer: Wuchunxia
Adjusted range / Étendue d'essai   Examiner / Vérifieur

Seriennummer: 30854428   Datum: 08.11.10
Serial number / No~. de série   Test date / Date d'essai

Prüfergebnisse:
Test results / Résultats d'essai

Eingangsgröße [kN]   Ausgangsgröße [mV/V]
Input quantity / Grandeur d'entrée   Output quantity / Grandeur de sortie

        0   0.00603
      500N   2.00531

Aus den Prüfergebnissen berechnete messtechnische Kenngrößen:
Metrological characteristic quantities calculated from the test results
Grandeurs caractéristiques de mesure calculées à partir des résultats d'essai

Kennwert C [mV/V]   1.99928
Sensitivity / Sensibilité

Allgemeine Zusatzinformationen:
General information / Informations complémentaires

Alle weiteren messtechnischen Eigenschaften des Aufnehmers sind durch Typprüfungen und laufende Produktaudits des
Qualitätswesens garantiert.
All other metrological characteristics of the transducer are verified by type testing and regular product audits of the quality department.
Toutes les autres caractéristiques techniques du capteur sont garanties par le Service Qualité, au moyen d'essais et d'audits suivis sur
le produit.

Figure D.2: Calibration sheet of force transducer 2

Hottinger Baldwin Messtechnik GmbH

Im Tiefen See 45
D-64293 Darmstadt

Zertifiziert nach ISO 9001 und ISO 14001
ISO 9001 and ISO 14001 certified / Certification selon ISO9001 et ISO 14001

Prüfprotokoll/Test certificate/Protocole d'essai

Typ:	S9M/500N	**Auftrag:** 4500337542	
Type / Type		Order no. / Commission	
Justiermessbereich:	500N	**Prüfer:** Wuchunxia	
Adjusted range / Étendue d'essai		Examiner / Vérifieur	
Seriennummer: 30854426		**Datum:** 08.11.10	
Serial number / No-. de série		Test date / Date d'essai	

Prüfergebnisse:
Test results / Résultats d'essai

Eingangsgröße [kN]	Ausgangsgröße [mV/V]
Input quantity / Grandeur d'entrée	Output quantity / Grandeur de sortie
0	0.00699
500N	2.00706

Aus den Prüfergebnissen berechnete messtechnische Kenngrößen:
Metrological characteristic quantities calculated from the test results
Grandeurs caractéristiques de mesure calculées à partir des résultats d'essai

Kennwert C [mV/V]   2.00007
Sensitivity / Sensibilité

Allgemeine Zusatzinformationen:
General information / Informations complémentaires

Alle weiteren messtechnischen Eigenschaften des Aufnehmers sind durch Typprüfungen und laufende Produktaudits des Qualitätswesens garantiert.
All other metrological characteristics of the transducer are verified by type testing and regular product audits of the quality department.
Toutes les autres caractéristiques techniques du capteur sont garanties par le Service Qualité, au moyen d'essais et d'audits suivis sur le produit.

Figure D.3: Calibration sheet of force transducer 3

HBM

Hottinger Baldwin Messtechnik GmbH

Im Tiefen See 45
D-64293 Darmstadt

Zertifiziert nach ISO 9001 und ISO 14001
ISO 9001 and ISO 14001 certified / Certification selon ISO9001 et ISO 14001

Prüfprotokoll/Test certificate/Protocole d'essai

Typ:
Type / Type — S9M/500N

Auftrag:4500339441
Order no. / Commission

Justiermessbereich: 500N
Adjusted range / Étendue d'essai

Prüfer: Wuchunxia
Examiner / Vérifleur

Seriennummer: 30835210
Serial number / No-. de série

Datum: 25.10.10
Test date / Date d'essai

Prüfergebnisse:
Test results / Résultats d'essai

Eingangsgröße [kN]
Input quantity / Grandeur d'entrée

Ausgangsgröße [mV/V]
Output quantity / Grandeur de sortie

0
500N

0.00850
2.00747

Aus den Prüfergebnissen berechnete messtechnische Kenngrößen:
Metrological characteristic quantities calculated from the test results
Grandeurs caractéristiques de mesure calculées à partir des résultats d'essai

Kennwert C [mV/V]
Sensitivity / Sensibilité

1.99897

Allgemeine Zusatzinformationen:
General information / Informations complémentaires

Alle weiteren messtechnischen Eigenschaften des Aufnehmers sind durch Typprüfungen und laufende Produktaudits des Qualitätswesens garantiert.
All other metrological characteristics of the transducer are verified by type testing and regular product audits of the quality department.
Toutes les autres caractéristiques techniques du capteur sont garanties par le Service Qualité, au moyen d'essais et d'audits suivis sur le produit.

Figure D.4: Calibration sheet of force transducer 4